CHALMERS

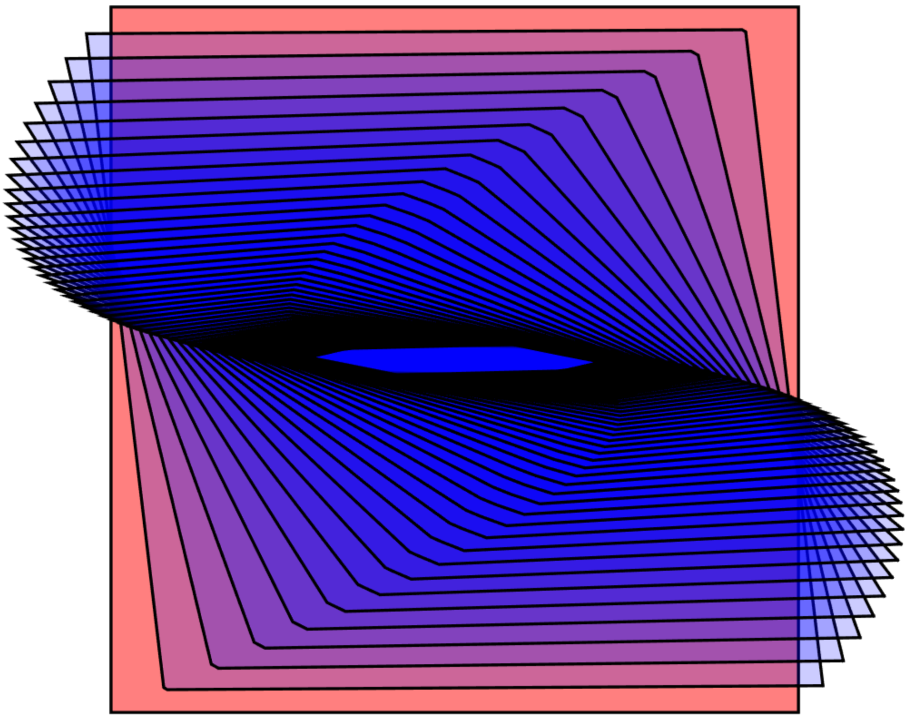

Formal Model Validation by Reachset Conformance between Low and High Order Tractor Semitrailer Vehicle Models

Master's thesis in Automotive Engineering

MOHAMED TAKKOUSH

Department of Mechanics and Maritime Sciences
CHALMERS UNIVERSITY OF TECHNOLOGY
Göteborg, Sweden 2020

MASTER'S THESIS IN AUTOMOTIVE ENGINEERING

Formal Model Validation by Reachset Conformance between Low and High Order Tractor Semitrailer Vehicle Models

MOHAMED TAKKOUSH

Department of Mechanics and Maritime Sciences
Division of Vehicle Engineering and Autonomous Systems
CHALMERS UNIVERSITY OF TECHNOLOGY

Göteborg, Sweden 2020

Formal Model Validation by Reachset Conformance between Low and High Order Tractor Semitrailer Vehicle Models
MOHAMED TAKKOUSH

Master's thesis 2020:57
Department of Mechanics and Maritime Sciences
Division of Vehicle Engineering and Autonomous Systems
Chalmers University of Technology
SE-412 96 Göteborg
Sweden
Telephone: +46 (0)31-772 1000

Cover:
Reachable sets of a vehicle's dynamics starting from a cube set with zero inputs.

Chalmers Reproservice
Göteborg, Sweden 2020

Formal Model Validation by Reachset Conformance between Low and High Order Tractor Semitrailer Vehicle Models
Master's thesis in Automotive Engineering
MOHAMED TAKKOUSH
Department of Mechanics and Maritime Sciences
Division of Vehicle Engineering and Autonomous Systems
Chalmers University of Technology

Abstract

The blooming era of vehicle automation is shaping the future of transportation in ways that humans were not expecting a few decades ago. Autonomous vehicles rely on vehicle models to plan their trajectories and their control behaviour. In this thesis work, a formal model validation technique is presented to check for the validity of the dynamics of low order models against higher order models or even against real measurable systems. The aim is to determine the required bounds of unstructured uncertainties for model validation. First, a formal approach for modelling of the dynamics of vehicles with an arbitrary number of units is introduced which makes use of the Taylor series expansion. Next, the model validation procedure is carried out using reachset conformance falsification, where the dynamics of a high order model are explored using rapidly exploring random trees, and checked against reachable sets calculated for the linear low order model with uncertainties. While the method applied for quantifying the unstructured uncertainty between the low and high order models is based on a proportionality approach, it is also proposed that the higher order terms from the Taylor series could be a good candidate for the quantifying of the uncertainties.

The methods presented are applied to a tractor semitrailer model and tested upon a suite of lane change maneuvers of different aggressiveness. The outcome is that the models conform in conservative maneuvers but fail to conform in aggressive maneuvers unless more unstructured uncertainty is introduced to the low order model. The effect of increasing the uncertainties on the robustness and performance of the studied models is also touched upon in the presented work.

Keywords: Reachability analysis, Model validation, Reachset conformance, Vehicle modeling, Uncertainty Estimation, Tractor semitrailer, Rapidly exploring random trees

Acknowledgements

بِسْمِ ٱللَّهِ ٱلرَّحْمَٰنِ ٱلرَّحِيمِ

For the past 30 weeks, I have had the pleasure to work closely with some brilliant people. The work presented in this thesis could not have been achieved without the help and support of my supervisors, Mathias Lidberg and Peter Nilsson. I am grateful for the unmatched support and undivided attention you bestowed on me since the start of my thesis. Thank you Mathias for guiding me and teaching me your problem solving methods as well as sharing your clever and tactics. And Peter, thank you for treating me as a member of the VAS family and for steering the wheel of the thesis in the direction that benefits me and Volvo Group simultaneously. It has been a pleasure and an honor working with both of you and I couldn't have asked for any better.

I will also take the opportunity to thank my siblings and my friends who drained me with moral support as well as helped me overcome the small obstacles I faced along the road. And a special thanks to Ahmed and Elias for the day to day support and for making Sweden feel like my home since the very beginning.

And of course, the unrivalled thank you goes to my parents, my backbone, who stood by my side every single day of my journey. Thank you for cheering me up and making me feel close to home even when I am thousands of miles away. Everything I achieve is owed to your efforts and sacrifice. I only hope to make you proud.

Mohamed Takkoush
Gothenburg, Sweden
September 21, 2020

Nomenclature

Latin Alphanumerics

$\boldsymbol{a}$	Acceleration vector
a_x	Longitudinal acceleration
a_y	Lateral acceleration
A	Discrete system matrix
$A(p)$	Discrete system matrix with parametric dependencies
A_c	Continuous system matrix
B	Discrete input matrix
$B(p)$	Discrete input matrix with parametric dependencies
B_c	Continuous input matrix
C_c	Continuous output matrix
C_x	Longitudinal cornering stiffness
C_y	Lateral cornering stiffness
C_{fy}	Front axle lateral cornering stiffness
C_{ry}	Rear axle lateral cornering stiffness
D_c	Continuous feedthrough matrix
d_H	Hausdorff distance
$\boldsymbol{F_v}$	Force in vehicle coordinates
$\boldsymbol{F_w}$	Force in wheel coordinates
$\boldsymbol{F_f}$	Force on front wheel
$\boldsymbol{F_r}$	Force on rear wheel
I_z	Moment of inertia about $z-$axis
K_I	Controller integral gain
K_P	Controller proportional gain
l_f	Distance of front axle from COG
l_r	Distance of rear axle from COG
$l_{c,i}$	Distance from coupling point to COG of unit i
$l_{i,j}$	Distance from unit i COG to axle j of that unit
m	Unit mass
M_{zv}	Moment about $z-$ axis in vehicle coordinates
N	Normalization matrix for distance measure ρ
$n_{samples}$	Number of x_s samples in $\mathcal{X}_rel$
$x_{simulations}$	Number of RRT simulations per time step
$\mathbb{N}$	Natural number
$\mathcal{P}$	A polyhedron
$\mathcal{Q}$	A polyhedron
R	Wheel radius
$\mathbb{R}$	Space Dimension
$\mathcal{R}$	Reachable set of states
$\mathcal{R}^h$	Reachable set of states for homogenous solution
$\mathcal{R}^i$	Reachable set of states for inhomogeneous solution
R_δ	Rotation matrix about the wheel fixed reference frame
R_ψ	Rotation matrix about the global fixed reference frame
$R_{\Delta\psi}$	Rotation matrix about the unit fixed reference frame
S_A	Abstract system
S_I	Implementation system
$\mathcal{S}$	Current set of states
s_x	Longitudinal tire slip
s_y	Lateral tire slip

t	Time
u_0	Initial input
u	Input
$u^*(\cdot)$	Nominal input trajectory
$\boldsymbol{u}$	Input vector
$\mathcal{U}$	Set of inputs
$\boldsymbol{V}$	Global velocity vector of vehicle
$\boldsymbol{v}$	Vehicle velocity vector in unit coordinates
$\boldsymbol{v_w}$	Vehicle velocity vector in wheel coordinates
$\boldsymbol{v_x}$	Longitudinal velocity
$\boldsymbol{v_y}$	Lateral velocity
w	Uncertainty
$\boldsymbol{w}$	Uncertainty vector
w_k	Uncertainty estimated from RK-method
$W(p)$	Discrete uncertainty matrix with parametric dependencies
$\mathbb{W}$	Set of uncertainties
x_0	Initial state
$\mathcal{X}_0$	Set of initial states
x	State
$\dot{\boldsymbol{x}}$	State derivatives
$\dot{X}$	Global $x-$ velocity
x^i	Group of RRT states at time t_k
x_n	A single state in x^i
x_s	State defined in $\mathcal{X}_rel$
x_{add}	Closest output state to x_s
x^+	State in next time step
$\boldsymbol{x}$	State vector
$\mathcal{X}$	Set of states
$\mathcal{X}(t_k)$	Set of states at time t_k
$\mathcal{X}_{rel}$	Multidimensional rectangle centered about the nominal trajectory
$\dot{Y}$	Global $y-$ velocity
$\boldsymbol{y}$	Output vector
$\dot{Z}$	Global $z-$ velocity

Greek Characters

α	Tire slip angle
δ	Wheel steering angle
ω	Wheel rotational speed about its center
ω_z	Unit yaw rate
$\dot{\omega}$	Unit yaw acceleration
Ω	Unit angular velocity in 3D
$\dot{\psi}$	Unit yaw rate
$\ddot{\psi}$	Unit yaw acceleration
$\Delta\psi$	Relative yaw angle between units
$\Delta\dot{\psi}$	Relative yaw rate between units
ψ	Unit yaw angle
ρ	Distance measure

Acronyms

COG	Center of Gravity
CORA	Continuous Reachabaility Analysis toolbox
DOF	Degrees of Freedom
FEA	Finite Element Analysis
GTT	Group Trucks Technology
GSP	Global Simulation Platform
HCT	High Capacity Transport
MBD	Multi-Body Dynamics
MDR	Multi-Dimensional Rectangle
MPT3	Multi-Parametric Toolbox
ODE	Ordinary Differential Equation
OTM	One Track Model
PI	Proportional-Integral
RK	Runge-Kutta
RRT	Rapidly-Exploring Random Trees
STM	Single Track Model
TST	Tractor Semitrailer
VAS	Volvo Autonomous Solutions
VTM	Volvo Transport Model

Contents

Chapter 1

Introduction

Automated driving is nowadays in the center of all automotive discussions and research, whether in terms of communication [1], [2], economic and environmental measures [3],[4] or of course safety and traffic flow [5],[2] and more... Automated transport systems can and has significantly improved the transport efficiency of people and goods. Autonomous vehicles connected to control and command centers and used in confined areas like harbors and mines already exist. For example, the use of autonomous trucks at Qingdao New Qianwan Container Terminal in China has reduced labor cost by 70% while increasing efficiency by 30% [6]. However, significant improvements in transport efficiency require a multi-modal transport system with road vehicles.

The vehicle- and function safety of road vehicle automation are currently a major area of research and development. The demand on producing autonomous vehicles to increase safety for road occupants is putting a huge pressure on engineers to come up with innovative ideas and solutions where they can achieve their goals and conform to set regulations.

1.1 Model Based Approach in Vehicle Automation

Driving is a very dynamic task which requires quick decision making based on many different vehicular, environmental and communicative factors. In contrast to an automated driving system, humans are equipped with a highly efficient and optimized brain that helps in taking those decisions and making tough approximations. But when it comes to decision making for autonomous vehicles, the design engineers should have a model that can predict, calculate and act in all situations, especially safety critical ones. Safety is probably the most important aspect of an autonomous vehicle. It is the single aspect that can not be neglected in a production autonomous vehicle and it is also one of the most complicated aspects to design for.

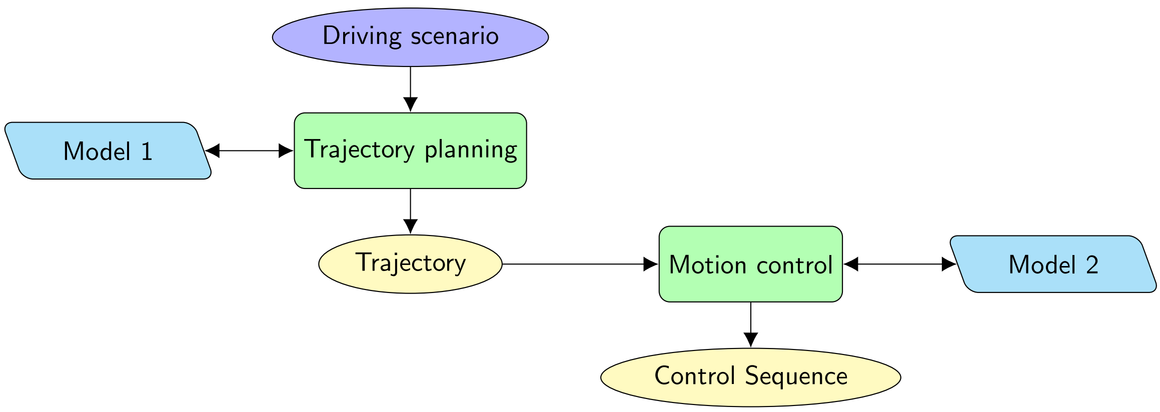

Figure 1.1: Current Workflow at VAS

To ease the process, engineers rely on vehicle models (and driver models [7],[8]) for achieving various safety functions, trajectory planning, motion control, etc. As of the time of writing, Volvo Autonomous Solutions (VAS) has a certain workflow when dealing with autonomous driving and controls. To put it in the simplest form possible, consider the diagram in Fig. 1.1. Here, it is clear how different tasks such as trajectory planning and motion planning depend on different models for calculation and estimation. Those models could be similar in some cases but often are derived from different general models and serve different purposes, with the simplest model being the Single Track Model (STM) and the most complex being the Volvo Transport Model (VTM) [9]. More details about those models and others used by Volvo GTT are presented in Appendix A.1.

1.1.1 Vehicle Modelling

The domain of vehicle modelling is a well established field with plenty of research poured into it. In modelling, there is always a trade off between the complexity and the performance of a model, that is, a mathematically and practically efficient model that could accurately and precisely capture the performance up to a certain standard [10]. Adding degrees of freedom to a model increases its complexity but does not necessarily improve it's performance. In a study carried out in Volvo GTT, Volvo's VTHAP simulation models with added frame roll stiffness behave in an opposite manner to the VTM model [11], a well recognized high fidelity model for trucks developed by Volvo.

In their paper, Hoel and Falcone model a Nordic combination for low speed maneuvering by eliminating roll and pitch motion, as well as considering that there is no sideways skidding and hence no lateral slip which, they claim, is a reasonable assumption for low speed cornering [12]. For a high-speed case on the other hand, some simplifications, or linearizations, are followed in [13] where pitch and roll motions are ignored, lateral and yaw motions are considered small and the tire cornering forces are taken proportional to the lateral slip angle. Those simplifications, along with the Lagrangian mechanics formulation approach, make the differential equations easier to solve [13].

The paper presented in [14] discusses a directional control method of a tractor semitrailer (TST). The article introduces two models, the first being a nonlinear model with 14 DOF used for testing the controller while the seconds model, which is a one track model of a TST, is a linear model with 4 DOF used for the design of the control system [14].

It is notable that the roll motion has a huge effect on the performance of the truck combinations and HCT vehicles. In his research, Santahuhta shows how pertinent is the reliance of roll motion on the height of the center of gravity. For a COG height of 1m, the rearward amplification increases by 0.4% while it increases by 12% for a COG of 2.5m [11]. As a compromise, the authors of [15] argue that the roll (and pitch) motion in their model are accounted for by the quasi-static acceleration of the center of gravity which is located above the ground plane. This way, the roll and pitch motion do not have to be included as additional degrees of freedom, giving the model a higher fidelity while keeping it simple.

When it comes to truck modelling, several directions are followed in modelling the dynamics of the system. Multibody dynamics (MBD) is one of the most common approaches used when modelling trucks and HCT vehicles. Several MBD programs have been developed for this cause and could be used in similar or different ways. Some of the known programs are Trucksim, ADAMS, ArcSim... Volvo GTT has also developed its own MBD model, the VTM. Those models are usually used in simulation environments, especially when real test data is not viable.

Finite element analysis (FEA) methods are also a possible way to study the dynamics of vehicles, although it is well known to be more computationally demanding. As a matter of fact, the combination of MBD with FEA for studying vehicle dynamics is used where the system is designed from several rigid bodies subject to joint constraints and where the structural behaviour of the system is of interest [16].

Analytical or mathematical models are probably the most common approach for modelling the dynamics of vehicles as well as trucks and HCT vehicles. While this could be the most simple approach for modelling, it allows for a deeper understanding of the physics of the model and enables the designer to include as much degrees of freedom required for capturing the needed dynamics. A detailed analytical model is developed by Kharrazi in her PhD book [17]. Her model is used as a reference in this thesis where the developed model here is directly compared to the one developed by Kharrazi. Analytical models could also be vectorized [18], [11] which simplifies the testing and simulation of several vehicle combinations by simply altering some parameters. This approach is also followed in this thesis as mentioned earlier.

1.1.2 Model Validation

A model is in general not of great use if it does not perform as it should. For that reason, the concept of model validation emerges. A vast number of validation techniques have been developed and advised. Some of those techniques are subjective and qualitative, while others are more formal, quantitative and statistical. Some of the most common model validation techniques are presented below [19]:

- *Face validation*: Checks the accuracy and soundness of a model based on the judgment of knowledgeable people.
- *Tracing*: Tracks the behaviour of a model's specific operations.
- *Internal validation*: Determines the variability of a model subject to a random and stochastic analysis.
- *Sensitivity analysis*: Studies how the model behaviour changes based on a change in input parameters.
- *Historical validation*: Relies on data to check if the model behaves like the real system does.
- *Predictive validation*: Checks whether the real system's behaviour complies with the predictions made with the model.
- *Events validation*: Provides a statistical comparison of the model's behaviour against the distribution of the such behaviours of the real system.
- *Turning tests*: Verifies whether the model behaviour and the system behaviour are distinguishable for experts.
- *Spectral analysis*: Evaluates the difference of the model and system's behaviours in the frequency domain.
- *Experimentation*: Compares the output of the model and the system by experimentally changing variables.
- *Convergent validation*: Estimates whether model's predictions are close to those of experts.

In model conformance, different combinations of such model validation techniques are intertwined to create formal links that allow for transference of properties from one model to another.

While model conformance has conventionally been deployed in validating hybrid systems and developed around cyber-physical systems [20], it has recently proven to be a useful tool for validation in different fields. Schurmann et al. [21] have introduced trace conformance in a formal framework for ensuring driveability of planned motions of a vehicle. The method presented studies the behaviour of the real system through real testing data as well as through a suite of Monte-carlo simulations. Their framework is adapted by Lattarulo et al. [22] where a vehicle model is validated with open- and closed-loop controllers with trace conformance. The validation is done against simulations of a high fidelity model based in Dynacar, a virtual platform and a simulation tool for vehicle dynamics systems [23]. Reachset conformance has been used in the field of robotics [24] where the implementation model's behaviour is tested in a feed-forward testing rig. In the field of biomechanics, reachset conformance has been used alongside RRT explorations to test for the safety margins of a human arms with a biomechanical model [25]. In the field of electronics, analog circuits are studied where measurement data from the implementation system are used for carrying out reachset conformance [26].

1.2 Purpose

There seems to be a trend in the work related to model validation where the researchers and authors do not explicitly focus on the model development but rather on the validation process. It is noticed that some authors use the same models from previous work [27], [28] or from other authors [22] even when the models are applied in different driving scenarios or even different driving contexts. This reinforces the need to focus on the development of the vehicle models in relation to the model validation process and the driving context.

VAS is always looking for improvements in their workflow to improve their performance and excel in their work. There is an increasing interest at VAS to develop a common model which is used for different vehicle automoation tasks. Fig. 1.2 depicts an example where a common model is used for both trajectory planning and motion control. It could be that the common model is a complex one and the different planning tasks rely on simplified variants of the common complex model.

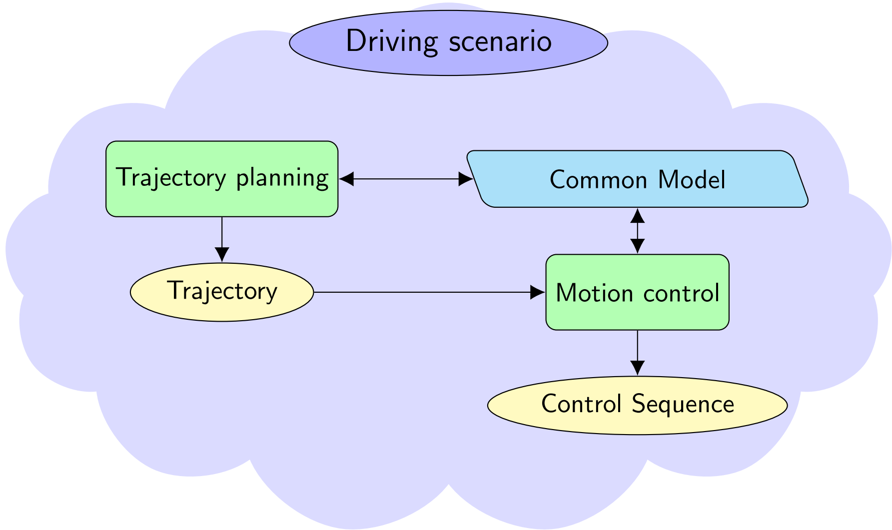

Figure 1.2: Desired Workflow at VAS

Safety assessment requires models which are complex enough for capturing real dynamics, yet simple enough for efficient real time computations. It is not straightforward to decide if a certain model complies with this statement. Hence, there is a high demand on having valid dynamics models that are to be used in different vehicle automation tasks.

1.3 Problem Formulation

The work in this thesis proposes a formal framework as an answer to the high demand on valid vehicle dynamics models. The presented framework is designed for the validation of low order models against higher order models that are to be used in safety assessment, trajectory planning and motion control, etc. The framework can also be used for validation against high fidelity models and even real systems. The aim behind proposing this framework is to quantify the required unstructured uncertainties used for model validation. In this thesis, the framework is implemented on a tractor semitrailer model as a proof of concept.

The framework is be broken down into three main phases:

1. A definition of a driving context
2. A method for vehicle dynamics modelling
3. A method for model validation using reachset conformance falsification

These steps are shown Fig. 1.3, where the blue bounding box representing the driving context spans the whole framework while the yellow bounding box represents the vehicle modelling phase. The model validation takes place in the green block. More information about the validation will follow. In the following sections is a quick introduction to each of the 3 main stages of the framework.

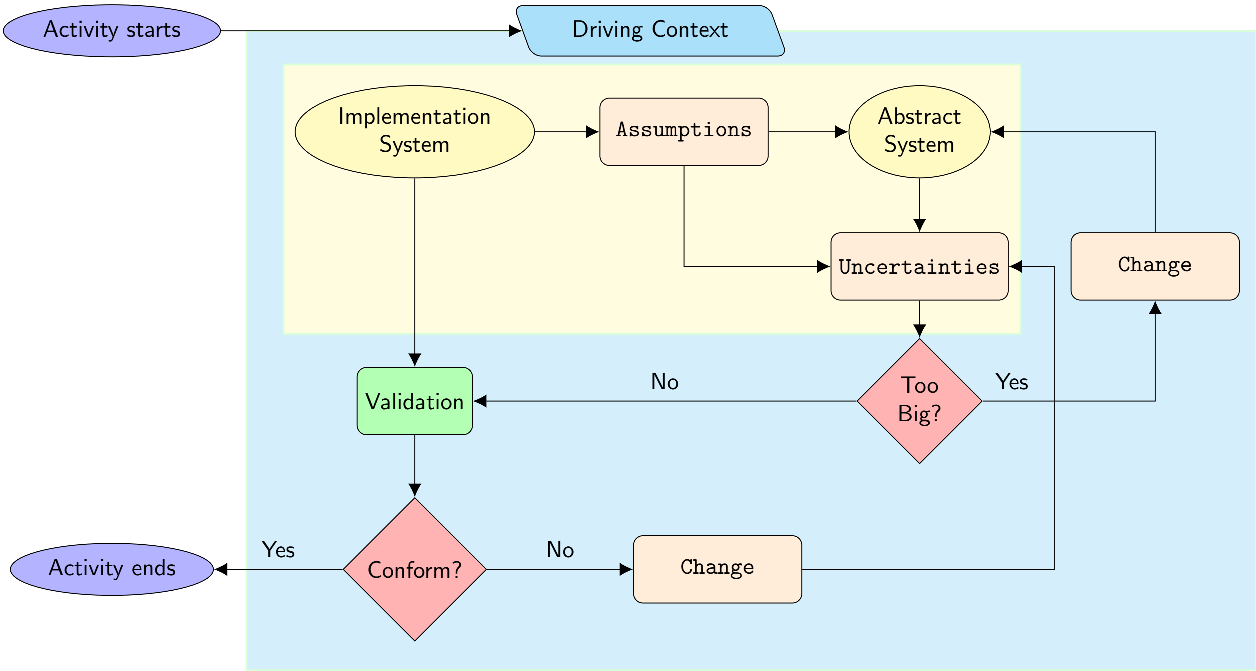

Figure 1.3: Overview Flowchart

1.3.1 Driving Context

The first step in the proposed framework is to define a driving context. This step is arguably among the most important phases in any design problem, yet it is often overlooked and overshadowed by other design phases. The choice of a driving context is reflected throughout the whole framework, in the modelling stage as well as the validation stage.

In this thesis, the concept of a driving context is defined as a set bounded and described by vehicular characteristics, such as the vehicle speed and acceleration, steering angles, aggressiveness in driving, etc. Those could also include road and environmental conditions for instance. These sets are intentionally portrayed as clouds to emphasize the fact that the edges or bounds of the sets are vague by design, and not limited. This is reflected in how different driving contexts could overlap. One important note is that the vehicle being studied is also considered as part of defining the driving context, that is because vehicle characteristics for passenger vehicles are different than those for trucks or sports cars for example. All these characteristics are what distinguish driving contexts from one another. Fig. 1.4 shows an example of three driving contexts divided based on their characteristics. It is clear how each driving context has some characteristics which are unique and some which overlap with other driving contexts.

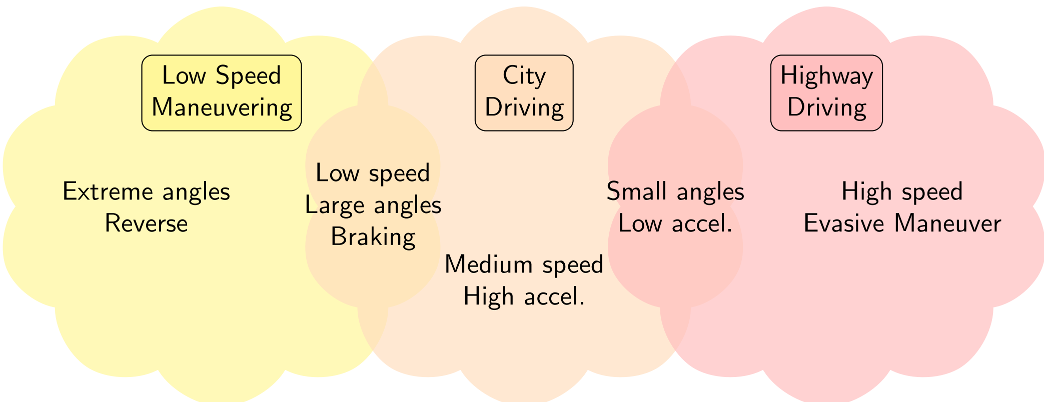

Figure 1.4: Driving context by characteristics

A closer look at a single driving context can describe how the set is structured. Each driving context is defined as a set which contains different driving scenarios. Each driving scenario is by itself a subset of driving maneuvers. This hierarchy is better depicted in Fig. 1.5 which shows the sets and the overlapping subsets as well as the ladder order for defining a driving maneuver. In this thesis, the considered maneuver used in the implementation of the suggested framework is shown in the red boxes in Fig. 1.5 which shows that the tackled driving maneuver is a single lane change in the scenario of driving straight on a city road, hence the driving context being city driving.

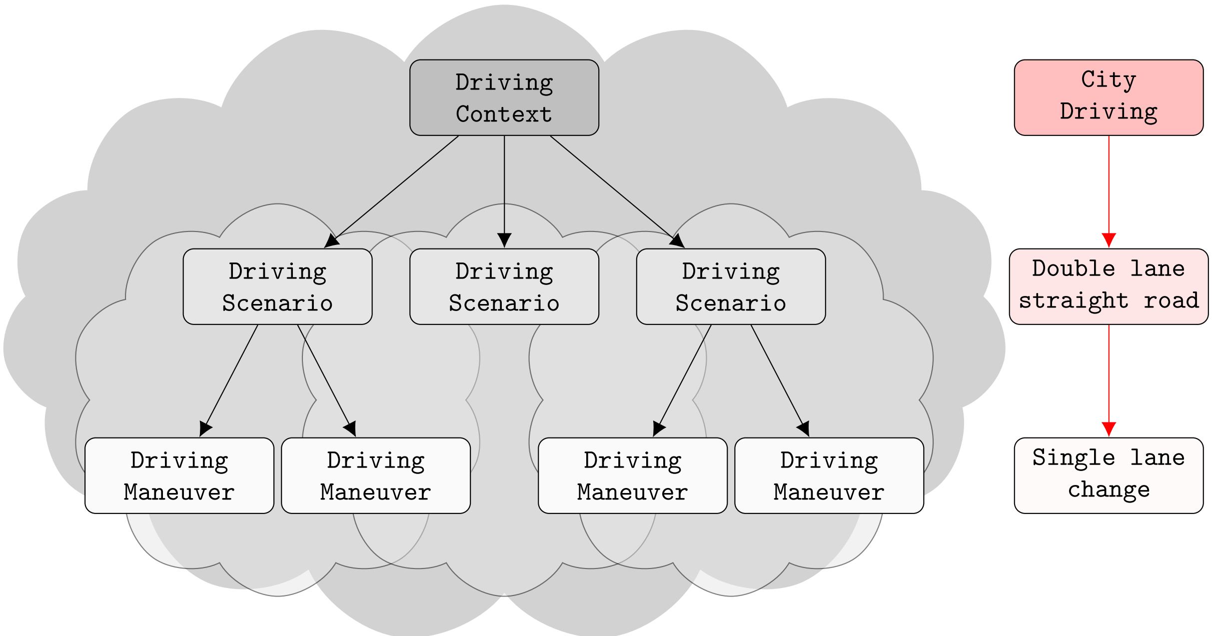

Figure 1.5: Driving context hierarchy

Another vivid example to better explain the hierarchy is that of a steady state cornering maneuver. This maneuver is performed in a roundabout scenario which falls under the driving context of low speed maneuvering. In fact, the roundabout scenario contains several driving maneuvers as shown in Fig. 1.6, those are the deceleration maneuver before reaching the roundabout, entering the roundabout, steady state cornering, exiting the roundabout and accelerating.

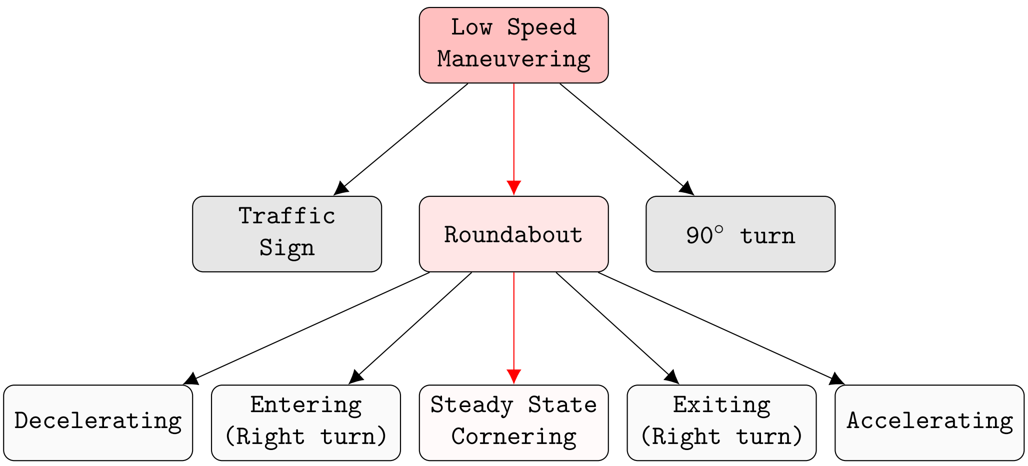

Figure 1.6: Driving context example: Low speed maneuvering

Having a concrete driving context is emphasized in this thesis to make sure that the subsequent design phases yield relevant results. With regards to the modelling phase, having a tangible driving scenario directly affects the assumptions that could be made to simplify the model in hands. As for the validation process, the driving context is key in defining acceptable limits.

1.3.2 Vehicle Modeling

As a part of the formal framework presented in this thesis, the vehicle modelling phase is also derived in a formal manner. The formal part of the modelling is mainly be seen in making assumptions and simplifying the models. The vehicle modelling phase of the presented framework is illustrated in Fig. 1.3 in the yellow bounding box. In this thesis, the development of the vehicle dynamics models are developed in a vectorized manner for an arbitrary number of units. The models follow the newtonian method, and the simplification of the system relies on the Taylor series expansion and the concept of dimensional analysis which results in a linear model of the tractor semitrailer.

1.3.3 Model Validation

After defining the driving scenario and deriving a model, it is left to validate the model in hand, that is by finding suitable levels of uncertainties for which the model is valid. A formal method for validation is presented in this thesis, and that is through reachset conformance by falsification which is presented by Althoff et al. in [24], [25], and [29]. The techniques in the presented work rely on studying the discrete reachability analysis of a low order model, exploring the dynamics of higher order model using a method called rapidly-exploring random trees (RRT), and finally checking whether the performance of the high order model can be predicted from this reachability analysis. An iteration of the framework is carried out until certain levels of uncertainties is reached, for which the models are validated.

1.3.4 Application of the Framework

In this thesis, the proposed framework is applied on a tractor semitrailer model in two main applications; the first one focuses on studying the full reachable space of the models to examine the driving scenario of a double lane straight road, and the second one examines the dynamics in a single lane change maneuver. The single lane change maneuver in a low to medium speed driving is used as a proof of concept to show that the framework is capable of validating models. The single lane change maneuver falls under the driving context of city driving. Setting this driving context implicitly affects the modelling and validation phases of the framework.

A one track model of the tractor semitrailer is developed to set up the nonlinear one track model, then simplified with the Taylor series expansion method to give rise to the linear one track model. The two models are used for the model validation process in the setting of reachset conformance by falsification. In this process, a reachability analysis is performed on the linear model with unstructured model uncertainties and uncertain input trajectories. In this thesis, two methods for quantifying the unstructured uncertainties are presented where one is based on higher order terms of the Taylor series expansion while the other is based on a proportionality approach. The former is expected to give a mathematical relation between the uncertainties and the states of the models which allows for formal error modelling. Meanwhile, the nonlinear model has its dynamics explored using a method called rapidly exploring random trees. Conformance falsification is then applied to validate the linear one track model against the nonlinear one.

Relevant Toolboxes for Reachability Analysis

The choice of toolboxes and programs is an integral part of the presented work. In fact, the framework is developed in MATLAB® where the RRT algorithm as well as the falsification algorithm are executed. As for the reachability analysis, the choice of the Julia language with the Lazysets package is more complicated. The field of reachability computation is flourishing in recent years. A concise rundown of some available toolboxes for reachability analysis is given here.

- **SpaceEX:** Is a mathematical software for the reachability analysis of continuous and hybrid systems using polyhedra to represent sets. The software is also able to handle zonotopes, which are a different representation of geometric sets using a central point and directional vectors pointing out of that center.
- **CORA:** Is a toolbox developed for MATLAB® that is focused on continuous reachability of hybrid systems. It is initially developed for cyber-physical systems and is based on the analysis of zonotopes. It also supports polyhedra representation of sets and is equipped to read and transfer models from SpaceEX.

- **MPT3:** The multi-parametric toolbox is another toolbox developed for MATLAB®. It is mainly designed for model predictive control on the basis of parametric optimization and computational geometry.
- **Lazysets:** The Lazysets package in Julia language is one of the recent approaches for computing the reachability analysis in a symbolic manner. This is discussed in Sec. 4.3.1 in more detail.

1.4 Structure of Thesis

The work in this thesis is structured as follows. Ch. 2 introduces the set theory which paves the way to performing reachability analysis used in the work of the thesis. Ch. 3 introduces the vehicle modelling techniques for a single unit as well as for an arbitrary number of units. Following that, Ch. 4 introduces model conformance as an approach for model validation where the method of reachability analysis from Ch. 2 are applied on the tractor semitrailer model developed in Ch. 3. Chs. 5 and 6 showcase the conformance results for a tractor semitrailer in a double lane change driving scenario as well as a single lane change maneuver respectively. Finally, the conclusion Ch. 7 wraps up the thesis with a discussion about the proposed framework, and finally ends the thesis with a summary as well as mentioning possible future work related to the presented work.

Chapter 2

Set Theory and Reachability Analysis

This chapter introduces the invariant set theory used in this thesis, leading to the definition of reachability analysis and the procedure for computing reachable sets.

2.1 Invariant Set Theory

Set theory is a branch in mathematics that deals with geometrical objects. It is a powerful tool for tackling countless problems in different domains. This section presents the methods used in this thesis for calculating reachable sets for eventually carrying out model conformance. For more details regarding set theory, refer to [30] and [31].

2.1.1 Convex Sets

A set $\mathcal{S} \in \mathbb{R}^n$ is a convex set if [30]

$$\forall x_1, x_2 \in \mathcal{S} \text{ and } \lambda \in [0,1],\ (\lambda x_1 + (1-\lambda)\, x_2) \in \mathcal{S} \tag{2.1}$$

Simply put, this means that a line joining any two points in a convex set is also contained in that set. This can be clearly seen in Fig. 2.1.

Figure 2.1: A simple representation of a non-convex set (left) and convex set (right)in $\mathbb{R}^2$

Hyperplanes and Halfspaces

A hyperplane in $\mathbb{R}^n$ is the set of points orthogonal to a non-zero vector $\mathbf{a} \in \mathbb{R}^n$. This can be described as

$$\mathcal{S} = \{x \in \mathbb{R}^n \mid a^T x = b\} \tag{2.2}$$

where b is a scalar $\in \mathbb{R}$.

The area on either side of a hyperplane is called a halfspace, and is defined as a linear inequality such as

$$\mathcal{S} = \{x \in \mathbb{R}^n \mid a^T x \leq b\} \tag{2.3}$$

Fig. 2.2 portrays an example of a hyperplane and a halfspace in $\mathbb{R}^2$

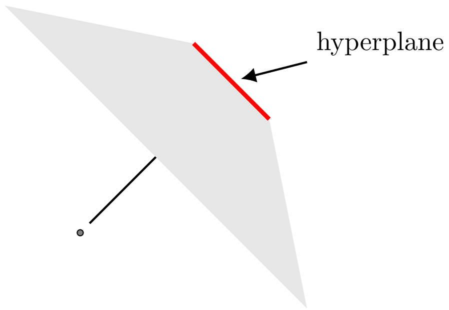

Figure 2.2: A simple example in $\mathbb{R}^2$ of a hyperplane (red) and a halfspace (gray area)

Polytopes and Polyhedra

Polyhedra are geometrical shapes with flat polygon faces and flat sides. They can be represented by a finite number of halfspaces or even a finite number of vertices.

A polytope is a bounded polyhedron which is finite in all its dimensions and has a finite volume in $\mathbb{R}^n$. This means that a polytope does not have any rays $\{x + ty \ : \ t \geq 0\}$ for any $y \neq 0$ [31].

2.1.2 Polytope Operations

In this section, some polytope operations used in the presented work are briefly discussed.

Convex Hull

The convex hull of a set $\mathcal{P}$ is the smallest intersection of all convex polygons containing the set $\mathcal{P}$ [32] and it is denoted by $conv()$ where

$$conv(\mathcal{S}) = \left\{ \sum_{i=1}^{k} \lambda_i x_i \ \middle| \ k \in \mathbb{N}, \ \sum_{i=1}^{k} \lambda_i = 1, \ i \in \{1, 2, ..., k\} \ : \ \lambda_i \geq 0, \ x_i \in \mathcal{S} \right\} \tag{2.4}$$

Projection

By projection, one can decrease the dimensional order of a set from $n+m$ to n by dropping m relations between the dimensions. Projection is used for several purposes, such as simplifying a problem or, as will be seen later, for calculating the reachable set. It is also used in other set operations which are not discussed in this thesis. Fig. 2.3 shows an example of a polyhedron in $\mathbb{R}^3$ being projected on the different planes of $\mathbb{R}^2$.

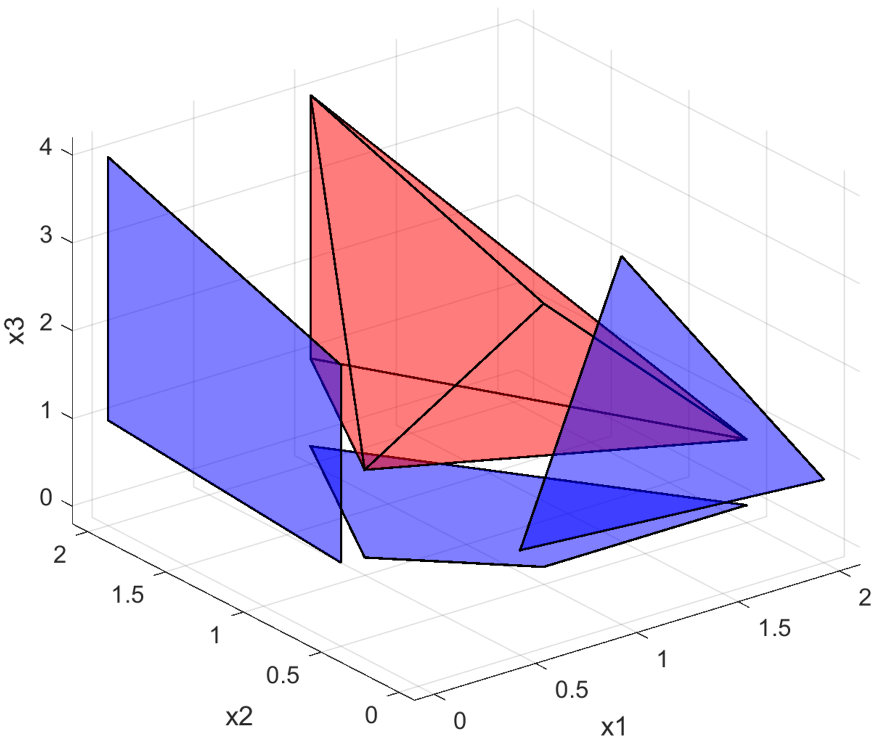

Figure 2.3: Projection of $\mathcal{P}$ from $\mathbb{R}^3$ to $\mathbb{R}^2$

There exist several methods and techniques for performing projections of polytopes. Those techniques can be classified as: Fourier elimination, block elimination and vertex based approaches. Fourier elimination, initially described by Fourier in 1824, has witnessed many improvements throughout the years [33]. One downside for this approach is the redundancy in the generated constraints for the resultant projected polytope. This makes the Fourier-Motzkin elimination method tough for solving projections of complex polytopes iteratively. The other approaches also suffer from similar downsides and perform differently in different problems. For example in low dimensional problems, vertex based approaches provide better performance compared to the other methods, especially if the number of vertices do not outnumber the inequalities.

Minkowski Sum

The minkowski sum $\oplus$ is an operation on two polytopes of the same dimension $\mathbb{R}^n$ giving rise to a third polytope in the same dimension such that

$$\mathcal{P} \oplus \mathcal{Q} = \{p + q \in \mathbb{R}^n \mid p \in \mathcal{P},\ q \in \mathcal{Q}\} \tag{2.5}$$

This is depicted in Fig. 2.4 which shows two polytopes $\mathcal{P}$ and $\mathcal{Q}$ and their minkowski sum.

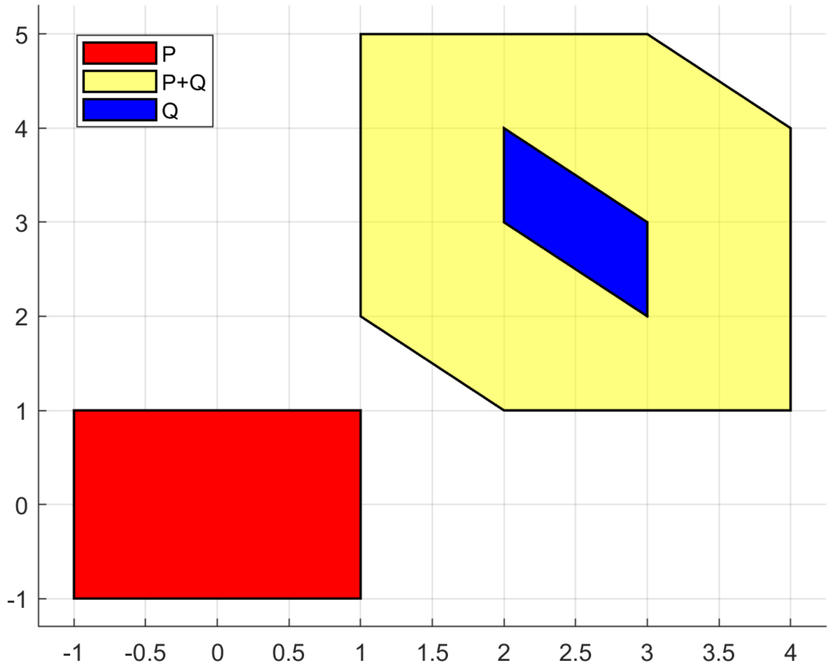

Figure 2.4: Minkowski sum of $\mathcal{P} \oplus \mathcal{Q}$

2.1.3 Set Representations

Ziegler defines two ways for representing polytopes: $\mathcal{V}-$representation and $\mathcal{H}-$representation where $\mathcal{V}-$representation is a convex hull of a finite set of points,

$$\mathcal{P} = \{conv(V) \mid \mathcal{P} \subseteq \mathbb{R}^d,\ V \in \mathbb{R}^{d \times n}\} \tag{2.6}$$

and $\mathcal{H}-$representation is a set of halfspaces whose intersections create a bounded space [31]

$$\mathcal{P} = \{\mathcal{P}(A, z) \mid \mathcal{P} \subseteq \mathbb{R}^d,\ A \in \mathbb{R}^{m \times d},\ z \in \mathbb{R}^m\}. \tag{2.7}$$

2.1.4 Reachable Sets

A continuous state space model is usually described by its system and input matrices as

$$\dot{\boldsymbol{x}}(t) = A_c \boldsymbol{x}(t) + B_c \boldsymbol{u}(t) \tag{2.8}$$

$$\boldsymbol{y}(t) = C_c \boldsymbol{x}(t) + D_c \boldsymbol{u}(t) \tag{2.9}$$

where the subscript c refers to the matrices being continuous in time. The solution of 2.8 with initial condition $x(t_0)$ is [34]

$$\boldsymbol{x}(t) = e^{A_c(t-t_0)}\boldsymbol{x}(t_0) + \int_{t_0}^{t} e^{A_c(t-\tau)} B_c \boldsymbol{u}(\tau) d\tau \tag{2.10}$$

Since the reachability analysis is carried out in a discrete manner, it is reasonable to discretize the previous equation. This can be done by performing the previous equation for one time step Δt such that $t = (k+1)\Delta t$ with $t_0 = k\Delta t$. Hence the discrete system can be described as

$$\boldsymbol{x}(k+1) = e^{A_c \Delta t}\boldsymbol{x}(k) + \left(\int_{0}^{\Delta t} e^{A_c \tau} B_c d\tau \right) \boldsymbol{u}(k) = A\boldsymbol{x}(k) + B\boldsymbol{u}(k) \tag{2.11}$$

The discrete time linear system can be presented in a simpler way using the state update $\boldsymbol{x}^+ = \boldsymbol{x}(k+1)$ of $\boldsymbol{x} = \boldsymbol{x}(k)$ subject to an input $\boldsymbol{u} = \boldsymbol{u}(k)$:

$$\boldsymbol{x}^+ = A\boldsymbol{x} + B\boldsymbol{u} \tag{2.12}$$

In the equation above, the system states and inputs are subject to constraints

$$\boldsymbol{x} \in \mathcal{X}, \ \boldsymbol{u} \in \mathcal{U} \tag{2.13}$$

Those constraints can be used to describe the state and input sets $\mathcal{X}$ and $\mathcal{U}$ as convex polytopes in terms of inequalities

$$\mathcal{X} := \{\boldsymbol{x} \mid H_S \boldsymbol{x} \leq h_S\} \tag{2.14}$$
$$\mathcal{U} := \{\boldsymbol{u} \mid H_U \boldsymbol{u} \leq h_U\} \tag{2.15}$$
$$\tag{2.16}$$

A reachable set of the system described in 2.12 is the set of reachable states that includes all possible outcomes of the system subject to a certain set of inputs $\mathcal{U}$ and starting from an initial set of states $\mathcal{S}$:

$$\text{Reach}(\mathcal{S}) = \mathcal{R} = \{\boldsymbol{x}^{+} \in \mathbb{R}^n \mid \exists\ \boldsymbol{x} \in \mathcal{S}, \exists\ \boldsymbol{u} \in \mathcal{U}\ s.t.\ \boldsymbol{x}^{+} = A\boldsymbol{x} + B\boldsymbol{u}\} \tag{2.17}$$

2.2 System Discretization

The previous section introduces the discretization of the continuous reachability equation (Eq. 2.10), and the resultant can be seen in Eq. 2.12 where the system and input matrices A and B are considered to be discrete. This section describes the techniques used for obtaining those discrete matrices.

The discretization method of a continuous system is key in defining the discrete system and input matrices A and B for calculating the reachable sets since the reachability analysis in this thesis is performed in discrete time domain. There are numerous methods used for discretization of systems. Here, two of many methods for discritization are presented since they are used later in the vehicle modelling chapter (Ch. 3) and the model validation chapter (Ch. 4) for discretizing the continuous vehicle dynamics equations to build up the system and input matrices, as well as discretizing the equations of uncertainties.

2.2.1 Bilinear Transform

The bilinear transform is a one-to-one mapping from the $s-$domain to the $z-$domain [35]. Being bilinear by nature, this method can be used for mapping in either direction, meaning that every point in the left plane of the $s-$domain maps exactly to one single point in the unit circle of the $z-$domain. The bilinear transformation can be described by

$$s = \frac{s-1}{z+1} \tag{2.18}$$

which is also written as

$$z = \frac{1+s}{1-s} \tag{2.19}$$

2.2.2 Discretization using Explicit Runge-Kutta Method

The Runge-Kutta (RK) method is a discretiatization method which relies on explicit or implicit iterations to approximate a function. The 4^{th} order RK method is used in this thesis to estimates a value in a subsequent time step based on the start point derivative, a first interior point derivative, a second interior point derivative and an approximate end point derivative. This can be described by the following algorithm:

Algorithm 1: Uncertainty Approximation

Result: w_k: discrete uncertainty estimated by Runge-Kutta 4^{th} order equations for time step k.
Inputs: X_k, U_k: current state and input. dt: sample period. f: continuous time dynamics equations.
$K_1 = f\left(X_k, U_k\right)$;
$K_2 = f\left(X_k + K_1 \frac{dt}{2}, U_k\right)$;
$K_3 = f\left(X_k + K_2 \frac{dt}{2}, U_k\right)$;
$K_4 = f\left(X_k + K_3 dt, U_k\right)$;
$w_k = \frac{dt}{6}\left(K_1 + 2K_2 + 2K_3 + K_4\right)$;

It can be noted here that using only the first order RK results in the Euler forward method.

2.3 Reachability Analysis

In this section, several approaches for reachability set computation are discussed which include model uncertainties. These methods can be used to analyze different case studies, which is discussed shortly. Reachability analysis, in general, tackles linear systems [36], [37]. However, some modifications can be applied to account for nonlinear systems by applying simple differential inclusions, that is generalizing the computed ordinary differential equations such that their output is mapped to a set rather than a single point. This has been done in several manners in literature, whether by simplifying the dynamical system itself in certain performance regions [38],[39], or by simplifying the reachable set computation such as over approximating reachable sets [40],[41]. Set outer approximation is also introduced in this chapter as well as parametric dependencies but the latter are not considered in the reachset conformance applied in the model validation chapter, see Ch. 4. Since the reachset conformance method in this thesis relies on discrete reachability analysis, the following sections present the technique used for this reachability analysis in discrete time.

2.3.1 Reachable Set Computation for Linear System

Consider the linear system in 2.12. Analytically, the discrete state evolution is defined as [34]

$$\begin{bmatrix} x_1 \\ x_2 \\ \vdots \\ x_N \end{bmatrix} = \begin{bmatrix} A \\ A^2 \\ \vdots \\ A^N \end{bmatrix} x_0 + \begin{bmatrix} B & 0 & \dots & 0 \\ AB & B & \ddots & 0 \\ \vdots & \ddots & \ddots & \vdots \\ A^{N-1}B & A^{N-2}B & \ddots & B \end{bmatrix} \begin{bmatrix} u_0 \\ u_1 \\ \vdots \\ u_{N-1} \end{bmatrix} \tag{2.20}$$

where the matrix exponential refers to matrix multiplication such that $A^2 = AA$ and so on.

To compute the reachable sets using set theory, consider the set of current states $\mathcal{S}$ and the set of inputs $\mathcal{U}$. $\mathcal{S}$ and $\mathcal{U}$ can be represented, in the $\mathcal{H}$-representation form, in terms of inequalities such that

$$H_S \boldsymbol{x} \leq h_S \tag{2.21}$$

$$H_U \boldsymbol{u} \leq h_U \tag{2.22}$$

By substituting Eq. 2.12 in Eq. 2.21 the following relations are obtained

$$H_S \boldsymbol{x} \leq h_S$$

$$H_S \left(A^{-1} \left(\boldsymbol{x}^+ - B\boldsymbol{u} \right) \right) \leq h_S \tag{2.23}$$

$$H_S A^{-1} \boldsymbol{x}^+ - H_S A^{-1} B \boldsymbol{u} \leq h_S \tag{2.24}$$

Eq. 2.22 and 2.24 constitute the new set of inequalities that define a new polyhedron $\mathcal{P}$. This can be portrayed as

$$\underbrace{\begin{bmatrix} H_S A^{-1} & -H_S A^{-1} B \\ 0 & H_u \end{bmatrix}}_{H_P} \begin{bmatrix} \boldsymbol{x}^+ \\ \boldsymbol{u} \end{bmatrix} \leq \underbrace{\begin{bmatrix} h_S \\ h_U \end{bmatrix}}_{h_P} \tag{2.25}$$

The projection of $\mathcal{P}$ on the dimensions of the set of states $\mathcal{S}$ results in the reachable set $\mathcal{R}$

$$\mathcal{R} = \mathcal{P}.Projection(dim(\mathcal{S})) \tag{2.26}$$

One other way of obtaining the reachable set is by benefiting from the linearity of the system and the superposition property. This is done using the Minkowski sum between the homogeneous solution $\mathcal{R}^h$ and the inhomogeneous solution $\mathcal{R}^i$ of the affine function in Eq. 2.12, and the corresponding reachable set becomes

$$\mathcal{R} = \mathcal{R}^h \oplus \mathcal{R}^i \tag{2.27}$$

where

$$\mathcal{R}^h = A\mathcal{S} \tag{2.28}$$

$$\mathcal{R}^i = B\mathcal{U} \tag{2.29}$$

2.3.2 Reachable Set Computation with Uncertainties

Dynamical systems are not always linear, especially not real ones, making linear reachability limited. As mentioned earlier, there are several ways to deal with system nonlinearity in reachability analysis. One way of doing that is to include system nonlinearities as bounded uncertainties or disturbances $w \in \mathbb{W}$ to the linear system. The resulting system becomes

$$\boldsymbol{x}^{+} = A\boldsymbol{x} + B\boldsymbol{u} + \boldsymbol{w} \tag{2.30}$$

Analytically, the state evolution can be computed as shown in the previous section (Sec. 2.3.1). The difference here is the additional disturbance term w.

$$\begin{bmatrix} x_1 \\ x_2 \\ \vdots \\ x_N \end{bmatrix} = \begin{bmatrix} A \\ A^2 \\ \vdots \\ A^N \end{bmatrix} x_0 + \begin{bmatrix} B & 0 & \dots & 0 \\ AB & B & \ddots & 0 \\ \vdots & \ddots & \ddots & \vdots \\ A^{N-1}B & A^{N-2}B & \ddots & B \end{bmatrix} \begin{bmatrix} u_0 \\ u_1 \\ \vdots \\ u_{N-1} \end{bmatrix} + \begin{bmatrix} 1 & 0 & \dots & 0 \\ A & 1 & \ddots & 0 \\ \vdots & \ddots & \ddots & \vdots \\ A^{N-1} & A^{N-2} & \ddots & 1 \end{bmatrix} \begin{bmatrix} w_0 \\ w_1 \\ \vdots \\ w_{N-1} \end{bmatrix} \tag{2.31}$$

The difference now from the linear system is in the additive set of disturbances. The bounds of the disturbance set can be expressed as

$$H_w \boldsymbol{w} \leq h_w \tag{2.32}$$

In a similar derivation as with the linear system, the resultant polyhedron $\mathcal{P}$ is portrayed as

$$\underbrace{\begin{bmatrix} H_S A^{-1} & -H_S A^{-1} B & -H_S A^{-1} \\ 0 & H_u & 0 \\ 0 & 0 & H_w \end{bmatrix}}_{H_P} \begin{bmatrix} \boldsymbol{x}^{+} \\ \boldsymbol{u} \\ \boldsymbol{w} \end{bmatrix} \leq \underbrace{\begin{bmatrix} h_S \\ h_U \\ h_w \end{bmatrix}}_{h_P} \tag{2.33}$$

The projection of $\mathcal{P}$ on the dimensions of the set of states $\mathcal{S}$ results in the reachable set $\mathcal{R}^w$ which now includes the system nonlinearity.

$$\mathcal{R}^w = \mathcal{P}.Projection(dim(\mathcal{S})) \tag{2.34}$$

Similar to before, the nonlinearity can be added to the reachability set using the Minkowski sum method. The resultant set $\mathcal{R}^w$ including the nonlinearities becomes:

$$\mathcal{R}^w = \mathcal{R} \oplus \mathbb{W} = \mathcal{R}^h + \mathcal{R}^i \oplus \mathbb{W} \tag{2.35}$$

2.3.3 Reachable Set Computation for Certain and Uncertain Inputs

So far, the reachability is discussed in terms of half spaces, hyperplanes and inequalities, and in terms of Minkowski sums of the system and input matrices A and B as well as the uncertainties w. One term that has not been discussed yet is the input term or the control signal u in the discrete system equation (Eq. 2.30). This input term can be interpreted in several ways, three of which are discussed here. The input can be certain as in it is definite without any uncertainty, or it can be an uncertain input meaning that the input has an uncertainty of a certain magnitude above or below a nominal input value, or it can be a set or a range of all inputs that the system can be subjected to.

The choice of the input set is directly related to the problem being handled. In the following example, three cases for the choice of input set are discussed. Consider a simple system of two states and one input defined as in the discrete system equation (Eq. 2.30)

$$\begin{bmatrix} x_1^{+} \\ x_2^{+} \end{bmatrix} = A \begin{bmatrix} x_1 \\ x_2 \end{bmatrix} + B \left[u \right] + w \tag{2.36}$$

$$A = \begin{bmatrix} 0.8 & 0.4 \\ -0.4 & 0.8 \end{bmatrix}, \quad B = \begin{bmatrix} 1.5 \\ 1 \end{bmatrix} \tag{2.37}$$

$$x_1,\ x_2 \in \mathcal{X}, \quad u \in \mathcal{U}, \quad w \in \mathbb{W} \tag{2.38}$$

$$\mathcal{X}_0 = \begin{bmatrix} 0 \\ 0 \end{bmatrix} \tag{2.39}$$

Among the three cases presented below, the cases of certain and uncertain inputs make use of a nominal trajectory, which is defined as the trajectory followed by a linear system subject to a predefined nominal input trajectory $u^{*}(\cdot)$.

Full Input Range

For the first case, consider the input set $\mathcal{U}$ to be the set of all admissible inputs to the system. This set allows the reachability analysis to discover the full potential of a system for a specified number of steps starting from an initial set $\mathcal{X}_0 = \mathcal{S}$.

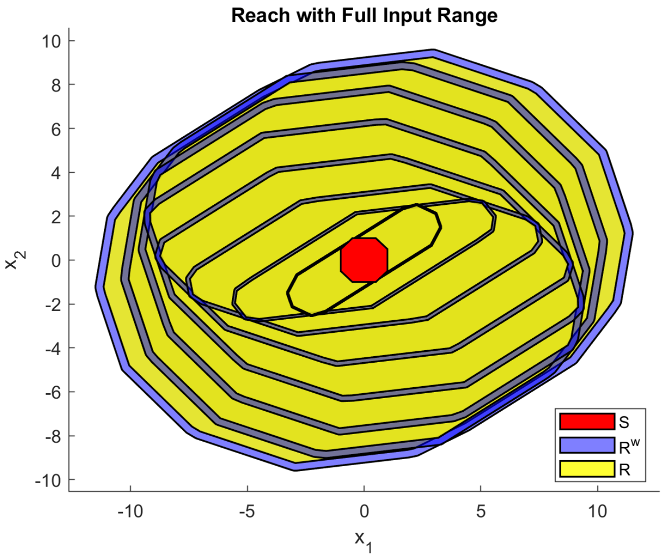

Figure 2.5: Reachability analysis with full input range for 8 steps (For clarity, R is the reachable set of S and R^w is the reachable set with disturbances)

Fig. 2.5 shows the reachable sets obtained by using the full input range. With this simplest definition of reachable sets, it is easy to explore the space that a system can reach. This has been used for guaranteeing safety of robotic arms [25], and is used in the model validation chapter (Ch. 4) for studying the reachable space of a tractor semitrailer model.

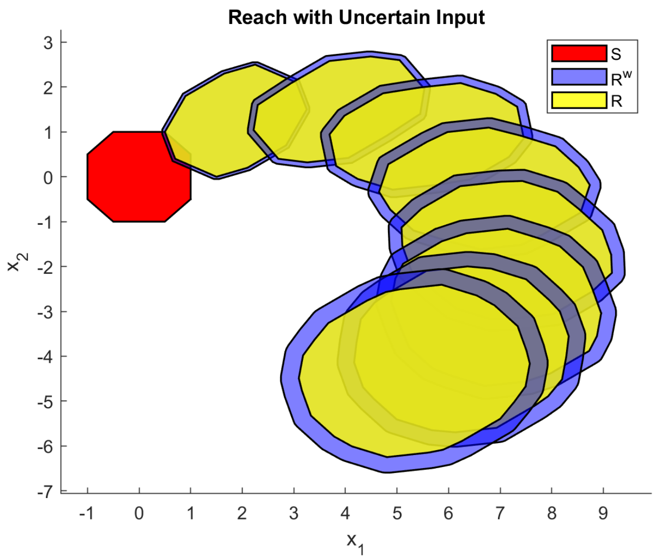

Figure 2.6: Reachability analysis with uncertain input for 8 steps (For clarity, R is the reachable set of S and R^w is the reachable set with disturbances)

Uncertain Inputs

For the second case, consider the input set $\mathcal{U}$ to be the set of uncertain inputs centered at the nominal input trajectory $u^*(\cdot)$. This set allows for the study of the evolution of the admissible states affected by the uncertainty in the inputs.

Fig. 2.6 shows the evolution of 8 steps for the system starting from the initial set $\mathcal{X}_0$ with the uncertain input set $\mathcal{U}$ following the input trajectory $u^*(\cdot)$. It is clear here how the sets are growing in size as the system evolves. Note that the figure also shows the sets including the uncertainty set $\mathbb{W}$ in blue which is another reason for the inflation in the sets.

Certain Inputs

For the third case, consider the input set $\mathcal{U}$ to be a singleton corresponding to an instance in the input trajectory $u^*(k)$ along $u^*(\cdot)$. This case is considered when there is no uncertainty in the inputs. Here, the evolution of the system uncertainties and disturbances can be studied.

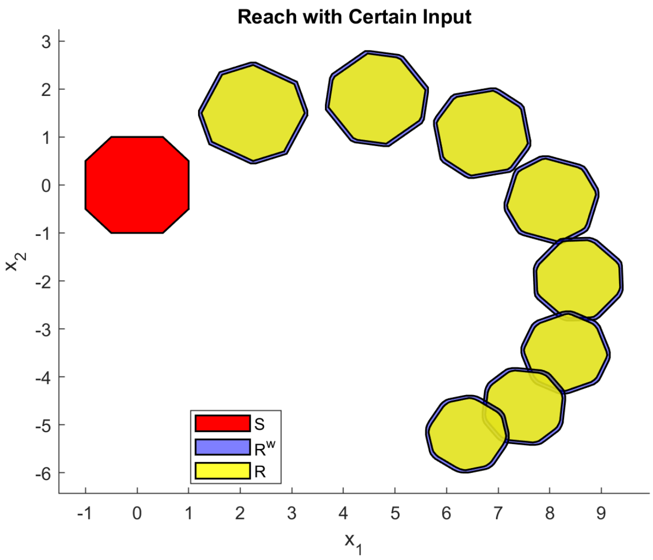

Figure 2.7: Reachability analysis with certain input for 8 steps (For clarity, R is the reachable set of S and R^{w} is the reachable set with disturbances)

Fig. 2.7 shows the evolution, similar to that in Fig. 2.6 but without the uncertainty in the inputs. Here, even though there is uncertainty in the system, it can be seen that the sets are getting smaller, and that is due to the stability of the system. In case the initial set is smaller, the trend in the figure would be the opposite, that is, the sets grow with time until they reach a point where the system stability counteracts the disturbances and the sets stabilize in size.

It is notable that the sets obtained in each of Figs. 2.6 and 2.7 are subsets of the reachable sets computed with the full input range in Fig. 2.5.

2.3.4 Outer Approximations

To increase the efficiency of solvers and allow them to solve complex problems by decreasing the computational costs, outer approximations of sets have been deployed in set based problems. There are numerous techniques to tackle outer approximation of sets. The outer approximation of sets in this thesis is based on Hausdorff distance, a mathematical metric that measures the closeness between sets and hence measures their resemblance. It has been developed and used in numerous fields such as in image comparison [42] and object detection [43]. It is also used in approximating polygons and set in an optimization manner [44]. The Hausdorff distance is later used for over-approximating sets for model validation Ch. 4. The Hausdorff distance d_H can be computed as

$$d_H(A, B) := \max\left(h(A, B),\ h(B, A)\right) \tag{2.40}$$

where

$$h(A, B) := \max_{a \in A} \min_{b \in B} \left\| a - b \right\| \tag{2.41}$$

Here, $a,\ b \in \mathbb{R}^n$, A and B are sets $\subset \mathbb{R}^n$, and $\left\| \cdot \right\|$ is the L_2 norm [42].

2.3.5 Parametric Dependencies in Reachable Set Computations

While not particularly tackled in this thesis work, it is worth mentioning parametric dependencies in the calculation of reachable sets. Parameter dependencies show up in several stages of a reachability analysis, whether in the system matrix $A(p)$, the input matrix $B(p)$ or even the uncertainty in the inputs $u(p)$. The importance of parametric dependencies is highly related to the linearization points since reachability analysis ideally deals with linear systems. The inclusion of parameter dependencies can be accounted for in an over approximation manner [27]. Even though parametric dependencies are not considered in this thesis, the effects of excluding those relations are reflected upon in the results.

Chapter 3

Vehicle Modeling

This chapter introduces the vehicle modeling that is used in the thesis. Since the point of designing models is to study a vehicle's performance in different situations, the models are evidently be different, or of different complexity depending on the use case of the model. While linear models are generally used in most practical control theory applications, there exist high fidelity models that capture the dynamics of a vehicle more profoundly. Those models are used for example in offline computations since their complexity requires greater computational power and hence is harder to perform in real time.

3.1 Assumptions

What distinguishes simpler models from one another are the assumptions chosen before the design phase. Extensive consideration should be invested in a model's assumptions since they play a huge role in the performance of that model. Since this thesis is devoted for providing a procedure for modeling and validating models in a formal framework, the choice of assumptions should also be part of the framework. Those assumptions are directly affected by the driving context and driving scenario being studied which implicitly set the limits on the dynamics of the vehicle, such as accelerations, steering angles, etc. Based on those limits, the assumptions can be made in such a way that the simplified model can still capture the right dynamics of the real system to a certain extent.

It is important to stay reminded of the assumptions throughout the design process for several reasons. One of those reasons is to understand the limits of the model being designed. The assumptions should also be reflected in the resulting performance of the model. It goes without questioning that introducing the assumptions certainly reduces the fidelity of the model.

3.1.1 Dimensional Analysis

Dimensional analysis is a method widely used in the fields of physics and engineering, such as in fluid dynamics. Here, a concept called smallness is introduced. The concept of smallness plays an important role in making assumptions and simplifying models. Smallness is introduced for dimensionless parameters and variables, such as angles, which allows for their comparison with 1. A variable a is called small when it is 1 order of magnitude smaller than 1 ($a << 1$) and is considered negligible when it is two orders of magnitude smaller than one. This is helpful when simplifying equations using the Taylor series expansion as it is discussed shortly.

3.1.2 Series Expansion

In mathematics, functions that cannot be expressed using regular mathematical operations such as addition and subtraction are often quantified by using series expansion methods. There are numerous methods used for different purposes and for the expansion of different functions. Of the most common series expansions are the Taylor series, Fourier series, Newtonian series and many others.

The simplification and linearization of the models in this thesis follow the Taylor Series expansion method which states that

$$f(x) = f(a) + f'(a)(x-a) + \frac{f''(a)}{2!}(x-a)^2 + ... + \frac{f^{(k)}(a)}{k!}(x-a)^k + h_k(x)(x-a)^k \tag{3.1}$$

where the last term is the remainder of order $k+1$. However, due to the presence of states and inputs in the models that are to be developed, the multi-parametric representation of the Taylor series expansion follows

$$\begin{aligned} f(x,u) &= f(a,b) + [f_x(a,b)(x-a) + f_u(a,b)(u-b)] \\ &+ \frac{1}{2!}\left[f_{xx}(a,b)(x-a)^2 + 2f_{xu}(a,b)(x-a)(u-b) + f_{uu}(a,b)(u-b)^2\right] \\ &+ \mathcal{O}(x^3,u^3) \end{aligned} \tag{3.2}$$

In order to combine the dimensional analysis method with series expansion, assume an angle α to be small and consider the following Taylor series expansion of $\cos\alpha$

$$\cos\alpha = 1 - \frac{\alpha^2}{2} + \frac{\alpha^4}{24} + ... \tag{3.3}$$

This means that the 2^{nd} order terms, which are the square of α are in the order of 10^{-2} which is two orders of magnitude less than 1 and are hence considered to be negligible. Assuming that the error is negligible if it is 2% or less, and solving the following equation

$$0.02 = \frac{\alpha^2}{2} \tag{3.4}$$

$$\Rightarrow \ \alpha = 0.2[\text{rad}] \approx 12^\circ \tag{3.5}$$

one gets that a small angle is considered to be 12° or less. This also applies when more than one variable are considered small such that the first order Taylor series gives

$$a << 1,\ b << 1 \ \Rightarrow \ ab \approx 0 \tag{3.6}$$

$$\alpha << 1 \ \Rightarrow \ \sin(\alpha) = \tan(\alpha) \approx \alpha \tag{3.7}$$

$$\Rightarrow \ \cos(\alpha) \approx 1 \tag{3.8}$$

3.2 Single Unit One Track Model

In the vehicle modeling presented in this chapter, the motion is described in different reference frames, namely the global fixed reference (inertial frame), the unit fixed reference frame and the wheel reference frame. The relation between those reference frames is described by the following rotation matrices:

$$R_\psi = \begin{bmatrix} \cos\psi & -\sin\psi \\ \sin\psi & \cos\psi \end{bmatrix} \tag{3.9}$$

$$R_\delta = \begin{bmatrix} \cos\delta & -\sin\delta \\ \sin\delta & \cos\delta \end{bmatrix} \tag{3.10}$$

$$R_{\Delta\psi} = \begin{bmatrix} \cos\Delta\psi & \sin\Delta\psi \\ -\sin\Delta\psi & \cos\Delta\psi \end{bmatrix} \tag{3.11}$$

where R_ψ represents the rotation matrix from unit to global coordinate system, R_δ represents the rotation matrix from wheel to unit coordinate system, and $R_{\Delta\psi}$ represents the rotation matrix from unit $i+1$ to unit i coordinate system. Those rotation matrices are used in the subsequent sections to transform forces, velocities and accelerations between different frames.

Fig. 3.1 shows the model for the single unit one track model that is used for developing the equations in the subsequent sections.

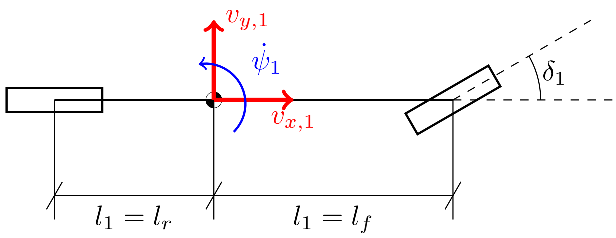

Figure 3.1: Single unit one track model

3.2.1 Equations of Motion

Starting from Newton's Second law,

$$\sum \boldsymbol{F_v} = m\boldsymbol{a} \tag{3.12}$$

$$\sum M_{zv} = I_z\ddot{\psi} \tag{3.13}$$

and defining the wheel forces (in the wheel's coordinate systems) to be

$$\boldsymbol{F^w} = \begin{bmatrix} F_{xw}^w & F_{yw}^w \end{bmatrix}^{\mathrm{T}} \tag{3.14}$$

and applying the transformation from the wheel to the unit coordinates, the forces become

$$\begin{aligned} \boldsymbol{F_w} &= R_\delta \boldsymbol{F_w^w} \\ \begin{bmatrix} F_{xv} \\ F_{yv} \end{bmatrix} &= \begin{bmatrix} \cos\delta & -\sin\delta \\ \sin\delta & \cos\delta \end{bmatrix} \begin{bmatrix} F_{xw}^w \\ F_{yw}^w \end{bmatrix} \\ &= \begin{bmatrix} F_{xw}\cos\delta - F_{yw}\sin\delta \\ F_{xw}\sin\delta + F_{yw}\cos\delta \end{bmatrix} \end{aligned} \tag{3.15}$$

The moment arm vectors from the wheels to the center of gravity of the vehicle are relatively l_f and l_r for the front and rear moment arms. Also, the moment exerted by one wheel on the center of gravity of the vehicle is defined as

$$\sum M_z = \boldsymbol{r} \times \boldsymbol{F_w} \tag{3.16}$$

where $\boldsymbol{r}$ is the moment arm from the center of gravity to the respective wheel. This means that the moments about the z-axis passing through the center of gravity are

$$\sum M_z = F_{fyv}l_f - F_{ryv}l_r \tag{3.17}$$

Let the vehicle speed be defined as

$$\boldsymbol{v} = \begin{bmatrix} v_x & v_y & 0 \end{bmatrix}^{\mathrm{T}} \tag{3.18}$$

Since the analysis is about planar motion, the only relevant angular rotation in this study is the yaw rate $\dot{\psi}$.

Let the angular velocity vector of the vehicle be defined as

$$\boldsymbol{\omega} = \begin{bmatrix} 0 & 0 & \dot{\psi} \end{bmatrix}^{\mathrm{T}} \tag{3.19}$$

Let the vehicle acceleration in planar motion be defined as

$$\begin{aligned} \boldsymbol{a} &= \frac{\partial \boldsymbol{v}}{\partial t} + \boldsymbol{\omega} \times \boldsymbol{v} = \frac{\partial \boldsymbol{v}}{\partial t} + \Omega\boldsymbol{v} \\ \begin{bmatrix} a_x \\ a_y \\ a_z \end{bmatrix} &= \begin{bmatrix} \dot{v}_x - \dot{\psi}v_y \\ \dot{v}_y + \dot{\psi}v_x \\ 0 \end{bmatrix} \end{aligned} \tag{3.20}$$

where Ω is the skew-symmetric matrix defined as

$$\Omega = \begin{bmatrix} 0 & -\dot{\psi} & 0 \\ \dot{\psi} & 0 & 0 \\ 0 & 0 & 0 \end{bmatrix} \tag{3.21}$$

Since the study is concerned with planar motion, the 2D skew-symmetric matrix becomes

$$\Omega = \begin{bmatrix} 0 & -\dot{\psi} \\ \dot{\psi} & 0 \end{bmatrix} \tag{3.22}$$

Hence, Newton's equations (3.12) and (3.13) can be rewritten as

$$F_{fxv} + F_{rxv} = m(\dot{v}_x - \dot{\psi}v_y) \tag{3.23}$$

$$F_{ryv} + F_{ryv} = m(\dot{v}_y + \dot{\psi}v_x) \tag{3.24}$$

$$F_{fyv}l_f - F_{ryv}l_r = I_z\ddot{\psi}_z \tag{3.25}$$

3.2.2 Tire Models

Tires play an essential role in a vehicle's dynamics. All interactions between the road and a vehicle are translated into forces that pass through the contact patch of the wheels, whether in the longitudinal, lateral or vertical direction. For this reason, a substantial amount of consideration is put into understanding how tires behave and perform, and for that, different tire models have been developed over the years.

Tire models can be divided into two categories: physical tire models and empirical tire models. Complex physical tire models quantitatively derive the performance of a tire based on material sciences and mechanical properties of the tire structure and compound, while empirical tire models rely on experimental data to tune certain parameters and capture the behaviour of a tire which is described by a mathematical formulation [45].

For the development of the models in this chapter, it is enough to state that the tires generally provide a relation between the tire forces and the tire slip angles (s_x and s_y) as well as the longitudinal and cornering stiffnesses (C_x and C_y). This can be written as

$$F_x = \boldsymbol{F_x}(C_x, s_x, F_z, \mu) \tag{3.26}$$

$$F_y = \boldsymbol{F_y}(C_y, s_y, F_z, \mu) \tag{3.27}$$

3.2.3 Constitution and Compatibility Relations

The longitudinal tire slip s_x and the lateral tire slip s_y also introduce more nonlinearity in modelling. Those are defined by

$$s_y = \frac{v_{yw}}{R\omega}, \quad s_x = \frac{R\omega - v_{xw}}{R\omega}, \quad \tan\alpha = \frac{v_{yw}}{v_{xw}} \tag{3.28}$$

$$\Rightarrow s_y = \tan\alpha(1 - s_x) = \frac{v_{yw}}{v_{xw}}(1 - s_x) \tag{3.29}$$

where α is the body slip angle. Here, the translational wheel speeds are defined such that

$$\begin{aligned} \boldsymbol{v_w} &= R_\delta^{-1} (\boldsymbol{v} + \boldsymbol{\omega} \times \boldsymbol{r}) \\ &= R_\delta^{-1} (\boldsymbol{v} + \Omega l) \end{aligned}$$

where $\boldsymbol{r} = l_f,\ l_r$ is the arm vector to the respective wheel.

3.2.4 Nonlinear Model

Using all the equations derived earlier and substituting them in equations (3.23-3.25) results in a highly nonlinear system of equations which are derived such that the Eqs. 3.24 and 3.25 are solved for

$$\dot{v}_y = \frac{F_{ryv} + F_{ryv}}{m} - \dot{\psi} v_x \tag{3.30}$$

$$\ddot{\psi}_z = \frac{F_{fyv} l_f - F_{ryv} l_r}{I_z} \tag{3.31}$$

where the forces are replaced by Eqs. 3.36-3.39. To write this more simply, consider the state vector $\boldsymbol{x} = \begin{bmatrix} v_y & \dot{\psi} \end{bmatrix}^{\mathrm{T}}$ and input vector $\boldsymbol{u} = [\delta]$. The nonlinear system for a single unit (su) is expressed as

$$\dot{\boldsymbol{x}} = f_{su}(\boldsymbol{x}, \boldsymbol{u}) \tag{3.32}$$

3.2.5 Linear Model

The simplification of Eqs. 3.30 - 3.31 in this section follows the concept of dimensional analysis and the approximation is based on the Taylor series expansion discussed earlier in the assumptions section, see Sec. 3.1.

For the single lane change maneuver considered in this thesis, assuming the vehicle does not harshly brake or steer for emergencies, it is relatively safe to assume a constant longitudinal speed and a small steering angle such that

$$\dot{v}_x \approx 0 \tag{3.33}$$

$$\delta << 1 \tag{3.34}$$

Other assumptions taken in such a scenario for designing a linear model can be small lateral and angular velocities which means

$$v_y\dot{\psi} \approx 0 \tag{3.35}$$

The tire model considered in the presented work is the linear tire model. This means that the constitution equations are written as

$$F_{xw} = C_x s_x \tag{3.36}$$
$$F_{yw} = C_y s_y \tag{3.37}$$

Therefore, for a single unit vehicle the lateral tire slip angles (s_{yf} and s_{yr}) for the steered and non-steered axles can be approximated by

$$s_{yf} \approx \frac{v_y + l_f\dot{\psi}}{v_x} - \delta_f \tag{3.38}$$
$$s_{yr} \approx \frac{v_y - l_r\dot{\psi}}{v_x} \tag{3.39}$$

Since the tire slip and slip angles are also considered to be small, then one can use the dimensional analysis and Taylor series expansion such that

$$s_x << 1 \;\Rightarrow\; s_x^2 \approx 0 \tag{3.40}$$
$$s_y << 1 \;\Rightarrow\; s_y^2 \approx 0 \tag{3.41}$$
$$\alpha << 1 \;\Rightarrow\; \alpha^2 \approx 0 \tag{3.42}$$
$$\Rightarrow\; \sin\alpha \approx \tan\alpha \approx 0,\; \cos\alpha \approx 1 \tag{3.43}$$

By using the assumption of Eq. 3.33 in Eq. 3.12 for longitudinal equilibrium, the sum of forces in the longitudinal direction results in

$$\sum F_x \approx 0 \;\Rightarrow\; F_{fx} + F_{rx} \approx 0 \tag{3.44}$$

Both front and rear axle are assumed to be either braking or propelling the vehicle which means that for the linear tire model used in this thesis,

$$F_{fx} \approx F_{rx} \approx 0 \;\Rightarrow\; s_x \approx 0 \tag{3.45}$$

All those assumptions allow for the simplification of the nonlinear system. This simplification can be carried out using the series expansion method discussed in the assumptions section, see Sec. 3.1.2. By considering only the 1^{st} order terms of the Taylor series, linearization about a constant longitudinal speed can be achieved, which takes care of the "smallness" attribute. The linearization introduces a new system defined as

$$\dot{v}_x = 0 \tag{3.46}$$
$$\dot{v}_y = -\frac{C_{fy}+C_{ry}}{mv_x}v_y - \left(v_x + \frac{C_{fy}l_f - C_{ry}l_r}{mv_x}\right)\dot{\psi} + \frac{C_{fy}}{m}\delta \tag{3.47}$$
$$\ddot{\psi} = -\frac{C_{fy}l_f - C_{ry}l_r}{J_z v_x}v_y - \frac{C_{fy}l_f^2 + C_{ry}l_r^2}{J_z v_x}\dot{\psi} + \frac{C_{fy}l_f}{J_z}\delta \tag{3.48}$$

Considering equations (3.46-3.48), the system can be written in state space formulation with a state vector $\boldsymbol{x} = \begin{bmatrix} v_y & \dot{\psi} \end{bmatrix}^{\mathrm{T}}$ and input vector $\boldsymbol{u} = [\delta]$ such that

$$\begin{bmatrix} \dot{v}_y \\ \ddot{\psi} \end{bmatrix} = \underbrace{\begin{bmatrix} -\frac{C_{fy}+C_{ry}}{mv_x} & v_x + \frac{C_{fy}l_f - C_{ry}l_r}{mv_x} \\ -\frac{C_{fy}l_f - C_{ry}l_r}{J_z v_x} & -\frac{C_{fy}l_f^2 + C_{ry}l_r^2}{J_z v_x} \end{bmatrix}}_{A} \begin{bmatrix} v_y \\ \dot{\psi} \end{bmatrix} + \underbrace{\begin{bmatrix} \frac{C_{fy}}{m} \\ \frac{C_{fy}l_f}{J_z} \end{bmatrix}}_{B} \delta \tag{3.49}$$

In order to express the position of the vehicle in global coordinates, consider the following kinematic equations for the global position (X, Y):

$$\boldsymbol{V} = \begin{bmatrix} \dot{X} \\ \dot{Y} \end{bmatrix} = R_\psi \boldsymbol{v} = \begin{bmatrix} \cos\psi & -\sin\psi \\ \sin\psi & \cos\psi \end{bmatrix} \begin{bmatrix} v_x \\ v_y \end{bmatrix} \tag{3.50}$$

This means that

$$\begin{bmatrix}\dot{X}\\ \dot{Y}\end{bmatrix} = \begin{bmatrix}\cos\psi\ v_x & -\sin\psi\ v_y\\ \sin\psi\ v_x & \cos\psi\ v_y\end{bmatrix} \tag{3.51}$$

Those equations can be linearized, using the 1^{st} order Taylor series expansion, about a constant velocity and for small heading angles as it is described earlier. This yields

$$\begin{bmatrix}\dot{X}\\ \dot{Y}\end{bmatrix} = \underbrace{\begin{bmatrix}1 & 0 & 0\\ 0 & 1 & v_x\end{bmatrix}}_{G} \underbrace{\begin{bmatrix}v_x\\ v_y\\ \psi\end{bmatrix}}_{\boldsymbol{y}} \tag{3.52}$$

The global position of the vehicle is not considered in this thesis since the focus is only on the dynamics of the system. Hence, no further development of the global position equations is carried out here.

3.3 Tractor Semitrailer One Track Model

As mentioned earlier, the modelling stage is developed for an arbitrary number of units, where i refers to the unit number and $i = 1, 2, ..., N$. In this section, the methods are developed for a tractor semitrailer but can easily be extended for more units. Fig. 3.2 shows the one track model of the tractor semitrailer where the 2 units are coupled with an angle $\Delta\psi$ between them.

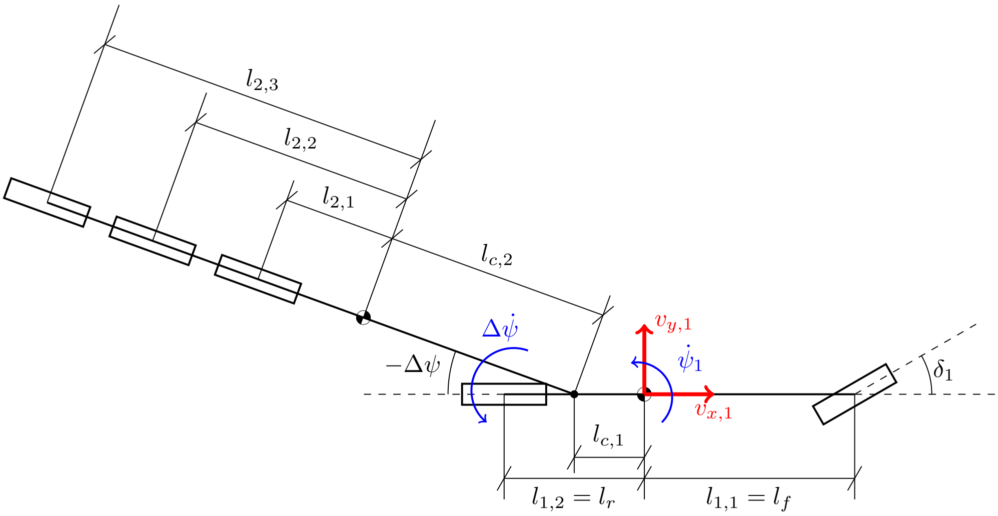

Figure 3.2: Tractor semitrailer one track model

While the equations in the previous section still hold in a tractor semitrailer model, introducing more units to the model increases its complexity. Due to the added units, there is now a new force in the couplings. By defining the coupling forces (in the global coordinate systems) between the units to be

$$\boldsymbol{F_{c,i}} = \begin{bmatrix}F_{xc,i} & F_{yc,i}\end{bmatrix}^{\mathrm{T}} \tag{3.53}$$

and applying the transformation from the global to the unit coordinates, the coupling forces in the unit coordinate system become

$$\begin{aligned} F_{vc,i} &= R_{\psi,i}^{-1} F_{c,i}\\ &= \begin{bmatrix}\cos\psi_i & \sin\psi_i\\ -\sin\psi_i & \cos\psi_i\end{bmatrix}^{-1} \begin{bmatrix}F_{xc,i}\\ F_{yc,i}\end{bmatrix}\\ &= \begin{bmatrix}F_{xc,i}\cos\psi_i - F_{yc,i}\sin\psi_i\\ F_{xc,i}\sin\psi_i + F_{yc,i}\cos\psi_i\end{bmatrix} = \begin{bmatrix}F_{xvc,i}\\ F_{yvc,i}\end{bmatrix} \end{aligned} \tag{3.54}$$

This force shows up in Newton's equations of motion such that Eqs. 3.23 - 3.25 are modified for a unit i such that

$$F_{fxv,i} + F_{rxv,i} + F_{fxvc,i} + F_{rxvc,i} = m_i(\dot{v}_{x,i} - \dot{\psi}_i v_{y,i}) \tag{3.55}$$

$$F_{ryv,i} + F_{ryv,i} + F_{fyvc,i} + F_{ryvc,i} = m_i(\dot{v}_{y,i} + \dot{\psi}_i v_{x,i}) \tag{3.56}$$

$$F_{fyv,i} l_{f,i} - F_{ryv,i} l_{r,i} + F_{fyvc,i} l_{c,i,f} + F_{ryvc,i} l_{c,i,r} = I_{z,i} \ddot{\psi}_{z,i} \tag{3.57}$$

Based on Newton's third law, the following relation for the coupling force in a tractor semitrailer model are used

$$\boldsymbol{F_{rc,i}} = -\boldsymbol{F_{fc,i+1}} \tag{3.58}$$

3.3.1 Kinematic Equations

To relate the motion of the units to one another, kinematic equations are used. This establishes relations for the velocities and accelerations between the units based on the yaw angles between them and allow for the simplification of the equations. To establish the motion of the coupling points, consider the unit i. The velocity of the rear coupling point of unit i is expressed as

$$\begin{aligned} \boldsymbol{v_{c,i,r}} &= \boldsymbol{v_i} + \boldsymbol{\omega}_i \times l_{c,i,r} && (3.59) \\ &= \boldsymbol{v_i} + \Omega_i l_{c,i,r} && (3.60) \end{aligned}$$

This velocity is then rotated from the coordinate system of unit i to $i+1$ using the rotation matrix $R_{\Delta\psi,i}$ such that the front coupling velocity becomes

$$\boldsymbol{v_{c,i+1,f}} = R^{-1}_{\Delta\psi,i} \boldsymbol{v_{c,i,r}} \tag{3.61}$$

Transforming this coupling velocity back to the center of gravity of unit $i+1$ eventually gives the velocity relation between the two units. The transformation is basically the opposite of that in Eq. 3.59 such that

$$\begin{aligned} \boldsymbol{v_{i+1}} &= \boldsymbol{v_{c,i+1,f}} - \boldsymbol{\omega_{i+1}} \times l_{c,i+1,f} && (3.62) \\ &= \boldsymbol{v_{c,i+1,f}} - \Omega_i l_{c,i+1,f} && (3.63) \end{aligned}$$

Eventually, the relation between the velocities of units i and $i+1$ becomes, in planar motion,

$$\boldsymbol{v_{i+1}} = \begin{bmatrix} v_{x,i+1} \\ v_{y,i+1} \end{bmatrix} = \begin{bmatrix} \cos(\Delta\psi_i)\, v_{x,i} + \sin(\Delta\psi_i)\left(l_{c,i,r}\dot{\psi}_i - v_{y,i}\right) \\ \sin(\Delta\psi_i)\, v_{x,i} + l_{c,i+1,f}\left(\Delta\dot{\psi}_i + \dot{\psi}_i\right) + \cos(\Delta\psi_i)\left(v_{y,i} - l_{c,i,r}\dot{\psi}_i\right) \end{bmatrix} \tag{3.64}$$

The same process is also applied for establishing a relation for the accelerations between units i and $i+1$. The resultant relations are as follows

$$\dot{\boldsymbol{v}}_{\boldsymbol{i+1}} = \begin{bmatrix} \dot{v}_{x,i+1} & \dot{v}_{y,i+1} \end{bmatrix}^{\mathrm{T}} =$$

$$\begin{bmatrix} \cos(\Delta\psi_i)\left(\Delta\dot{\psi}_i\left(l_{c,i,r}\dot{\psi}_i - v_{y,i}\right) + \dot{v}_{x,i}\right) - \sin(\Delta\psi_i)\left(-l_{c,i,r}\ddot{\psi}_i + \dot{v}_{y,i} + v_{x,i}\Delta\dot{\psi}_i\right) \\ \sin(\Delta\psi_i)\left(\Delta\dot{\psi}_i\left(l_{c,i,r}\dot{\psi}_i - v_{y,i}\right) + \dot{v}_{x,i}\right) + \cos(\Delta\psi_i)\left(-l_{c,i,r}\ddot{\psi}_i + \dot{v}_{y,i} + v_{x,i}\Delta\dot{\psi}_i\right) + l_{c,i+1,f}\left(\Delta\ddot{\psi}_i + \ddot{\psi}_i\right) \end{bmatrix} \tag{3.65}$$

3.3.2 Nonlinear Model

The full nonlinear equations are not presented in this section due to space limitations. The process of obtaining the equations is, however, the same as the one presented for a single unit vehicle. This means that the resultant equations for the tractor semitrailer model are highly nonlinear and can be expressed as ordinary differential equations such that

$$\dot{\boldsymbol{x}} = f_{TST}(\boldsymbol{x}, \boldsymbol{u}) \tag{3.66}$$

This nonlinear model is the model used as the implementation system S_I in the reachset model conformance.

3.3.3 Linear Model

Same as with the single unit vehicle, and for the lane change dynamics, the nonlinear system of equations for the two unit vehicle is linearized about a constant speed following assumptions similar to those presented in Sec. 3.2.5 based on series expansion and dimensional analysis. Here, the added unit calls for an extension of the assumptions such that the lateral and angular velocities are considered small ($v_{y,i}\dot{\psi}_i \approx 0$). The relative angle between the units is considered small

$$\Delta\psi_1 << 1 \tag{3.67}$$

along with the relative angular velocity and acceleration, which means that their multiplication with any other small term is considered negligible.

The linearization process follows that presented for the single unit model using the first order terms of the Taylor series. The resulting system can be expressed in state space formulation with a state vector $\boldsymbol{x} = [v_{y,1} \quad \dot{\psi}_1 \quad \Delta\psi \quad \Delta\dot{\psi}]^{\mathrm{T}}$ and input vector $\boldsymbol{u} = \delta$ such that

$$\dot{\boldsymbol{x}} = \mathrm{A}\boldsymbol{x} + \mathrm{B}\boldsymbol{u} \tag{3.68}$$

where A and B, the system matrix and the input matrix, are not shown here for spacial limitation reasons. Those are then discretized using the bilinear transform method, see Sec. 2.2, and then used for the reachability analysis.

Chapter 4

Model Validation by Reachset Conformance

In this chapter, the theory behind model conformance is introduced with a focus on reachset conformance. This is then applied on the tractor semitrailer developed in the modelling chapter (Ch. 3) using the reachability analysis techniques presented earlier in the set theory background, Ch. 2.

4.1 Model Conformance

Model conformance is a methodology used by engineers to ensure the behaviour of systems. The definition of a system's behaviour varies based on the field of research. An implementation system S_I is said to be conformant to an abstract system S_A if the behaviour of the implementation system S_I is a subset of the behaviour set of the abstract system S_A [20]. In this work, the behaviour is considered to be the dynamic performance of the systems, and an implementation system can be a high order model (i.e. nonlinear two track model), a high fidelity model (i.e. VTM), or even test data.

Achieving conformance between the implementation and abstract systems S_I and S_A is similar to building a bridge that links the two models allowing for the transference of properties or specifications from the abstract system S_A to the implementation system S_I [20]. This can be expressed as

$$S_I \text{ conf } S_A \quad \wedge \quad S_A \vDash \mathit{spec} \quad \Rightarrow \quad S_I \vDash \mathit{spec} \tag{4.1}$$

Conformance between two models can be achieved on several levels. Ranked from stricter to weaker conformance links, the types of model conformance are listed in the diagram of Fig. 4.1.

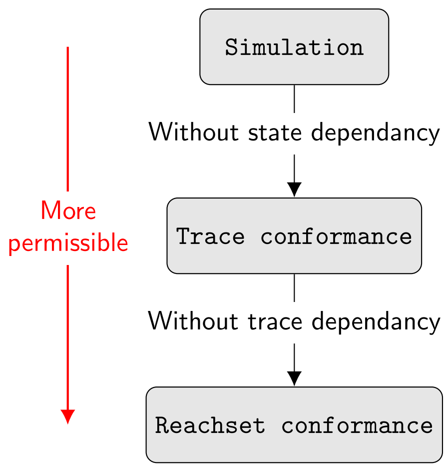

Figure 4.1: Types of model conformance

Here, conformance by simulation is the most accurate conformance link between an abstract and an implementation system where all states of the simulation of both systems overlap in time and space making the implementation system S_I conformant to the abstract system S_A. The relation gets more permissible, or weaker, by dropping state dependencies and looking at trace conformance. That is, for the same input set, the trace outputs of the implementation system S_I conform to those of the abstract system S_A for all input trajectories [29]. The weakest conformance link among the conformance types is reachset conformance in which trace dependencies are dropped and the states of the implementation system S_I are measured against the reachable space of the abstract system S_A for a certain input. The level of validity required is based on the properties of interest that are to be transferred between the models and also based on the use case of the model under development. This is reflected in the type of model conformance chosen for validation. The conformance choice should be as permissive as possible yet allowing to transfer properties that suits the desired objective. To put this into perspective, trace conformance relations are strong relations that allow for transference of all properties between models, but does not allow for transference of state dependant properties. Also, it is difficult to apply on abstract models. In case of safety of autonomous vehicles, a weaker or more permissive relation, reachset conformance, is enough to transfer the required properties, even where trace conformance does not hold [29].

4.1.1 Reachset Conformance

Formally, one can define reachset conformance between the implementation and abstract systems S_I and S_A as [20]

$$S_I \text{ conf } S_A \iff \forall t : \forall u \in \mathcal{U} : \; Reach(S_I, u) \subseteq Reach(S_A, u) \tag{4.2}$$

For carrying out any type of conformance, the implementation system's behaviour should be explored. Since the calculation of reachable sets for high order models and high fidelity models are computationally demanding, it is strenuous to perform conformance verification by comparing the reachabiliy of two systems. This also applies to model conformance with real systems where exploring the full behaviour is impossible, or requires plenty of data. For that reason, reachset model conformance by falsification is introduced where an under-approximation of the high order model is calculated and used for falsifying the validity of the model. This has been done in several ways in literature. Where the implementation system is a real physical system, real testing and data logging techniques are most commonly implemented. The implementation system can also be a high fidelity model, in which exploring the dynamics of the model can be tricky. Random Monte-Carlo simulations are often used to explore the dynamics of such models [21]. Another method for exploring the behaviour of an implementation system is by using a random exploration technique such as the rapidly exploring random trees (RRT) [27], [46]. Such methods have been tested with reachset conformance and proven to be a reliable method for examining extreme behaviours of a system.

In reachset conformance by falsification, in order to prove that a model is not valid, it is enough to prove that the under-approximative states of the high order model fall out of the reachable sets of the low order model. The implementation in this chapter follows four main steps. First, the models representing the abstract system S_A and the implementation system S_I used for conformance have to be chosen. Next, reachability analysis is applied on the abstract system S_A. Third, the dynamics of the implementation system S_I are explored with the RRT method and finally, an iterative falsification algorithm is applied to checked the RRT outputs against the reachable sets.

Before diving into the details of model conformance, one should always stay reminded of the driving context that encompasses the whole process, in this case it is city driving. What is important to know here is that the driving scenario defines a certain nominal trajectory which is used in the reachability analysis, see Sec. 2.3.3. As defined earlier, a nominal trajectory is the trajectory of states followed by the states of the linear system when a certain input trajectory is applied on that system.

4.2 Choosing Models for Conformance

The first task of model conformance should start by defining the models which are used for carrying out the study. It is decided that the nonlinear tractor semitrailer model represents the implementation system and the linear low order model represents the abstract system. Those were both obtained in the tractor semitrailer modelling in Sec. 3.3

4.2.1 Quantification of Uncertainty

Since the linear model has its limitations, it can not capture the complex dynamics of a nonlinear higher fidelity model. In this section, two methods to account for the uncertainties between the high and low order models are introduced. The first method is based on the explicit formula of the remainders of the Taylor series expansion. This approach is studied by Althoff in more detail in [47] and applied in some of his work on reachability analysis such as in [27]. The second method is based on a simple proportional approach.

Method 1: Higher order terms from series expansion

Recall the Taylor series Eq. 3.1. During the simplification in the modelinh chapter (Ch. 3), only the first order terms of the Taylor series are considered. Here, both the 2^{nd} and 3^{rd} order terms of the series expansion are used for the uncertainty quantification since some of the uncertainty equations are even functions while others are odd. This is due to the presence of sine and cosine terms in the equations. In fact, for a single unit vehicle, as well as for a two unit vehicle, linearizing about a constant speed leads to the uncertainty equations to be as follows:

$$\begin{aligned}
\dot{v}_{x,\text{uncertainty}} &\rightarrow \text{Even function} \\
\dot{v}_{y,\text{uncertainty}} &\rightarrow \text{Odd function} \\
\ddot{\psi}_{\text{uncertainty}} &\rightarrow \text{Odd function} \\
\Delta\dot{\psi}_{\text{uncertainty}} &\rightarrow \text{Odd function} \\
\Delta\ddot{\psi}_{\text{uncertainty}} &\rightarrow \text{Odd function}
\end{aligned} \tag{4.3}$$

This means that the uncertainty $\dot{v}_{x,\text{uncertainty}}$ shows up in the 2^{nd} order terms of the Taylor expansion while the other states have a lower uncertainty and show up in the 3^{rd} order terms.

All those equations are evaluated along the nominal trajectory, even before the reachability analysis is carried out. The values obtained are used to bound the uncertainty sets $\mathbb{W}$ in the reachability analysis. This means that the uncertainty set is changing in each time step. However, this approach poses a problem for the discrete reachability analysis presented in this thesis since the equations of the uncertainties are obtained from the continuous time dynamics equations while the reachability analysis is done in a discrete manner.

Since the 2^{nd} and 3^{rd} order terms from the Taylor series expansion are in continuous time domain, the 4^{th} order Runge-Kutta (RK) method is used to calculate the value of the state uncertainties in the succeeding discrete time step based on the nominal trajectory.

Method 2: Proportional uncertainties

This method is a simple approach to tackle the unstructured uncertainties in a model. This method is expected to be robust and its application must be straightforward.

The idea here is to find a percentage for which the added uncertainties yield a conformant model. This approach is not computed along the whole nominal trajectories of states, but rather as a proportion of the maximum value attained in each of the state trajectories. Since the uncertainty here is a constant for the whole maneuver, no discretization is required for the uncertainties.

4.3 Reachability Analysis of Low Order Model

Now that the models are defined, the reachable sets can be computed for the abstract system, or low order model. The reachable sets include the uncertainty sets $\mathbb{W}$ which are discussed earlier. The model shown in Eq. 3.68 with the 4 dimensional state vector $\boldsymbol{x} = [v_{y,1} \;\; \dot{\psi}_1 \;\; \Delta\psi \;\; \Delta\dot{\psi}]^{\mathrm{T}}$ is used here with the introduction of uncertainties such that the model becomes

$$\dot{\boldsymbol{x}} = A\boldsymbol{x} + B\boldsymbol{u} + W\boldsymbol{x} \tag{4.4}$$

The reachability analysis presented with and without uncertainties in Secs. 2.3.1 and 2.3.2 shows an ideal way to compute the reachable sets of a system. However, in practice, the projection carried out on the polyhedrons $\mathcal{P}$ introduces the reachable sets $\mathcal{R}$ and $\mathcal{R}^w$ with many hyperplanes causing the reachability analysis problem to explode in terms of the number of hyperplanes per set after calculating the reachable sets in just a couple of time steps, hence rendering the reachability analysis unsolvable. Of course, the reachable sets with uncertainties $\mathcal{R}^w$ include more hyperplanes due to the introduction of the uncertainty set $\mathbb{W}$ in the analysis. This is solved by using an over-approximative technique to outer approximate the reachable sets with polyhedrons having a low number of hyperplanes. This sets a limit on the computation time required to compute the reachable sets on the cost of reducing the accuracy of the calculation. The technique is based on the Hausdorff distance which is presented in the outer approximation Sec. 2.3.4 and its application in Julia language is discussed in the section describing the projection of reachsets, Sec. 4.3.1.

4.3.1 Projection of Reachsets

The reachability analysis in this thesis ought to be robust and used with different models and various dimensions. Due to the computational demands of the reachability analysis problem, the work done is carried out in the Julia language. Julia is an open source high-level programming language designed for fast computations [48]. One package that is useful in the context of this thesis is LazySets.jl, which is a package for calculus with convex sets. This package is designed for solving complex set-based problems in a symbolic manner, and hence the name LazySets. It is designed in the context of reachability analysis and model verification which makes it an ideal tool for the reachability analysis carried out in this thesis.

Lazysets are by definition a symbolic representation of sets, which makes them not useful right out of the box for explicit computations. The Lazysets should be evaluated in order to give useful sets for the conformance testing. The evaluation of Lazysets results in what is referred to as concrete sets. This evaluation is performed using an over-approximative function from the LazySets.jl library which uses the Hausdorff distance to approximate a Lazyset with an H-polygon. The approach with Lazysets over-approximation is not

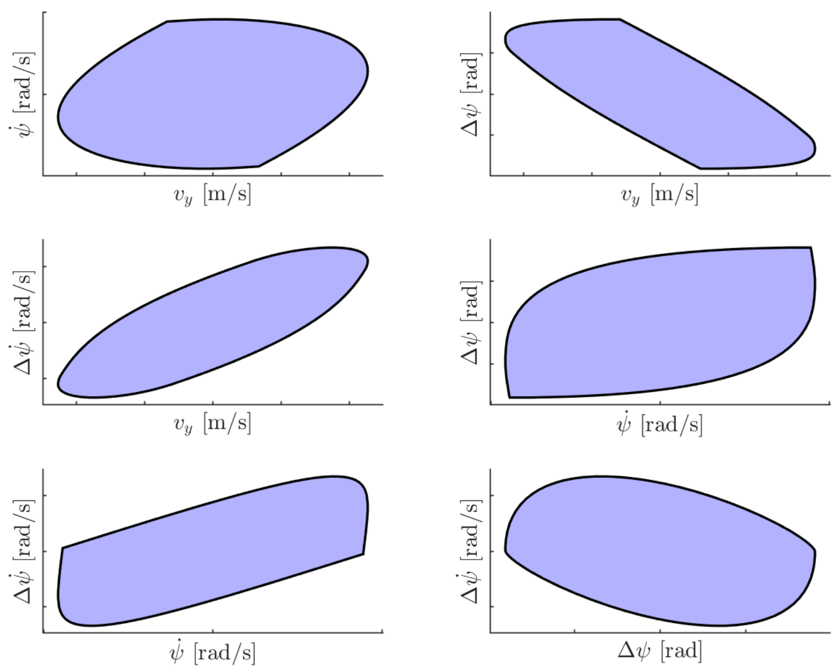

Figure 4.2: Phase planes of the different projection combinations of a 4 state tractor semitrailer model

ideal. Even though it provides a huge advantage in terms of computational time, it has it's own limitations. The over-approximative function is limited to 2D projections only. This means that the relations between different dimensions of the state space are lost upon projecting the Lazysets on the 2D space to allow for the over-approximations. To minimize the error from this limitation, all combinations between different two dimensions are established so the relations between the dimensions are captured as closely as possible. An example of the projection looks like the one in Fig. 4.2 where a single reachable set of the 4 dimensional system representing the dynamics of a tractor semitrailer is projected on the 6 combinations of states.

The resultant H-polygons from the reachability analysis are all projected in this manner then used for conformance testing as it is discussed in the next section.

4.4 Dynamics Exploration of High Order Model

The third step of the model conformance implementation is the exploration of the dynamics of the high order model. Remember that the high order model is highly nonlinear making the exploration of its dynamics cumbersome. For this reason, rapidly exploring random trees are introduced earlier as an efficient exploration method for pushing the limits of the high order model in order to achieve falsification of the model conformance, if any.

4.4.1 Rapidly-Exploring Random Trees Method

First introduced by LaValle in 1998, rapidly exploring random trees (RRT) is an exploration method designed for path planning problems which can handle high degrees of freedom and tackle holonomic as well as non-holonomic constraints. This technique of exploration iteratively expands towards undiscovered areas of the state space in a probabilistically complete manner while keeping the outcome connected. This makes it an ideal and simple method for path planning [49]. The main reason behind the use of RRT exploration method is because of the under-approximative nature of exploring the dynamics of the implementation system. The RRT method actively tries to find extreme cases for which model conformance can be falsified.

Inspired by the work of Alhoff & co. in [27], [50], and [46], the RRT method used in this thesis to perform the model conformance through falsification is an efficient method for exploring the dynamics of complex systems. Here, a more detailed description of the RRT calculation method used in the thesis is presented. The following procedure for rapidly-exploring random trees (RRTs) is developed.

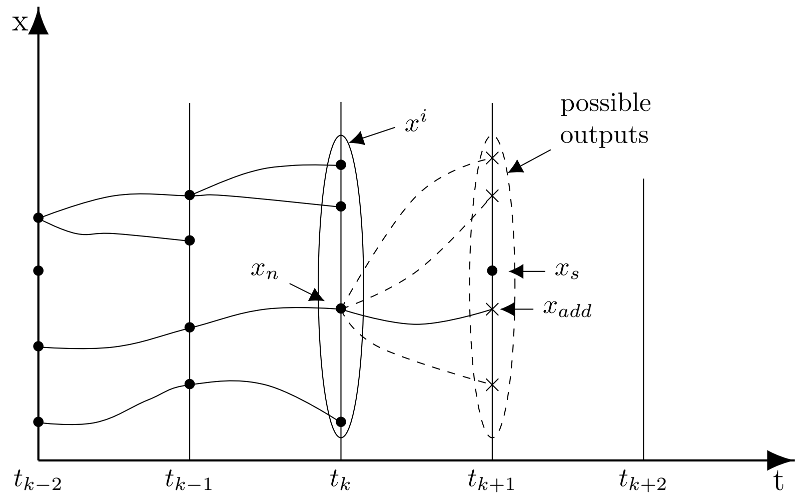

Figure 4.3: Scheme for the RRT algorithm. Reproduced from [27]

Starting from a time $t = t_k$ and a set , $\mathcal{X}(t_k)$

1. Initialize an empty set $\mathcal{X}(t_{k+1}) = \emptyset$.
2. Generate a sample x_s from the state space.
    - Create a multidimensional rectangle (MDR) $\mathcal{X}_{rel}$ with predefined edge lengths. The edge lengths (L_1, L_2...), which resemble the dimension states of the system, are chosen such that the largest reachable set is enclosed in the multidimensional rectangle which is centered about the nominal trajectory and hence moves in time.
    - Once $\mathcal{X}_{rel}$ is defined, sample the multidimensional rectangle starting with the vertices. Next, take the midpoints of all vertices as sample points, and finally take 30 random sample points from the set

$\mathcal{X}_{rel}$. Other approaches which show fruitful results can be by uniformly sampling the set $\mathcal{X}_{rel}$ [27] or by using combined deterministic and stochastic sampling [51].

3. Find the nearest state $x_n \in \mathcal{X}(t_k)$ to the sampled x_s based on a distance measure ρ.
   - The closest $x^{(i)} \in \mathcal{X}(t_k)$ is named x_n and is obtained by a predefined distance measure ρ. This distance is defined as the second norm such that

$$\rho = \left\| N(x_s - x^{(i)}) \right\|_2 \tag{4.5}$$

$$N = \begin{bmatrix} \frac{1}{L_1} & 0 & 0 \\ 0 & \frac{1}{L_2} & 0 \\ 0 & 0 & \ddots \end{bmatrix} \tag{4.6}$$

     where N is a normalization matrix with diagonal entries being the inverse of the multidimensional rectangle's edge lengths.
   - As it can be seen in Fig. 4.3, it is not necessary that all the states of $\mathcal{X}(t_k)$ are used as x_n. There might be some states $x^{(i)}$ which are not used, and others which are used more than once depending on the distance measure ρ.
4. Obtain the input u which drives the nearest state x_n to the new state x_{add} closest to the sampled state x_s.
   - The inputs are taken from uniformly sampling the predefined input set $\mathcal{U}$. Here, 10 samples are taken including the vertices of $\mathcal{U}$.
   - The inputs are applied on the nearest states x_n separately, and the outputs are states in $\mathcal{X}(t_{k+1})$.
   - The output that is closest to the sampled state x_s based on the distance measure ρ is called x_{add}. The other outputs are disregarded.
5. Add x_{add} to the set of states for the next time interval $\mathcal{X}(t_{k+1})$.
6. Repeat steps 2 through 5 are for the desired number of samples.
7. Move to the next time interval and start with step 1.

4.5 Falsification Testing

After obtaining the reachable sets of the low order model and having calculated the RRT states for the high order model, it is left to compare the outcome in an attempt to falsify the reachable sets using the RRT states. Since the study is in discrete time, each set of states $\mathcal{X}(t_k)$ from the RRT exploration is checked against the corresponding reachable set $\mathcal{R}(t_k)$. This is performed for all 6 combinations of projections of the reachable sets. In case an RRT state in any step falls out of the reachable sets, falsification is achieved and the models fail to conform. This can be expressed as

$$\{\forall\ t_k :\ \ \exists\ x \in \mathcal{X}(t_k) \mid x \notin \mathcal{R}(t_k)\ \Rightarrow\ \text{Conformance} = \text{false}\} \tag{4.7}$$

In case the falsification algorithm can falsify the conformance between the models, the uncertainties of the low order model have to be increased and the reachability analysis has to be recalculated. Conformance is achieved once the falsification algorithm fails to falsify conformance. It should be noted however, that since the exploration of the high order model relies on the RRT method instead of a reachability analysis, it means that absolute conformance can never be guaranteed. There are always some states that the RRT algorithm does not explore. The more the MDR is sampled, the less risk there is from missing out on important dynamics that can falsify the conformance.

Chapter 5

Double Lane Road Driving Scenario

This chapter portrays the results of the reachset conformance methods presented in Ch. 4 on a tractor semitrailer in a driving scenario of a double lane straight road with low city driving speeds ($v_x = 10$[m/s]). The idea here is to study the reachable performance of the tractor semitrailer in the presented scenario. The setup of the experiment and simulation are presented followed by the corresponding results.

5.1 Simulation Setup for Double Lane Driving Scenario

This study is essentially carried out by studying the full reachable space of the models and checking for their conformance in this scenario. In this section, the simulation setup to study the full reachable space is described and the respective results are portrayed in the subsequent sections.

Since this section is concerned with the full reachable space analysis, the input set $\mathcal{U}$ is chosen as the full input range case from the three input set options for reachable sets (Sec. 2.3.3). This allows the reachability analysis and the RRT to explore all the possible dynamics in this angle range of the linear model and the nonlinear model respectively. The limits to those input sets are what create the test suite for the full reachable space study. The limits can be considered as the step steering values chosen to be $\pm[2°, 4°, 6°, ..., 20°]$. Those are chosen even though some of the angles do not comply with the smallness attribute which states that small steering angles should not exceed 12°. The choice of higher angles induces non-linearity in the systems which is of interest for the conformance testing. The length of the maneuver is 5 seconds which is considered reasonable to study the reachable space in the context of safety for the presented driving scenario.

5.2 Reachability Analysis of Linear Low Order Model

For carrying out the reachability analysis for this driving scenario, the approach using Lazysets is considered. The Lazysets used in this simulation setup are projected onto the 6 combination of states and over-approximated with a Hausdorff distance of $d_H = 0.001$. The Hausdorff distance is presented in the outer approximations section, see Sec. 2.3.4. This distance is chosen such that the reachability analysis yields sensibly accurate results with a reasonable computational time. As a matter of fact, the yielded results are limited to no more than 200 hyperplanes per set. This also eases the falsification check in later stages.

Because the study is in discrete time domain, a time step of 0.01 seconds is chosen. In general, this value is chosen such that it is at least 5 times faster than the highest frequency happening in the system. The value of 0.01[s] is common in literature for applications similar to the work in this thesis [27]. This means that the output H-polygons representing the reachable sets are separated by 0.01 seconds. The first set $\mathcal{X}_0$ from which the reachability analysis starts from is set to be a 4 dimensional rectangle centered at zero with edge size 0.001 in all dimensions. The zero positioning refers to driving on a straight line with zero lateral and rotational velocities and no relative rotation between the tractor and the semitrailer. The choice of $\mathcal{X}_0$ is chosen to be a set instead of a singleton to account for sensor errors at the beginning of the analysis.

By carrying out this reachability analysis, the output results look like the ones in Fig. 5.1. This figure shows the reachable sets every 20^{th} step for the $\pm 10°$ case. It can be notices that after a certain number of steps, the dynamics of the system reach their maximum and are saturated, and hence the sets do not grow further.

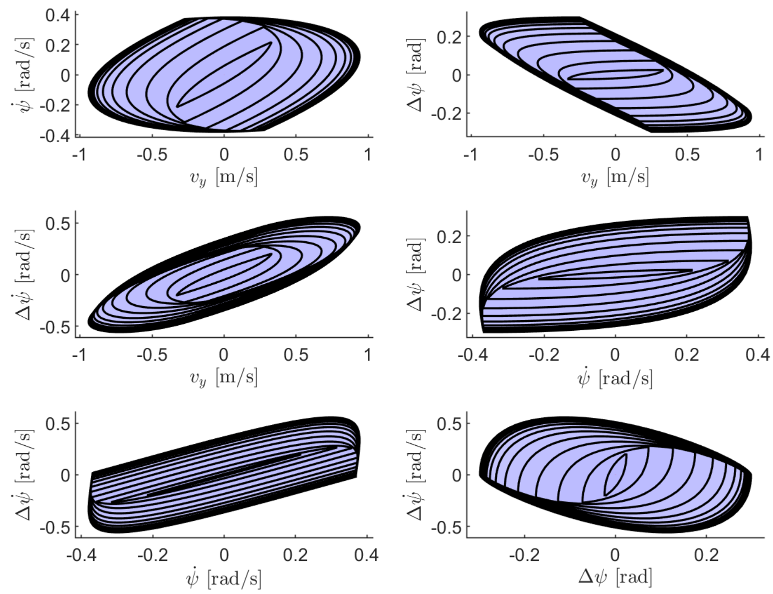

Figure 5.1: Reachable sets for driving scenario with 10° maximum steering angle

5.3 Nonlinear High Order Model Dynamics Exploration

The algorithm for the RRT method explained earlier is adopted for exploring the dynamics of the high order model. The sizing of the multidimensional rectangle used in the RRT is done by outer-approximating the biggest reachable set obtained from the reachability analysis with an outer rectangle and scaling it up by a factor of 1.5. The scaling is meant to create an outer rectangle which is bigger than any reachable set which means that the desired dynamics are always extreme. However, the system should also explore reachable and reasonable dynamics as well. If the scaling is too large, the desired dynamics will all lie outside the reachable space and hence will all be considered extreme dynamical states. The considered scaling here guarantees that the RRT generated states strive to falsify all reachable sets, even the biggest of them, while still discovering rational dynamics. It is notable that the RRT computation, since it relies on the equations of the high order model, requires the addition of a new state ψ_1 to the state vector since it appears in the nonlinear equations of motion. This results in the implementation system, or the higher order model, having 5 states instead of 4 and hence the MDR consists of 32 vertices.

Sampling the MDR is obtained by first taking all 32 vertices of the MDR, then by obtaining the midpoint of each combination of 2 vertices, and finally adding 30 random sample points from inside the MDR. The combinations of all 2 vertices is calculated as

$$\begin{aligned} C(n,r) = \binom{n}{r} &= \frac{n!}{(r!\,(n-r)!)} \\ &= \frac{32!}{(2!\,(32-2)!)} \\ &= 496 \end{aligned} \tag{5.1}$$

This means that the total number of sampling points adds up to be

$$n_{samples} = 32 + 496 + 30 = 558 \tag{5.2}$$

As for the input set, it is uniformly sampled with 10 samples in total. This means that in each time step the RRT calculation executes 5580 simulations of the high order model before choosing which states are used in the subsequent time step. Hence, with a 0.01 sampling time, the number of simulations realized for obtaining the RRT simulation for one realtime second becomes

$$n_{simulations} = 558 \times 10 \times \frac{1}{0.01} = 558000 \text{ simulations} \tag{5.3}$$

Those simulations are carried out using the MATLAB *ode*45() function which solves nonstiff type problems as the one presented here. Figs. 5.2, 5.3 show the time taken for each step to execute all the simulations of the RRT algorithm. It can be noticed that the execution time for one RRT step takes between 8 and 11 seconds with some exceptions. For the 8 second maneuver in Fig. 5.3, the simulation executes over 4.4 million sub-simulations where the average execution time for each time step is 9.276[s] with a total of 7977[s] = 132.95[min] execution time.

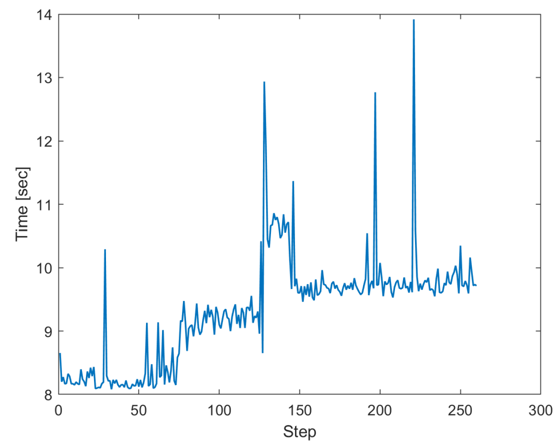

Figure 5.2: Simulation time versus time step for all RRT simulations of the 2 second maneuver

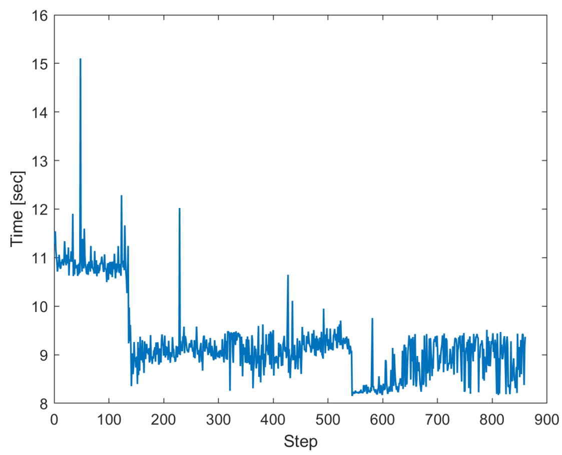

Figure 5.3: Simulation time versus time step for all RRT simulations of the 8 second maneuver

The resultant RRT states are plotted (in red) against the reachable sets (in blue) in Fig. 5.4 for the case of $\pm 10°$ as the input range. It is clear how the RRT states are trying to reach extreme dynamics and breach the reachable sets, and discover inner dynamics as well. In fact, the plotted reachable sets are inflated with the respective uncertainty which is obtained after the iterative falsification algorithm. This is discussed in the next section.

5.4 Conformance Falsification

Of course, the results shown in the previous sections are the findings of an iteration process lead by the falsification algorithm. The falsification algorithm works to find the right values of uncertainties for which the models are conformant.

Here, the two methods for uncertainty quantification presented in the model validation chapter (Sec. 4.2.1) are considered. However, the method of using higher order terms from series expansion does not yield conformant models. Hence, only the results of the proportional uncertainty method are presented here. The uncertainties are calculated as a percentage relative to the values of the state trajectories attained if the abstract system is simulated for a step steering input with the amplitude being specific for each test case in the test suite. The percentage values are based on the falsification testing such that the uncertainties are increased until no falsification resides and the models are conformant. Tab. 5.1 shows the percentage of uncertainty for each test case. It is noticeable that for the case of small angles no uncertainty is needed whatsoever for the models to conform. As the range of steering input increases, the uncertainty level required to hold the conformance increases as well. This is expected since the high steering angles induce non-linearities in the simulations and allow the model to behave more aggressively.

δ[°]	2	4	6	8	10	12	14	16	18	20
w [%]	0	0	0	0.01	0.01	0.02	0.03	0.07	0.11	0.15

Table 5.1: Test suite for the full reachable space analysis

It is also noticed that the falsification algorithm for higher angles detects the breach of the reachability

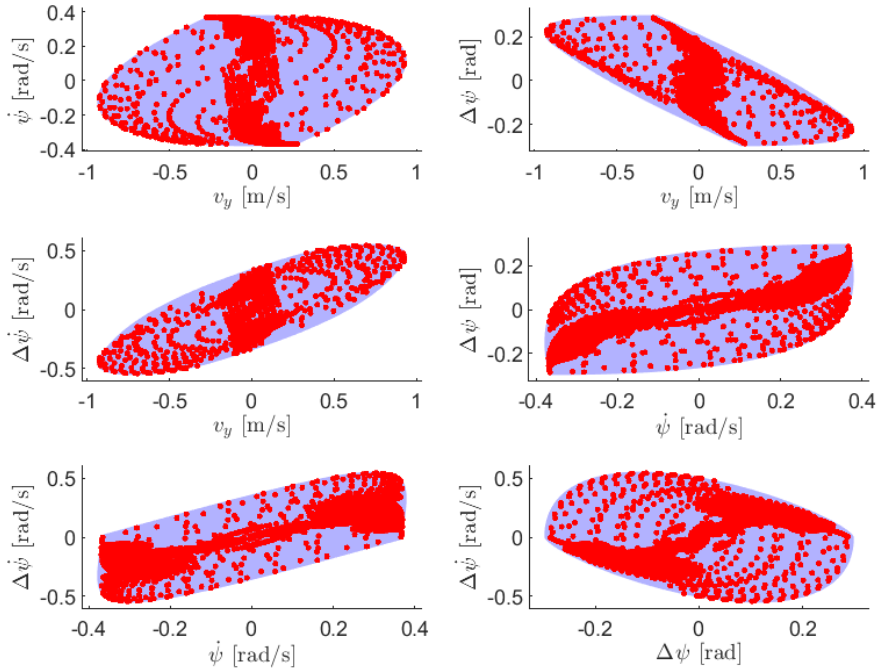

Figure 5.4: Full reachable state space for 10 degrees steering angle in 5 seconds.

space in the phase planes where the lateral velocity v_y is one of the considered states. In fact, most of the falsification occurs in the phase plane of the lateral velocity v_y and yaw rate $\dot{\psi}$.

5.5 Safety Road Occupation

Coupling the full reachable space analysis with the calculation of the global position of the tractor semitrailer is compelling for studying the safety road occupation of the vehicle. Even though the dynamics are limited and get saturated after a certain time, the global position of the vehicle is not limited in the same manner. In fact, if the dynamics are held at their limits, it means that the vehicle will keep deviating in the global coordinated from its initial position.

The calculation of global positioning of the vehicle can be done in different ways. One of those ways is to include the the position and orientation of the vehicle as one of the systems states. This evidently complicates the reachability analysis by increasing the dimensionality of the problem. The linearization of the equations are a detail worthy to be focused on in this case. Another method for calculating the position of the vehicle is to post process the reachability sets by integrating the calculated dynamics which include the uncertainties in the studied system.

Chapter 6

Single Lane Change Driving Maneuver

This chapter portrays the results of the model validation process in Ch. 4 of a tractor semitrailer performing a single lane change maneuver as a proof of concept for the presented framework. The single lane change is considered in the driving context of city driving on a double lane straight road. For that reason, the considered vehicle speed is $v_x = 10$[m/s]. The setup of the experiment and simulation are presented followed by the corresponding results.

The simulation setup is directly related to the application which is under study. Here, the application of the single lane change is used for motion prediction of the implementation system based on nominal dynamics and bounded uncertainties for a specific driving maneuver.

6.1 Setup of driving maneuver

To simulate a lane change maneuver with an open loop control input sequence, a sinusoidal steering input is implemented, and the longitudinal velocity is kept at a constant $v_x = 10$[m/s]. The steering profile introduced here is defined by the period of the sine wave and its amplitude. Those values are evaluated such that the intended lane change maneuvers follow Tab. 11 in Ch. 10.4 of the SAE J2944 Standard [52]. From this standard, it is noticed that on average, a lane change maneuver for heavy trucks is executed in around 8 seconds with a minimum of 3.6 seconds for a fast lane change and up to 22 seconds for slow ones.

Having this in mind as well as defining the lateral distance covered in the lane change to be 3.5 meters [52], a test suite of single lane change maneuvers is adopted starting from a conservative maneuver of 8 seconds. The maneuver is then made tighter and more aggressive to induce a nonlinear behaviour in the models where the most aggressive maneuver studied takes only 2 seconds to execute. The input profiles look like the ones in Figs. 6.1.

The test suite is shown in Tab. A.1 which presents the period of the sine wave as well as the amplitude of the steering angle in degrees. Here, the amplitude of the sinusoidal input is chosen by trial and error such that the vehicle executes a 3.5 meter lane change in the given time period. The resultant maneuver in global coordinates looks like the one shown in Fig. 6.2.

Period [s]	8	7.5	7	6.5	6	5.5	5	4.5	4	3.5	3	2.5	2
Amplitude $\delta[°]$	0.95	1.10	1.20	1.40	1.70	2.00	2.40	3.00	4.00	5.00	6.75	9.50	15.00

Table 6.1: Test suite for lane change maneuvers

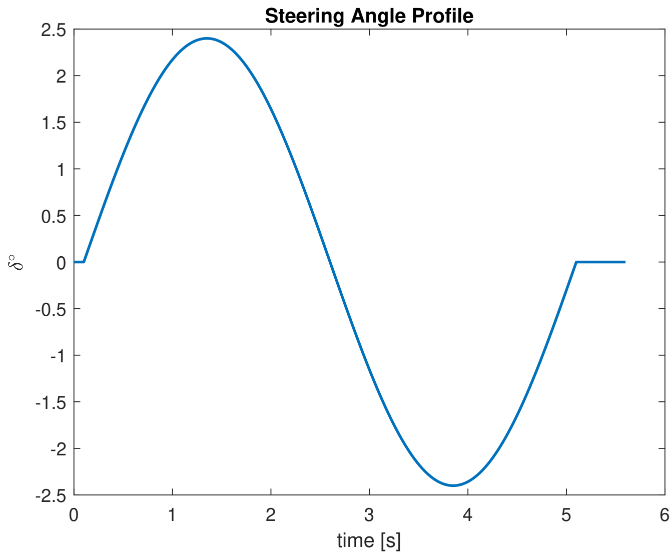

Figure 6.1: Steering profile for 5 second sinusoidal input

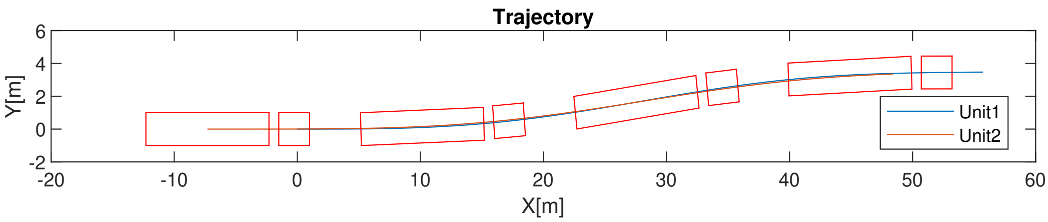

Figure 6.2: Trajectory for 5 second maneuver

All maneuvers from the test suite are simulated on the linear low order model to generate the nominal state trajectories that can be seen in Fig. 6.3. Here, it can be seen how the shorter maneuvers have more aggressive dynamics. This can also be portrayed in the lateral acceleration achieved during the maneuvers, as seen in Fig. 6.4.

It is important to check for the linearity in the simulations especially in the aggressive maneuvers. Based on the definition of smallness presented in the assumptions section for vehicle modelling, see Sec. 3.1.1, a steering angle above 0.2[rad] $\approx 12°$ is not considered small and hence exceeds the limits of linearity. This means that the steering inputs for the most aggressive maneuver has a steering angle that is considered to be outside of the linear range of the steering angle.

For that reason, the lateral accelerations are computed for the whole test suite and are shown in Fig. 6.4. The gray areas in the figure refer to the value of critical lateral acceleration above which heavy trucks are expected to roll-over or at least lift off one side of the axles. This evidently means that the simulations and the results are out of the linear region of study. This value is estimated to be between 0.3 to 0.4[g] [53]. This is in general considered when nonlinear tire models are used, and tire saturation plays a role in the dynamics of the models. Since the study does not consider nonlinear tire models and also does not consider load transfer, the limit for the linear region can actually be pushed up to 0.35[g] and in some cases to 0.45[g].

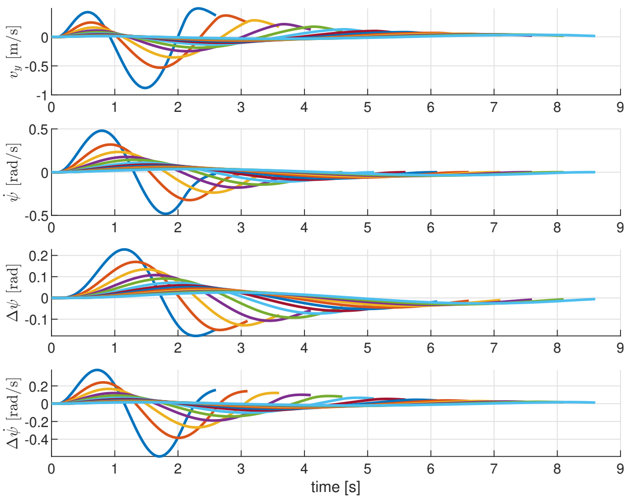

Figure 6.3: Nominal state trajectories for 5 second maneuver

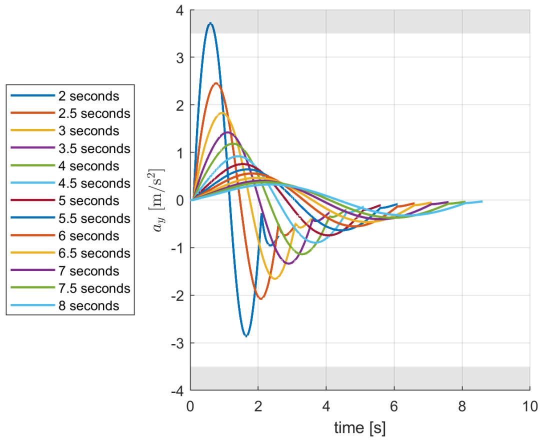

Figure 6.4: Lateral acceleration profiles for all tested maneuvers (gray area is considered to be outside the linear region)

It can be seen in Fig. 6.4 that for the aggressive 2 second maneuver, the lateral acceleration is around 3.7 [m/s^2] $\approx$ 0.38[g] which is considered to be a critical roll-over lateral acceleration. Because of that, this simulation in specific is expected to fail easier in the conformance testing compared to the other more conservative simulations. However, even though the lateral acceleration for the 2 second maneuver exceeds the critical rollover limit, the maneuver is kept in the study to have a relative idea of the uncertainty levels that are achieved in case the driving context limits are exceeded.

6.2 Reachability Analysis of Linear Low Order Model

Similar to the reachability analysis carried out for the double lane diving scenario in Ch. 5, the reachability analysis here is also based on using Lazysets with a similar value for the Hausdorff distance ($d_H = 0.001$) and a time step of 0.01[s]. The reachability analysis is also started from the same set $\mathcal{X}_0$ centered at zero with edge size 0.001 in all dimensions.

As for the input set $\mathcal{U}$, the uncertain input case is chosen from the three input cases presented earlier, where the input uncertainty is relative to each case with 10% the value of the maximum steering angle input. The main reason behind this uncertainty in the input is a mitigation for linearizing the high order dynamics about a constant longitudinal velocity in straight line driving. The more aggressive the maneuver gets, the farther away the inputs get from the linearization trajectory, and hence more uncertainty is added. The value of the percentage in fact depends on the modeled system and the decision of the design engineers. The more the engineers trust the model, the lower that percentage can be.

With this proportional approach to the uncertainty in the inputs, it means that for the case of the 5 second maneuver for example, the input set is a 1D set centered about the nominal input at each time instant with a range spanning $\pm 0.24°$ since the amplitude of the sine wave is 2.4°.

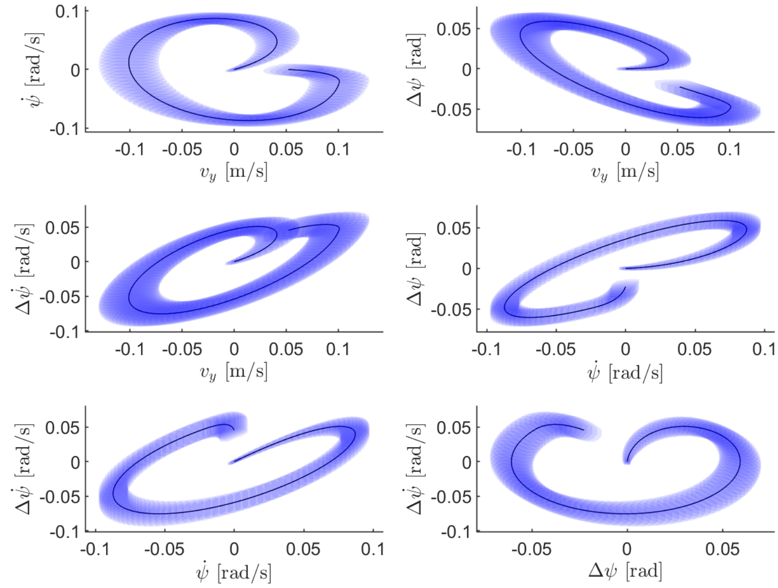

Figure 6.5: Phase planes with nominal trajectories and reachability sets

The 5 second maneuver is considered as an example of the results. Plotting the relations between the state trajectories results in the 6 aforementioned phase planes as shown in Fig. 6.5 with black lines. As discussed in the model validation chapter (Ch. 4), the first step in performing reachset conformance is to apply the reachability analysis on the abstract system starting from the initial set $\mathcal{X}_0$. The result can be seen in the same figure where the blue sets represent the reachable sets of the abstract system. It is to no surprise that the reachable sets overlap with the nominal trajectories. That is due to the choice of the input set $\mathcal{U}$ being the case of uncertain input around the nominal input trajectory.

6.3 Nonlinear High Order Model Dynamics Exploration

The second step in reachset conformance is to perform the exploration on the implementation system. The setup for the RRT simulations is similar to that implemented for the double lane driving scenario in terms of the scaling of the MDR sets and the sampling of the MDR and the input sets, even though the MDR sets and input sets have different sizes.

The outputs of this step are the RRT generated states which can be seen as red dots in Fig. 6.6. It is evident from this figure how the RRT algorithm is making the implementation system discover the whole range of dynamics of the system and pushing the model towards extreme dynamics in order to falsify the conformance. The rest of the results are shown in the appendix.

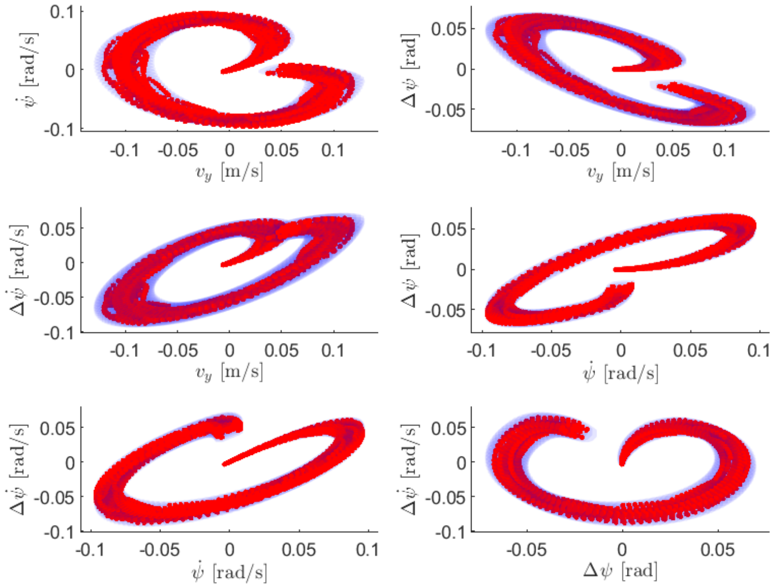

Figure 6.6: Phase planes with reachability sets and RRT generated states

6.4 Conformance Falsification

First, the method of using higher order terms from Taylor series expansion is considered. This means that the 2^{nd} and 3^{rd} order terms from the Taylor series expansion are used to quantify the structured uncertainties. However, the falsification algorithm reveals that those uncertainties are not enough to guarantee conformance. Hence, uncertainties have to be increased. The reasoning behind this result is touched upon in the discussion of the framework, see Ch. 7. Because of that, the proportional method for quantifying uncertainties is used in the falsification algorithm instead.

The RRT states are hence checked against their respective reachable sets in the falsification algorithm in an iterative manner. Similar to the process in the chapter of double lane driving scenario Ch. 5, the percentage of uncertainty is increased until the falsification algorithm fails to falsify the models and hence the models are considered conformant.

By performing this process on all the maneuvers of the test suite, a trend is noticed in the values of the uncertainties. In fact, as the aggressiveness of the maneuvers increases, the uncertainty value required to achieve model conformance has to be increased. This can be seen in Fig. 6.7 where the values of uncertainty for each state is plotted as a function of the lateral acceleration of the maneuver. It is clear that for the more aggressive maneuvers, which have a higher lateral acceleration, the uncertainty levels are higher.

It is also clear how the uncertainties increase faster for more aggressive maneuvers. In fact, when the angles are less than 12°, the required percentage of uncertainty to achieve conformance is less than 0.1%. For steering angles that do not abide by the smallness concept, that percentage is increased and the increments get bigger the more aggressive the maneuvers become. The main reason behind this increase is the nonlinearity that is induced in the models when they are driven away from the linearization points by using larger steering angles.

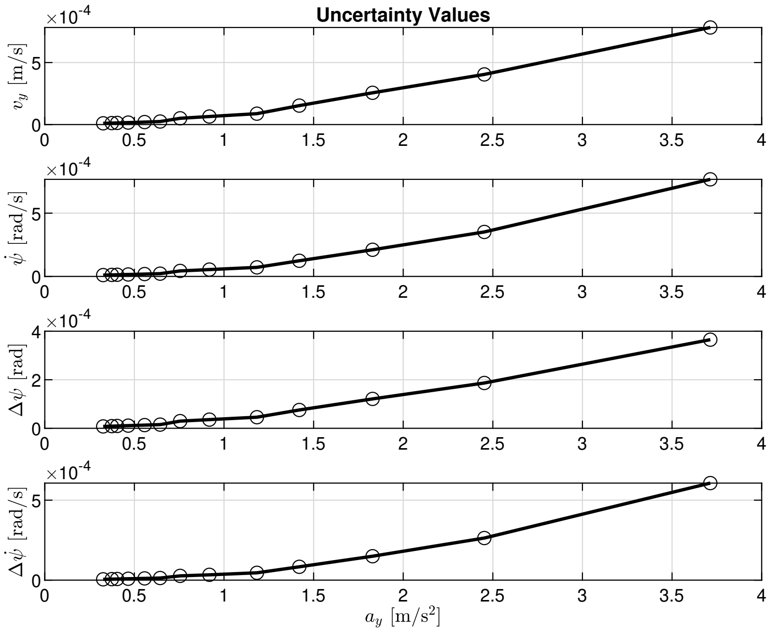

Figure 6.7: Uncertainty values for all maneuvers

In order to mitigate the loss of accuracy caused by projecting the reachable sets on 2D planes, the results from the falsification process are fortified by measuring the difference in the state trajectories between the implementation and the abstract system when simulated for each maneuver in the test suite. This difference is calculated and plotted in Fig. 6.8 as a percentage of the maximum attained value for each state throughout the maneuver. It can be clearly seen how the more aggressive maneuvers have high errors compared to the conservative ones, especially in the lateral velocity v_y where the difference reaches more than 10% of the maximum attained value of the lateral velocity v_y. The errors in the relative yaw rate between units $\Delta\dot{\psi}$ rank in second with a maximum of 4% error between the two models.

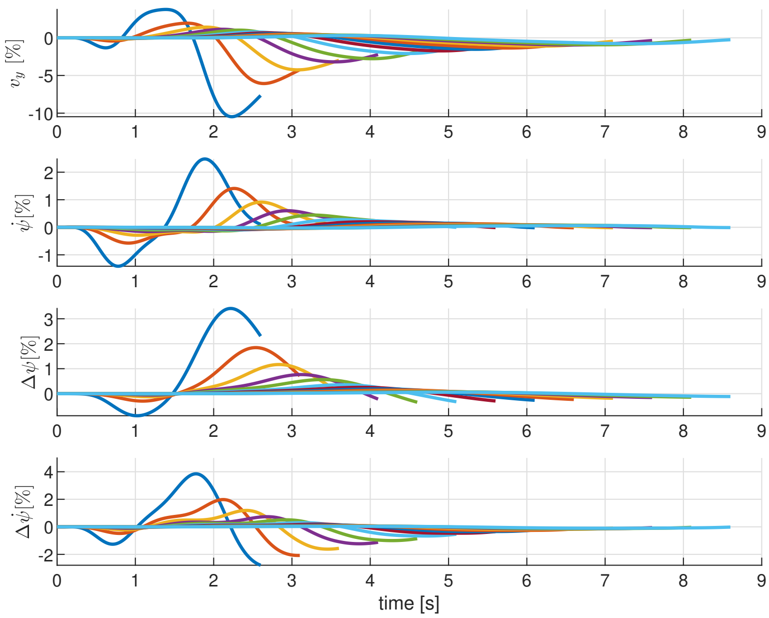

Figure 6.8: Percentage difference in states relative to the maximum attained value per maneuver for all tested maneuvers

During the iterative falsification process, the algorithm specifies in which of the 6 phase planes the reachability sets are breached. By looking back at Fig. 6.8, it can be noticed that the errors in v_y present the highest errors throughout the maneuver. This fortifies the results that are obtained from the falsification algorithm where the models fail mainly in the phase planes where the lateral velocity v_y is one of the dimensions. The second most common failure is in the realtive yaw rate $\Delta\dot{\psi}$ phase planes, however, lower levels of uncertainties resolved the falsification in $\Delta\dot{\psi}$ phase planes before reaching conformance in the v_y phase planes.

6.5 Prediction of Dynamics of Implementation System

After achieving conformance between the models, the link can be used to transfer properties between them. This section shows talks about the prediction of the dynamics of the implementation system as one of the applications in which the output of the framework can be used. The motion prediction is based on the nominal dynamics of the abstract system which is in most cases more computationally efficient compared to the simulation of the implementation system. Fig. 6.9 depicts the motion prediction for the 2 second and 3 second maneuvers.

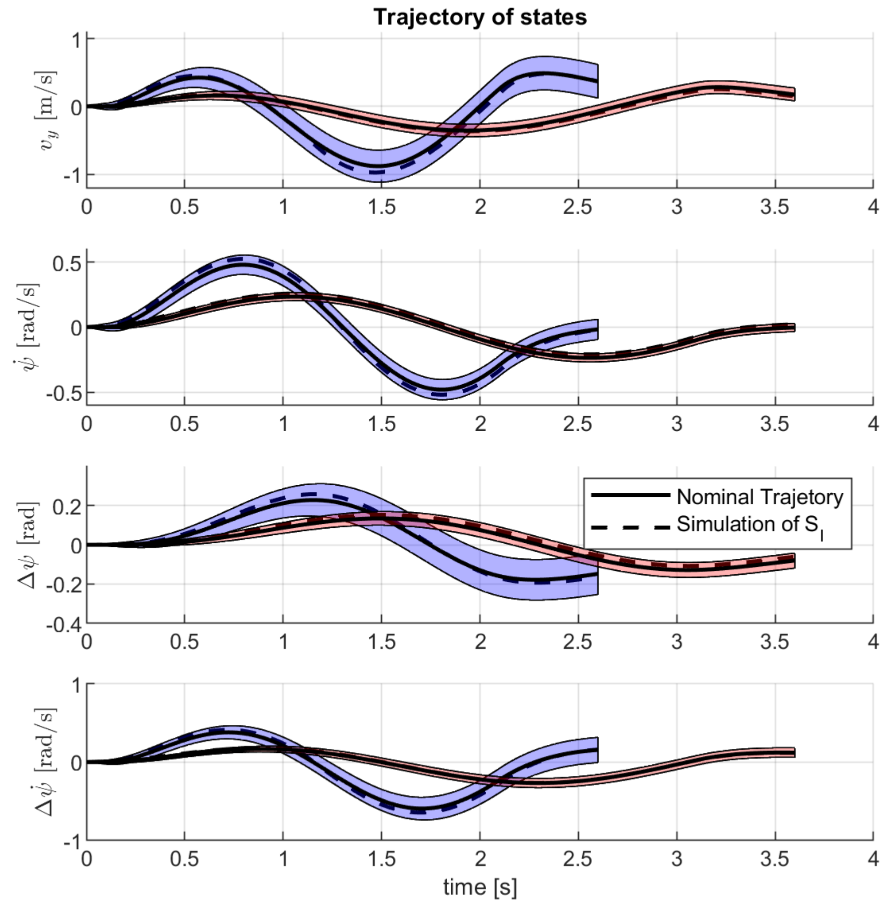

Figure 6.9: Trajectory of states with uncertainty bounds for 2 second (blue) and 3 second (red) maneuvers

Here, the nominal trajectories of states are bounded with the uncertainties obtained from the framework. Since the uncertainties are higher for more aggressive maneuvers, it comes to no surprise that the blue bounded area around the 2 second maneuver is wider than that for the 3 second maneuver which is shown in red. The dynamics of the implementation system are predicted to fall inside those bounded areas. One thing to note here is that the dashed lines in the figure represent the simulation of the implementation system for the same input as the abstract system but with an added noise that mimics the uncertainties in the input.

It is notable that even though those colored areas might seem small, they can get actually remarkable when the global positioning of the tractor semitrailer is computed, especially after a long maneuver where small errors pile up and cause the vehicle to reach unsafe road regions. This is another application that can be investigated using the results of the framework.

Chapter 7

Conclusion

In this thesis, a framework for model validation is proposed and tested upon a single lane change maneuver on a tractor semitrailer. This chapter concludes the work done in this thesis by taking a closer look at the performance of the proposed framework in reference to the results from the double lane driving scenario and the single lane change maneuver of Chs. 5 and 6 respectively. A short summary is then given followed by a list of recommended future work.

7.1 Discussion about Framework

The different stages of the framework are inspected and discussed here, showing the strengths and weaknesses of the proposed methods.

Driving context

It is clear at this point how important the choice of the driving context is for the whole process of model validation. The values of the unstructured uncertainties that are increased during the iteration of the conformance are controlled by the driving context under study. The limits for those values are set by the engineers or designers before conducting the framework based on the application of interest. However, this is not the only degree of freedom on the limits set in the framework. In fact, additional limitations are recommended to be added to the framework to ensure that the study is abiding by the limits of the driving context. In case many of the studied maneuvers exceed such a criteria, it means that the driving context should be reconsidered, as well as the assumptions and the developed models. This is seen in the single lane change application in Ch. 6 where the lateral acceleration of the tractor semitrailer is put under the microscope throughout all the maneuvers. Ideally, the aggressive maneuver (2 seconds) can be counted out of the test suite because it exceeds the critical rollover lateral acceleration of 0.3[g]. However, as mentioned earlier, this is kept in the study in order to understand how exceeding the boundaries of the driving context affects the conformance results.

Vehicle modelling

The models developed in this work are in planar motion only, meaning that vertical loads and load shifting are neglected. Also the longitudinal velocities are considered to be constant. The simplification of the nonlinear model based on Taylor series expansion and coupled with dimensional analysis prove to be a simple and robust method for linearization. One major drawback of the tractor semitrailer model that is developed in this thesis is its lack of roll dynamics which is a characteristic feature of heavy vehicles. The reason behind that is to develop a simple model that is used in the framework's proof of concept. Another important characteristic is infused in the tire model that has been used in the work. At slow dynamics and low speeds, tire relaxation plays an important role in the dynamics of a vehicle, and that is not well captured with the linear tire model.

When it comes to model simplifications, it is common practice to linearize a model around a certain nominal trajectory. However, in this thesis the linearization is done about straight driving at a constant speed of 10 [m/s]. The focus on this speed level is actually related to one of the assignments that Volvo's autonomous truck, Vera, is being studied for. In fact, it can be interesting to increase that speed for the single lane change maneuvers in order to study the effects of that on the validation process and the uncertainty levels. At the given 10 [m/s] velocity, larger steering angles are possibly applied on the models, breaking the concept of smallness in the steering angles. This means that the driving context should be reconsidered, as well as the assumptions and simplifications made in the modelling stage of the framework.

By doing the linearization as such, only one linearization of the model is required and the linearized model can then be validated for different aggressiveness of a certain maneuver. This is reflected in the uncertainty of the input sets as it is mentioned in the single lane change application in Ch. 6. The conformant models are, however, only validated for the maneuver for which the framework is applied on. For having a model which is validated for a full driving assignment, the framework can be then applied on all the other expected maneuvers in the assignment, and the highest uncertainty value can be chosen for achieving conformance for all the autonomous driving tasks of that vehicle. This is easily done for autonomous vehicles which are operated in controlled environments such as in harbours or mines.

Structured and unstructured uncertainties

It is obvious that the increase of unstructured uncertainties has a direct effect on the robustness of the models, making them more versatile for the different automation tasks. However, this comes on the cost of their performance. By increasing the uncertainties, and hence the robustness of the models, their use in motion control, decision making, safety assessment, etc. is compromised. This compromise is related to the limits of the driving context. Accounting for structured uncertainties can be one way to remedy this problem. By including structured uncertainties in the study, the performance of the models will be affected in certain parts of a maneuver, but not throughout the whole maneuver. A suggested method to approach this task is to also use series expansion as a way to formally represent those structured uncertainties.

The hypothesis of having the higher order terms from the Taylor series represent the unstructured uncertainties between the models is put to test in the conformance testing of the single lane change maneuver. However, the results show that those uncertainties are not enough to account for the difference between the models. While not much focus is invested in verifying this hypothesis, there are some reasons which are thought to be causing this hypothesis to be falsified. By looking back at the parity of the uncertainties that results from the higher order terms of Taylor series in Eqs. 4.3, it is noticed that the Taylor series equations for the 4 system states ($v_{y,1},\ \dot{\psi}_1,\ \Delta\psi,\ \Delta\dot{\psi}$) are odd functions, meaning that the higher order terms show up in the 3^{rd} order. On the other hand, the equation for the longitudinal velocity v_x is even and the higher order terms start from the 2^{nd} order which means that they have a higher value compared to the other 4 states. However, in the application of the single lane change maneuver, the longitudinal velocity is considered to be a constant parameter in the system and input matrices, and hence its uncertainties are neglected. This is related to the assumptions made for linearization based on the driving context under study.

One way to account for this structured uncertainty while keeping velocity vx as a parameter in the system instead of a state is to account for parametric dependencies in the system and input matrices (A and B) of the linear system (Eq. 4.4). This idea of parametric dependencies can be employed for accounting for structured uncertainties in the semitrailer load for example, or even road friction uncertainties. With that, the system matrix A can be augmented by the uncertainty matrix $\mathbb{W}$ to include uncertain parameters. This makes the parametric dependent matrices $A(p)$ and $B(p)$ more flexible which in turn affect the reachability analysis and lower values for the unstructured uncertainties can be expected.

Conformance testing

One topic related to conformance theory that is touched upon in the thesis is that the desired properties to be transferred from the abstract to the implementation system are what dictate the type and level of conformance required. This is a current focus in the topic of model conformance and it can be seen that some efforts are already put in order to build those links. In a recent survey, Althoff et al. provide guidelines for selecting the right conformance relations based on the properties of interest [20]. It is important to carry out more studies that build links between the levels of conformance and the properties that can be transferred via those links. That is because it is not always easy to know which conformance type is able to transfer a certain property.

Since the reachset conformance is performed using a falsification approach, one should stay reminded that absolute conformance is never considered to be achieved. The reason is that there is always the risk of having some cases that are not explored by the exploration algorithm. However, this does not diminish the superior ability of the RRT algorithm. In fact, the RRT algorithm proves to be a reliable method to minimize that risk by pushing the dynamics limits of the implementation system to their extreme cases and falsify the conformance in most cases. In the presented framework, the RRT is applied on an implementation system being the nonlinear

ODEs. However, the RRT algorithm is capable of handling more complex systems. One such cases can be to use the dynamics of a high fidelity model, such as the VTM, to carry out all the required simulations that are performed inside the RRT algorithm.

The framework is also able to handle real life systems. Carrying out conformance testing based on reachset falsification with a real system comes with its share of drawbacks. Logically, testing out a real system inherently means that not all possible dynamics are explored, which makes the falsification of the conformance a weak statement. There is a high risk of not exploring certain dynamics cases for which the conformance does not hold. This is a threat for several safety factors. In that case, a reinforcement learning approach can be a viable option, where the framework is continuously executed, and the values of uncertainties are modified based on any new dynamics that the vehicle exhibits.

Toolboxes Used for Reachability Analysis

As mentioned earlier, the reachability analysis is carried out using the Lazysets package. While this approach is limited by the 2D projections of the outer-approximated reachable sets, it proved to be the most applicable method based in relation to the other steps of the framework. One major advantage about the Lazysets package is that the reachability analysis is performed symbolically in the full dimension of the state space. This means that the reachability set computation is not compromised by the outer-approximation of the sets. The outer-approximation is a post-processing functionality that quantifies the reachable sets in 2D projections. This increases the credibility of the reachable sets and decreases the errors that can be developed in case the reachability analysis is carried out numerically, as it is the case with using the MPT3 or the CORA toolboxes in MATLAB.

In fact, a MATLAB algorithm for reachability analysis is developed in-house for the work of this thesis. The main reason why the framework does not eventually rely on this approach for reachability analysis is the fact that it is not capable to handle complex dynamics in high dimensions. Two instances where this is encountered can be summarized in the following:

1. Based on the presented method for reachability analysis of a nominal and a disturbed system, Secs. 2.3.1 and 2.3.2, it is noticed that the projection of the set $\mathcal{P}$ causes the reachability analysis to explode in terms of the number of hyperplanes defining the reachset $\mathcal{R}$. The algorithm hence is very sensitive to the dimension of the system as well as the complexity of the reachable sets. In fact, the algorithm is not able to compute a 5 step reachability analysis of the tractor semitrailer's 4 dimensional system.

2. As an attempt to solve this problem, an optimization algorithm for outer-approximating the reachable sets is developed, and is shown in Appendix A.3. However, some functions used in this approach are limited in their dimensionality.

Control Verification

While control functions are fundamental when dealing with vehicle automation, it is clearly noticed that not much attention is given to them in this thesis. That is because the focus here is about model validation and not control verification. By taking out all control attributes from the equation, the framework is able to focus on validating models and their dynamics regardless of their source of input, whether it is given as a feed forward open loop input or if it is from a feedback closed loop controller. This, however, does not diminish the importance of having verified controllers for vehicle automation tasks. The framework is still under development and formal control functions verification can be added to it in later stages.

7.2 Summary

In conclusion, a formal framework for model validation is proposed in this thesis to manage the high demand on having valid models for different vehicle automation tasks. The framework is applied on a tractor semitrailer model in a single lane change maneuver as a proof of concept, and the results are used in predicting the dynamics of an implementation system based on nominal dynamics and bounded unstructured uncertainties. The structure of the framework is divided into three main stages, where the validation process is dependent on the concept reachset conformance by falsification. The proposed framework for model validation proved to perform well. It is able to falsify conformance between different models until certain levels of uncertainties are introduced for which the models are conformant.

The simple application of the framework on a single lane change maneuver shows the performance of the framework in achieving conformance between models. It is noticed that the uncertainties required to realize the conformance between two models increase as the aggressiveness of the lane change maneuver increases.

7.3 Future Plans

This thesis sets the work path and the building blocks of the framework. The framework is versatile and can be applied on different engineering applications. However, it is evident that further development is required in order to enhance the performance of the framework and optimize its usage. This section is dedicated for recommendations to help develop the framework even further. All of those recommendations have been touched upon throughout the report. Hence, the following is a simple and comprehensive list for the suggested future work.

- Add parametric dependencies in models to account for structured uncertainties such that:

  $$\dot{\boldsymbol{x}} = A(p)\boldsymbol{x} + B(p)\boldsymbol{u} + W(p)\boldsymbol{x}$$

  A similar approach can be applied for unstructured uncertainties as it is discussed earlier. Those should improve the capability of the reachability analysis as well as improve the performance of the models in different vehicle automation tasks.

- Enhance the computational efficiency of the reachability analysis by improving over-approximations of polytopes. The over-approximation presented works only in two dimensions. It is important that more work and research is invested in optimizing over approximation algorithms and reachability computations.

- Investigate the levels of conformance required for transferring properties.

- Evaluate global position of the vehicle from the acquired states.

- Further development of uncertainty quantification using higher order terms from series expansion.

- Extend the framework to include control design.

- Test the framework on more maneuvers to cover the whole driving scenario and generalize the results from the framework.

- Due to the use of different programs and coding languages, the framework should be automated and optimized to ease the connection between the different programs and toolboxes being used.

References

[1] L. Hobert, A. Festag, I. Llatser, L. Altomare, F. Visintainer, and A. Kovacs, “Enhancements of V2X communication in support of cooperative autonomous driving”, *IEEE Communications Magazine*, vol. 53, Institute of Electrical and Electronics Engineers Inc., Dec. 2015, pp. 64–70. DOI: 10.1109/MCOM.2015.7355568.

[2] P. Fernandes, U. N. .-. I. T. o. Intelligent, and u. 2012, Platooning with IVC-enabled autonomous vehicles: Strategies to mitigate communication delays, improve safety and traffic flow, *ieeexplore.ieee.org*, [Online]. Available: https://ieeexplore.ieee.org/abstract/document/6135795/?casa_token=0vVCbj5CJrkAAAAA:BqTPCarNKaybImx1vvOS3UUQHm6CrVvIE_teQiEoY3iwz5BlK2S1r8PGNgJnyF61pHqFUS4.

[3] D. G. .-. 2. A. A. Meeting and u. 2005, The economics of autonomous vehicles in agriculture, *elibrary.asabe.org*, [Online]. Available: https://elibrary.asabe.org/abstract.asp?aid=18842.

[4] M. Lu, M. Taiebat, M. Xu, A. M. Asce, and S.-C. Hsu, Multiagent Spatial Simulation of Autonomous Taxis for Urban Commute: Travel Economics and Environmental Impacts, *ascelibrary.org* **144**, no. 4 Dec. 2018, Dec. 2018. DOI: 10.1061/(ASCE)UP.1943-5444.0000469. [Online]. Available: https://orcid.org/0000-0002-7232-9839..

[5] S. Heinrich, “Obstacle Avoidance with Safety Guarantees Feasibility of MPC-based Steering Algorithms Master’s thesis in Signals and Systems”, Tech. Rep. [Online]. Available: http://publications.lib.chalmers.se/records/fulltext/229150/229150.pdf.

[6] L. Doe, *Asia Enters Fully Automated Terminal Era*, 2017. [Online]. Available: https://www.porttechnology.org/news/asia_enters_fully_automated_terminal_era/.

[7] G. Reymond, A. Kemeny, J. Droulez, and A. Berthoz, Role of lateral acceleration in curve driving: Driver model and experiments on a real vehicle and a driving simulator, *Human Factors* **43**, no. 3 2001, 483–495, 2001, ISSN: 00187208. DOI: 10.1518/001872001775898188.

[8] A. Y. Ungoren and H. Peng, An adaptive lateral preview driver model, *Vehicle System Dynamics* **43**, no. 4 Apr. 2005, 245–259, Apr. 2005, ISSN: 00423114. DOI: 10.1080/00423110412331290419. [Online]. Available: https://www.tandfonline.com/doi/abs/10.1080/00423110412331290419.

[9] J. Hebib and S. Dam, “Vehicle dynamic models for virtual testing of autonomous trucks”, Tech. Rep., 2019. [Online]. Available: http://www.diva-portal.org/smash/record.jsf?pid=diva2:1297688.

[10] P. Fancher and C. Winkler, Directional performance issues in evaluation and design of articulated heavy vehicles, *Vehicle System Dynamics* **45**, no. 8 2007, 607–647, 2007. DOI: 10.1080/00423110701422434. [Online]. Available: https://www.tandfonline.com/action/journalInformation?journalCode=nvsd20.

[11] V. Santahuhta, “Roll dynamics and tyre relaxation in heavy combination vehicle models for transient lateral manoeuvres”, Tech. Rep., 2019. [Online]. Available: https://odr.chalmers.se/handle/20.500.12380/300379.

[12] C. Hoel, P. F. .-. 2. I. I. Vehicles, and u. 2013, Low speed maneuvering assistance for long vehicle combinations, *ieeexplore.ieee.org*, [Online]. Available: https://ieeexplore.ieee.org/abstract/document/6629532/?casa_token=E7fwvfxujYQAAAAA:Uw_cgTecEPYe2Mo3DYyWoVhISGrbKV0yV2kIqIMDqQxM6wpIvdGkeTYsX0juI
M.

[13] C. Chen, M. T. .-. P. o. 1. A. Control, and u. 1995, Dynamic modeling of articulated vehicles for automated highway systems, *ieeexplore.ieee.org*, [Online]. Available: https://ieeexplore.ieee.org/abstract/document/529331/?casa_token=9Dohnr9UjMkAAAAA:pqQ55KyddKBOjkKv1xQy5386Qsk37CrA3WTggvV3f-eFP2RqG9yM86iCyTb4ZoW0oDrC9_w.

[14] S. T. Oreh, R. Kazemi, S. Azadi, A. Z. .-. A. J. o. B. and, and u. 2012, A new method for directional control of a tractor semi-trailer, *Australian Journal of Basic and Applied Sciences.* **6**, no. 12 2012, 396–409, 2012.

[15] P. L. .-. S. Transactions and u. 1970, The directional dynamics of the commercial tractor-semitrailer vehicle during braking, *JSTOR*, [Online]. Available: `https://www.jstor.org/stable/44644487`.

[16] J. Christl, S. Kunz, P. Bayrasy, I. Kalmykov, and J. Kleinert, "FEA-MBS-Coupling-Approach for Vehicle Dynamics", Tech. Rep.

[17] S. Kharrazi, *Steering Based Lateral Performance Control of Long Heavy Vehicle Combinations*. Chalmers, 2012, ISBN: 9789173857246. [Online]. Available: `http://publications.lib.chalmers.se/records/fulltext/160463.pdf`.

[18] P. Sundström, B. Jacobson, and L. Laine, Vectorized single-track model in Modelica for articulated vehicles with arbitrary number of units and axles, *publications.lib.chalmers.se*, DOI: `10.3384/ECP14096265`. [Online]. Available: `http://publications.lib.chalmers.se/records/fulltext/190501/local_190501.pdf`.

[19] M. Landry, J. L. Malouin, and M. Oral, *Model validation in operations research*, Nov. 1983. DOI: `10.1016/0377-2217(83)90257-6`.

[20] H. Roehm, J. Oehlerking, M. Woehrle, R. Bosch GmbH MATTHIAS ALTHOFF, and M. Althoff, Model Conformance for Cyber-Physical Systems: A Survey, *Cyber-Physical Systems: A Survey. ACM Trans. Cyber-Phys. Syst* **26**, no. 3 2019, 2019. DOI: `10.1145/3306157`. [Online]. Available: `https://doi.org/10.1145/3306157`.

[21] B. Schürmann, D. Heß, J. E. .-. 2. I. 2. . . ., and u. 2017, Ensuring drivability of planned motions using formal methods, *ieeexplore.ieee.org*, [Online]. Available: `https://ieeexplore.ieee.org/abstract/document/8317647/?casa_token=EwKgVqfTQmoAAAAA:BvFuA6biMhT1Ecl0PMiUSBkVMxym7Lyx4pdIk-EGMnyqClfIemp0-HJ5J9ByuTS_n8gVAy8`.

[22] R. Lattarulo, D. Hes, J. A. Matute, and J. Perez, "Towards conformant models of automated electric vehicles", *2018 IEEE International Conference on Vehicular Electronics and Safety, ICVES 2018*, Institute of Electrical and Electronics Engineers Inc., Oct. 2018, ISBN: 9781538635438. DOI: `10.1109/ICVES.2018.8519484`.

[23] J. Cuadrado, D. Vilela, I. Iglesias, A. Martín, and A. Peña, "A Multibody Model to Assess the Effect of Automotive Motor In-wheel Configuration on Vehicle Stability and Comfort", Tech. Rep. [Online]. Available: `http://lim.ii.udc.es/docs/proceedings/2013_07_ECCOMAS_AMultibody.pdf`.

[24] S. Liu, M. A. .-. 2. I. I. C. on, and u. 2018, Reachset conformance of forward dynamic models for the formal analysis of robots, *ieeexplore.ieee.org*, [Online]. Available: `https://ieeexplore.ieee.org/abstract/document/8593975/?casa_token=UzZ3kdO1VLMAAAAA:pmo3mWsJnO744Mhrczk7zgESe6BBRHPsBUFxGbaShdnefQ1GHfjY YPrfZa98-Yrs3b8`.

[25] C. Stark, A. Pereira, M. A. .-. 2. S. I. International, and u. 2018, Reachset conformance testing of human arms with a biomechanical model, *ieeexplore.ieee.org*, [Online]. Available: `https://ieeexplore.ieee.org/abstract/document/8329909/?casa_token=GwMcbe_gSgcAAAAA:RIEV_w1bDbOJ9UMS_hhmHk8-njiSplssGFa1pKPoEylOPGLDGZbmkscHQBqCFfF8lZphfGc`.

[26] N. Kochdumper, A. Tarraf, M. Rechmal, M. Olbrich, L. Hedrich, and M. Althoff, "Establishing Reachset Conformance for the Formal Analysis of Analog Circuits", *Proceedings of the Asia and South Pacific Design Automation Conference, ASP-DAC*, vol. 2020-January, Institute of Electrical and Electronics Engineers Inc., Jan. 2020, pp. 199–204, ISBN: 9781728141237. DOI: `10.1109/ASP-DAC47756.2020.9045120`.

[27] M. Althoff and J. M. Dolan, "Reachability Computation of Low-Order Models for the Safety Verification of High-Order Road Vehicle Models", Tech. Rep. [Online]. Available: `https://ieeexplore.ieee.org/abstract/document/6314777/`.

[28] M. Althoff, J. D. .-. 2. 1. I. I. Conference, and u. 2011, Set-based computation of vehicle behaviors for the online verification of autonomous vehicles, *ieeexplore.ieee.org*, [Online]. Available: `https://ieeexplore.ieee.org/abstract/document/6083052/?casa_token=C0mP41u3wj8AAAAA:Qx7g9C-rNUlxionEI6PCIK9isvGUykiklY7kN9rj7oc03LGf9ZUUrQ2drJuyy7gAkoVXigU`.

[29] H. Roehm, J. Oehlerking, M. Woehrle, and M. Althoff, Reachset Conformance Testing of Hybrid Automata, *dl.acm.org* Apr. 2016, 277–286, Apr. 2016. DOI: `10.1145/2883817.2883828`. [Online]. Available: `http://dx.doi.org/10.1145/2883817.2883828`.

[30] J. Rawlings, D. Mayne, and M. Diehl, *Model Predictive Control: Theory, Computation, and Design*, 2nd ed. Madiscon, Wisconsin: Nob Hill Publishing.

[31] G. M. Ziegler, *Lectures on Polytopes*, ser. Graduate Texts in Mathematics. New York, NY: Springer New York, 1995, vol. 152, ISBN: 978-0-387-94365-7. DOI: `10.1007/978-1-4613-8431-1`. [Online]. Available: `http://link.springer.com/10.1007/978-1-4613-8431-1`.

[32] D. G. Kirkpatrickf and R. Seidel, "THE ULTIMATE PLANAR CONVEX HULL ALGORITHM?*", Tech. Rep. 1, 1986. [Online]. Available: http://www.siam.org/journals/ojsa.php.

[33] C. N. Jones, E. C. Kerrigan, and J. M. Maciejowski, "Equality Set Projection: A new algorithm for the projection of polytopes in halfspace representation", Tech. Rep., 2004. [Online]. Available: https://infoscience.epfl.ch/record/169768.

[34] B. Egardt, *Model Predictive Control - Lectures*, Gothenburg, 2017.

[35] K. Deergha Rao and ·. M. N. S. Swamy, *Digital Signal Processing Theory and Practice*. Springer Nature Singapore, 2018.

[36] M. Althoff, O. Stursberg, M. B. .-. 2. 4. I. C. on, and u. 2007, Reachability analysis of linear systems with uncertain parameters and inputs, *ieeexplore.ieee.org*, [Online]. Available: https://ieeexplore.ieee.org/abstract/document/4434084/?casa_token=luPEDlv8VU0AAAAA:baTTU6l1_BAsGmJMHJx6LKfj8nF5ViWs6P6g8Z6prp8
7g.

[37] M. Althoff, C. Le Guernic, and B. H. Krogh, "Reachable set computation for uncertain time-varying linear systems", *HSCC'11 - Proceedings of the 2011 ACM/SIGBED Hybrid Systems: Computation and Control*, 2011, pp. 93–102, ISBN: 9781450306294. DOI: 10.1145/1967701.1967717.

[38] T. Dang, Approximate Reachability Computation for Polynomial Systems, *Springer* **3927 LNCS** 2006, 138–152, 2006. DOI: 10.1007/11730637{_}13. [Online]. Available: https://www.researchgate.net/publication/221422362.

[39] A. Chutinan, B. K. .-. I. t. o. a. control, and u. 2003, Computational techniques for hybrid system verification, *ieeexplore.ieee.org*, [Online]. Available: https://ieeexplore.ieee.org/abstract/document/1166525/?casa_token=hU3Yj0YERt0AAAAA:UZnDZXkzzCtpA3EdUdi8UcWWPc8eKqm8AyZ1nSsnuf4lQ3NdMRvFWogsn-wjQ1UlAeDNuy0.

[40] T. Dang and O. Maler, "Reachability analysis via face lifting", *Lecture Notes in Computer Science (including subseries Lecture Notes in Artificial Intelligence and Lecture Notes in Bioinformatics)*, vol. 1386, Springer Verlag, 1998, pp. 96–109, ISBN: 3540643583. DOI: 10.1007/3-540-64358-3{_}34.

[41] T. A. Henzinger and P. H. Ho, "Algorithmic analysis of nonlinear hybrid systems", *Lecture Notes in Computer Science (including subseries Lecture Notes in Artificial Intelligence and Lecture Notes in Bioinformatics)*, vol. 939, Springer Verlag, 1995, pp. 225–238, ISBN: 9783540600459. DOI: 10.1007/3-540-60045-0{_}53.

[42] D. Huttenlocher, G. K. .-. I. T. o. …, and u. 1993, Comparing images using the Hausdorff distance, *ieeexplore.ieee.org*, [Online]. Available: https://ieeexplore.ieee.org/abstract/document/232073/?casa_token=EtFeXjsK3zEAAAAA:Fucir4QQDK9pnMWTkPQddV1rueW-PyL4AWxzp_VWHSj7zN45hTDBj6ueyygftyAqEsLGh

[43] O. Jesorsky, K. J. Kirchberg, and R. W. Frischholz, Robust face detection using the Hausdorff distance, *Lecture Notes in Computer Science (including subseries Lecture Notes in Artificial Intelligence and Lecture Notes in Bioinformatics)* **2091** 2001, 90–95, 2001, ISSN: 16113349. DOI: 10.1007/3-540-45344-x{_}14.

[44] D. P. Huttenlocher and K. Kedem, "Computing the minimum hausdorff distance for point sets under translation", Publ by ACM, 1990, pp. 340–349, ISBN: 0897913620. DOI: 10.1145/98524.98599.

[45] J. Pauwelussen, Essentials of vehicle dynamics 2014, 2014. [Online]. Available: https://www.google.com/books?hl=sv&lr=&id=aJ3vAwAAQBAJ&oi=fnd&pg=PP1&dq=Essentials+of+vehicle+dynamics+joop&ots=C4iJtUwMfx&sig=N9R-LlRSXfEex0NLy30_MtDK7iA.

[46] D. Heß, M. Althoff, and T. Sattel, "Comparison of Trajectory Tracking Controllers for Emergency Situations", Tech. Rep. [Online]. Available: http://vehiclecontrol.it.cx/ttb.

[47] M. Althoff and O. Stursberg, "Reachability Analysis and its Application to the Safety Assessment of Autonomous Cars", Tech. Rep., 2010. [Online]. Available: https://mediatum.ub.tum.de/doc/1287517/file.pdf.

[48] J. Bezanson, A. Edelman, S. Karpinski, and V. B. Shah, Julia: A fresh approach to numerical computing, *SIAM review* **59** 2017, 65–98, 2017. [Online]. Available: https://doi.org/10.1137/141000671.

[49] S. M. Lavalle and S. M. Lavalle, Rapidly-Exploring Random Trees: A New Tool for Path Planning 1998, 1998. [Online]. Available: http://citeseerx.ist.psu.edu/viewdoc/summary?doi=10.1.1.35.1853.

[50] M. Koschi, C. Pek, S. Maierhofer, and M. Althoff, "Computationally Efficient Safety Falsification of Adaptive Cruise Control Systems", Tech. Rep. [Online]. Available: https://ieeexplore.ieee.org/abstract/document/8917287/.

[51] S. M. Lavalle, M. S. Branicky, and S. R. Lindemann, On the Relationship Between Classical Grid Search and Probabilistic Roadmaps, *The International Journal of Robotics Research* **23**, no. 8 Jul. 2004, 673–692, Jul. 2004. DOI: 10.1177/0278364904045481. [Online]. Available: https://journals.sagepub.com/doi/abs/10.1177/0278364904045481?casa_token=DMSymku3kHYAAAAA:xS4GUo2uA4Ds2B95eBBPYIwndFkyTJUi9WvA7Vlfm5jXl

[52] *Operational Definitions of Driving Performance Measures and Statistics J2944_201506*. DOI: https://doi.org/10.4271/J2944{_}201506.
[53] B. Jacobson, *Vehicle Dynamics Compendium*. Gothenburg: Chalmers University of Technology, 2018.
[54] J. Wong, Theory of ground vehicles 2008, 2008. [Online]. Available: https://www.google.com/books?hl=sv&lr=&id=Blp2D1DteTYC&oi=fnd&pg=PR11&dq=theory++of++Ground++Vehicles&ots=Xttv3lT3aj&sig=bozUEDv6L062CELP_9m3qGtu0Hk.
[55] M. M. Islam, N. Fröjd, S. Kharrazi, and B. Jacobson, How well a single-track linear model captures the lateral dynamics of long combination vehicles, *Vehicle System Dynamics* **57**, no. 12 Dec. 2019, 1874–1896, Dec. 2019, ISSN: 17445159. DOI: 10.1080/00423114.2018.1556796.
[56] M. Burhaumudin, P. S. .-. I. . . ., and u. 2012, "Modeling and validation of magic formula tire model", Tech. Rep. [Online]. Available: https://pdfs.semanticscholar.org/04aa/8fa25886103a97b92443346fc94bf4c6c50b.pdf.
[57] D. John and M. Sampson, "Active Roll Control of Articulated Heavy Vehicles", Tech. Rep., 2000. [Online]. Available: http://www.sampson.id.au/david/work/phd.pdf.
[58] M. Gäfvert, O. Lindgärde, A. Afvert, O. Lindg, and A. Arde, A 9-DOF Tractor-Semitrailer Dynamic Handling Model for Advanced Chassis Control Studies, *Vehicle System Dynamics* **41**, no. 1 Jan. 2004, 51–82, Jan. 2004, ISSN: 1744-5159. DOI: 10.1076/vesd.41.1.51.23408. [Online]. Available: https://www.tandfonline.com/action/journalInformation?journalCode=nvsd20.
[59] J. R. Ellis, A Model of Semi Trailer Vehicles Including the Roll Modes of Motion, *Vehicle System Dynamics* **6**, no. 3 Sep. 1977, 124–129, Sep. 1977, ISSN: 1744-5159. DOI: 10.1080/00423117708968521. [Online]. Available: https://www.tandfonline.com/action/journalInformation?journalCode=nvsd20.

Appendix A

Work Material

A.1 Volvo GTT Truck Models

As mentioned earlier, Volvo GTT currently relies on several models which are developed for tackling specific tasks or scenarios. Those models are described here briefly. For more details, refer to [9].

A.1.1 Single Track Model (STM)

The single track model is one of the simplest internal models in Volvo GTT. It is used in their in-house simulator and is based on C++ programming language. The truck semitrailer combination is modeled as two separate single track models, or bicycle models [54].

The models have very simple longitudinal and lateral dynamics, and are kinematic (i.e. the position is calculated as a function of time and and not forces. This is also why the models exhibit no slip. The model has a 12 gear transmission which is responsible for propulsion. The frame of reference in use is odd, with the x-axis pointing to the right and the y-axis pointing forward.

As for the way this model works, it can be described in 3 main steps (this also applies to reverse driving).

1. The tractor unit moves forward as it's bicycle model would.
2. The semitrailer fixes the articulation angle between the two units such that it's kingpin is pointing towards the tractor's fifth-wheel.
3. The semitrailer moves forward towards the tractor.

A.1.2 One Track Model with Linear Tire Slip (OTM)

The one track model is another single track model used in Volvo GTT. While the name is close to the STM, probably the only thing they share in common would be having two separate units for the tractor and the semitrailer, although the coupling forces are well defined. The model is dynamic and modeled in MATLAB, but does not have a simulation interface. There is also no propulsion or braking system so the model cannot accelerate nor decelerate.

The model is clearly described by mathematical equations following a Newtonian formulation and showing the longitudinal, lateral and yaw motion of the tractor and semi-trailer. The equations are available in [9]. The tractor is modeled with two axles while the semitrailer has 3 axles. As the name suggests, a linear tire model is considered and the wheel lateral forces are hence linear with respect to the slip angle.

A.1.3 Global Simulation Platform (GSP)

The GSP is not a standalone platform. It requires a vehicle dynamics model to function, and is now hosting the STM model in the in-house simulator. The GSP offers a complete powertrain with realistic gear changes which considers the total mass of the heavy combination vehicle to be lumped into one mass. Even though the model is designed in Simulink, the interface is not available for the users who use this platform as a black box through a *User Datagram Protocol (UDP)*. The platform takes as input the throttle, gear, brake and inclination and returns the engine speed, fuel consumption and vehicle speed as outputs.

A.1.4 Volvo Transport Model (VTM)

One more complex model, if not the most complex model at Volvo GTT, is the VTM. The VTM library offers several truck combination models which are simulated in Simspace Multibody^{TM} using a Simulink environment and are parameterized in MATLAB [55]. Those high fidelity 3D multi-body dynamic models follow the ISO8855 standard in their frame of reference. The different bodies are modeled separately with some preset degrees of freedom between them. The thesis work presented in [9] gives more detailed information about the division and lumping of masses as well as the different degrees of freedom between the different bodies.

The complexity of those models comes from the various degrees of freedom and compliances that they host. The suspension is sensitive to vertical bounce, pitch and roll motions, whereas the steering system in the VTM has an inertia and damping effect while the wheels are physically connected by a rigid link.

The wheels' longitudinal and lateral rotation are modeled in Simulink with an S function, while the tires are non-linearly modeled after the famous Pacejka magic tire formula of version PAC2002. This formula is compliant to the normal forces as well as the slip of the tire is both the longitudinal and lateral directions. This tire formula is also several properties such as a stiffness, shape, peak and curvature [56]. One thing the VTM lacks is a propulsion system.

The VTM is a well defined model and has been tested and verified against measured data from physical on-track tests. For that reason, the VTM will be considered throughout the modeling phase of this thesis for performance comparison.

Flexible Frames

One particularly important characteristic of truck frames is their flexibility, and that is a distinguishing characteristic of the VTM. The VTM model is a unique high fidelity model which accounts for frame flexibility by modelling it as two parallel beams which exhibit a warp motion. For several factors including their heavy weight, long wheel bases and high center of gravity, truck frames are designed to have more flexibility compared to passenger vehicles. They also have to withstand much higher forces. This significance in frame compliance has a noticeable effect on roll hand handling performance [57].

There are several ways used for studying frame flexibility and simplifying the dynamics. In his paper, Sampson designed his truck model with frame flexibility represented by two generic vehicle units connected by a torsional spring to model the torsional stiffness in the frame. Similarily, in [58], a model of a tractor with a semitrailer which considers the tractor's chassis torsional stiffness is introduced. The model is characterised by 9-DOF which include the relative roll motion caused by the chassis stiffness in the body. The model is divided into 5 separate bodies, where the tractor itself is composed of 2 bodies connected by a torsional spring. Torsional stiffness can also be added in the 5^{th} wheel connecting the tractor to the semitrailer as shown in [59]. Finite element methods are also used in the modelling of flexible frames as mentioned earlier.

A.2 Comparison with Volvo GTT Models

A.2.1 Comparison Between Volvo GTT Models

Since the models are each developed to tackle a specific scenario, they behave and perform different than each other. To understand the difference between them, [9] performs testing on 4 scenarios and find out which model performs best in each:

1. Acceleration and deceleration test: GSP
2. Sinusoidal maneuver test: VTM
3. Steady-state cornering test: VTM
4. Uphill driving test: GSP

It is clear that the VTM did not perform well in tests concerned with longitudinal dynamics since it does not host a propulsion system as mentioned earlier. However, the VTM performs best in maneuvering tests when lateral dynamics are of concern. This is why the VTM is chosen as the reference against which the designed models are going to be compared.

In [55], Islam & co. compare the high-speed performance of Volvo GTT's single track model (STM) to their high fidelity 3D model VTM. It comes to no surprise that the STM, with less degrees of freedom is less computationally expensive. However, the performance deemed unsatisfactory in general, and sometimes even unacceptable.

A.2.2 Comparison of Developed Linear Model Against VTM

This section will show a comparison between the linear model with uncertainties that is developed in Ch. 3 and Volvo's high fidelity model, the VTM. The results shown in this section are used to set a reference of how far away the developed linear model is from reality.

Volvo's VTM is tested for the same lane change maneuvers as before which are also presented in Tab. A.1. In fact, the same resultant reachable sets are used here as well, but rather than checking for the falsification from the RRT states, here the output of the VTM simulations are shown against the reachable sets. In this section, only two cases will be shown, a conservative maneuver (8 seconds) and an aggressive maneuver (2 seconds).

The VTM is simulated with an open loop feed forward steering input and a feedback PI controller for controlling the longitudinal speed. The reason behind introducing this controller is to keep the longitudinal speed constant since the linear model's longitudinal speed does not change under lateral maneuvering only. Hence, the results should be more comparable if the longitudinal speeds are kept constant. The PI controller has the gains $K_P = 17860$ and $K_I = 100$ which are obtained from calculated guesses and manually optimised to give a longitudinal speed that does not fluctuate when the model is maneuvering. The controller controls the longitudinal velocity based on the difference between the desired velocity and the current VTM longitudinal velocity.

To make the comparison fair, the steering inputs on the wheels should be the same for both the linear model and the VTM. However, because of the complex steering and suspension systems of the VTM, the steering input on the steering wheel have to be modified so that the steering at the wheels is the same sinusoidal function used for the linear model. The modification in the steering input can be seen in Tab. A.1 where the steering amplitude is shown for the linear model as well as the VTM.

Period [s]	8	7.5	7	6.5	6	5.5	5	4.5	4	3.5	3	2.5	2
Linear model $\delta[°]$	0.95	1.10	1.20	1.40	1.70	2.00	2.40	3.00	4.00	5.00	6.75	9.5.	15
VTM $\delta[°]$	1.17	1.35	1.45	1.70	2.05	2.40	2.85	3.50	4.70	5.80	7.75	10.80	16.70

Table A.1: Test suite for lane change maneuvers

The steering inputs are used in an open loop manner as it is done for the reachable set calculations. Fig. A.1 shows a block diagram of the VTM in the control loop.

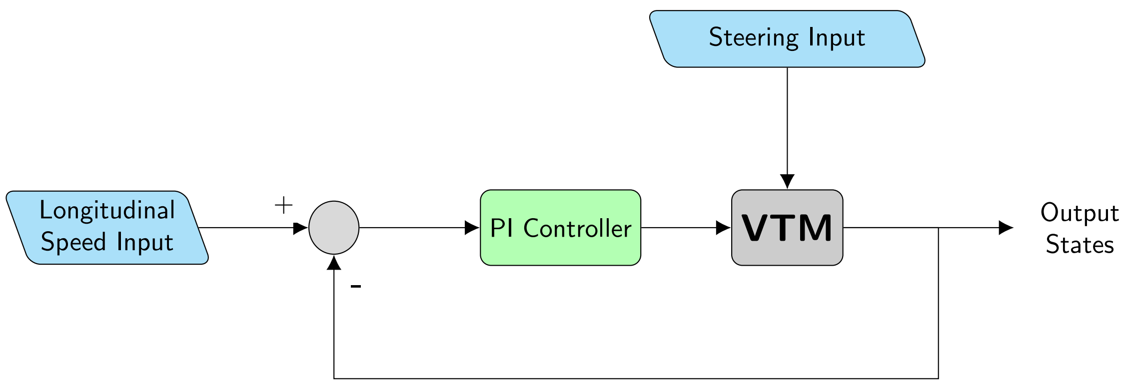

Figure A.1: VTM in the loop

The VTM is now chosen as the implementation system. Ideally, the VTM would be used in the RRT simulation between each step in order to explore all its possible dynamics. However, for the simple comparison of the models, this section focuses on the simulation of the VTM in comparison with the abstract system's reachable sets. Both systems are measured at the center of gravity of the first unit to keep the comparison reasonable. It is clearly noticed from Figs. A.2 and A.4 that the outputs from the VTM do not completely comply with those of the linear model in the state v_y where there is an obvious phase shift between the models in the more conservative maneuvers. The differences can also be seen in Figs. A.3 and A.5 where the phase planes showing the state v_y are all not overlapping with the blue reachsets. As for the other states ($\dot{\psi}$, $\Delta\psi$, $\Delta\dot{\psi}$), a short phase shift can be noticed for the conservative maneuver. The phase shift seems to get smaller and disappear as the maneuver gets more aggressive.

Those speculations can be attributed to several reasons, which mainly arise from the complexity of the VTM model in comparison to the simple linear model presented in the thesis. The linear model is not designed to capture the dynamics of the VTM. For instance, at such low speeds as the one considered in the work (10 [m/s]), it is well known that tire relaxation plays an important in the performance and the dynamics of the model. In addition, the complex steering gear that is implemented in the VTM is not accounted for in the linear model. Those can be complex steering compliances or passive steering effects which could be accounted for in the linear model if needed. It could be speculated that other compliances inside the VTM model occur at a lower frequency compared to the dynamics of the aggressive lane change maneuvers which could be the reason behind the smaller phase gap.

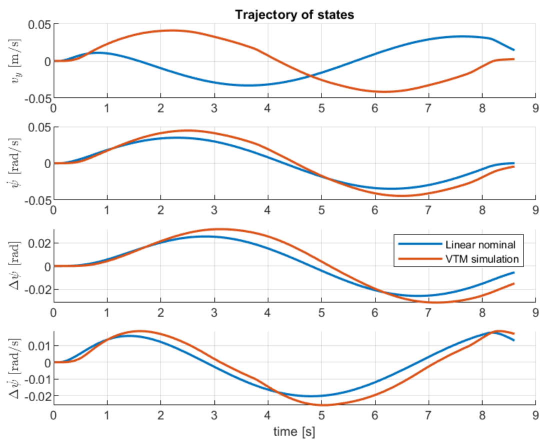

Figure A.2: VTM simulation for sinusoidal maneuver of 8 seconds

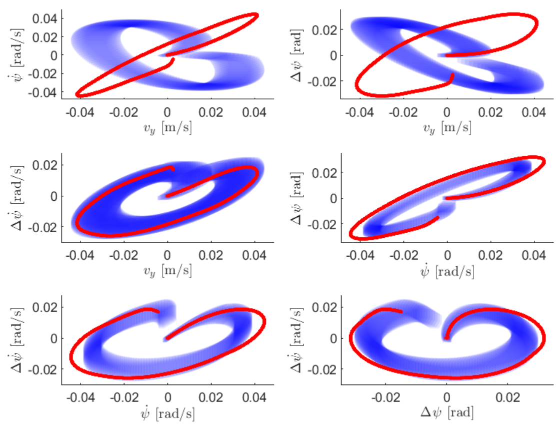

Figure A.3: Phase plane projections and VTM simulation for sinusoidal maneuver of 8 seconds

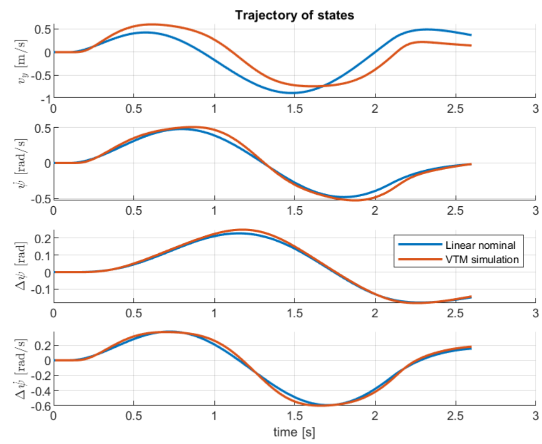

Figure A.4: VTM simulation for sinusoidal maneuver of 2 seconds

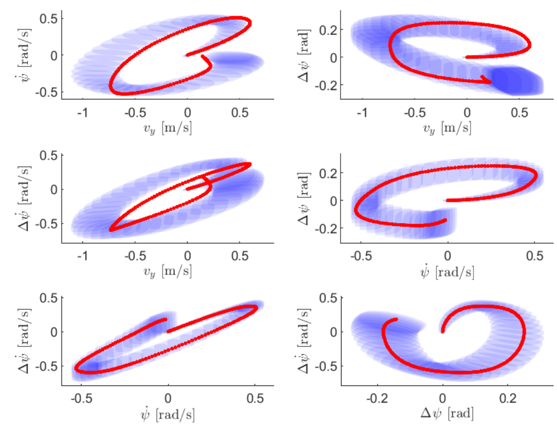

Figure A.5: Phase plane projections and VTM simulation for sinusoidal maneuver of 2 seconds

A.3 Matlab Outer Approximation Algorithm

The suggested technique is to solve an optimization problem which minimizes the size of an overapproximative polyhedron while abiding by certain measures. The problem is solved using the *fmincon()* function from MATLAB®. This function attempts to solve problems of the form:

$$\begin{aligned} \min_x J(x) \text{ subject to: } Ax \leq B, \quad A_{eq}x = B_{eq} \quad & \text{(linear constraints)} \\ C(x) \leq 0, \quad C_{eq}(x) = 0 \quad & \text{(nonlinear constraints)} \\ LB \leq x \leq UB \quad & \text{(bounds)} \end{aligned} \tag{A.1}$$

The problem of interest here is, as mentioned earlier, to optimize an overapproximative polyhedron. Assume that a polyhedron $\mathcal{P}_{initial}$ is to be outer-approximated with a polyhedron $\mathcal{P}_{out}$. For that, cost function J to be minimized is defined as

$$J = \sum_{i=1}^{N} d_{V,i}^{2n} \tag{A.2}$$

where N is the predefined number of vertices of $\mathcal{P}_{out}$ and $d_{V,i}$ is the distance measure of the i^{th} vertex of $\mathcal{P}_{out}$ to $\mathcal{P}_{initial}$. n is the order number of the optimization in a sequential optimization problem where the output of one optimization is used as an initial guess for the consecutive optimization problem in the sequence.

The constraints that are opted for are in terms of the volumes of the polyhedrons $\mathcal{P}_{initial}$ and $\mathcal{P}_{out}$. Hence, the nonlinear constraints are used for solving the problem in hand. First of all, for the nonlinear inequality in A.1, function $C(x)$ is defined as

$$C = volume\left(\mathcal{P}_{initial}\right) - volume\left(\mathcal{P}_{out}\right) \tag{A.3}$$

since $\mathcal{P}_{out}$ is an outer approximation and should have a bigger volume than $\mathcal{P}_{initial}$. However, this constraint is not limiting enough, and the resultant $\mathcal{P}_{out}$ could ideally have a bigger volume than $\mathcal{P}_{initial}$ while still cutting through it. This will cause the loss of some parts of $\mathcal{P}_{initial}$ which is not accepted. Therefore, the other nonlinear equality constraint in A.1 is introduced such that

$$C_{eq} = volume(\mathcal{P}_{initial}) - volume(\mathcal{P}_{intersect}) \tag{A.4}$$

where $\mathcal{P}_{intersect} = \mathcal{P}_{initial} \cap \mathcal{P}_{out}$. This should force $\mathcal{P}_{out}$ to enclose all of $\mathcal{P}_{initial}$, and along with the constraint in equation A.3 should be enough for solving the optimization problem.

In Figure A.6, an optimization problem is solved for overapproximating a polyhedron $\mathcal{P}_{initial}$ with $\mathcal{P}_{out}$ starting from an initial guess. In this example, the initial guess is a square polyhedron. Five vertices are defined at the vertices of the initial guess (in this case, there are 2 overlapping vertices) which eventually constitute the vertices of $\mathcal{P}_{out}$. The optimitzation problem shown has a sequence of 2, meaning that $\mathcal{P}_{out}$ is refined in two steps with the first $\mathcal{P}_{out}$ being used as the initial guess of the second $\mathcal{P}_{out}$.

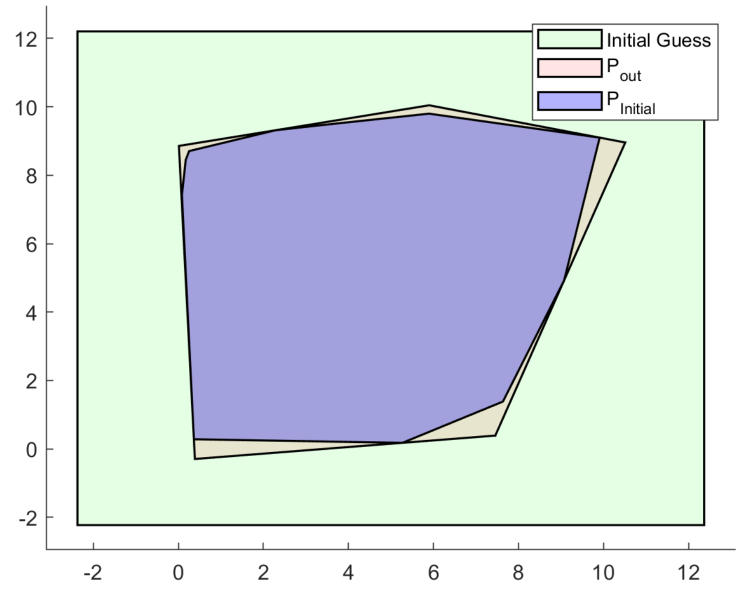

Figure A.6: Example of an outer approximation using 5 vertices

However, this approach to overapproximate polyhedrons is not ideal. The function $volume()$, from MPT3 toolbox, used in the optimization problem in several instances has its limitations. First of all, while the $volume()$ function works fairly well for 2D and 3D dimensions, higher dimensions are less computationally friendly. This is because the $volume()$ function relies on a different algorithm for 4D problems and higher. The algorithm for higher dimensional problems has a limitation as well. In the case of vehicle dynamics and very short time steps (0.01 sec), the initial polyhedra $\mathcal{P}_{initial}$ are too small for being calculated. This might be solved by scaling the polyhedra then re-scaling the volumes back to their actual value.

However, since several problems appeared with the MPT3 toolbox and its functions, it was decided eventually to opt for a different approach based on the LazySets package in Julia as explained in Chapter 4.

Appendix B

Extra Figures

B.1 Full Reachable Space

The following figures show the full reachable state space for the tractor semitrailer in 5 seconds for different steering angle ranges.

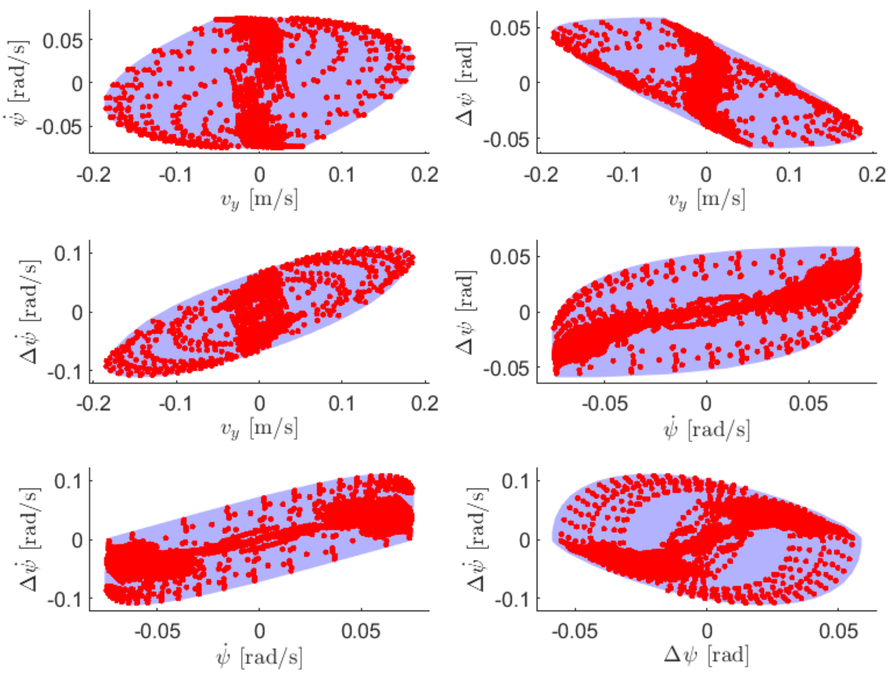

Figure B.1: Full reachable state space for 2 degrees steering angle in 5 seconds.

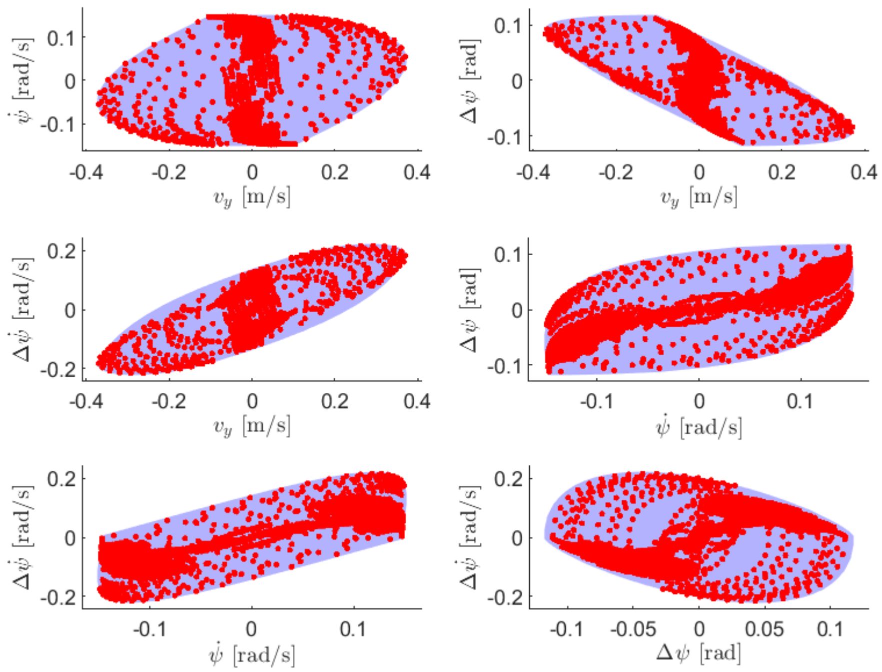

Figure B.2: Full reachable state space for 4 degrees steering angle in 5 seconds.

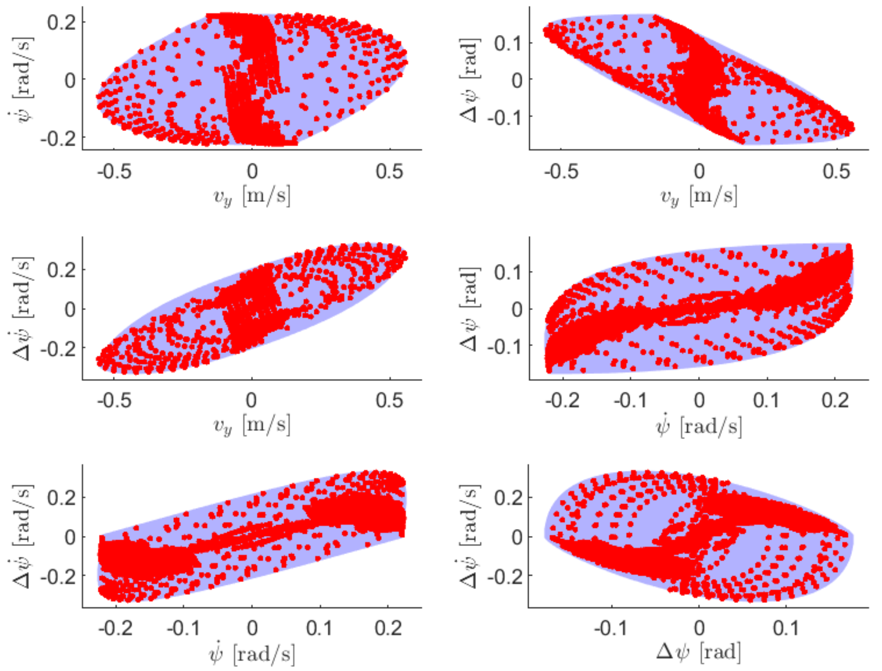

Figure B.3: Full reachable state space for 6 degrees steering angle in 5 seconds.

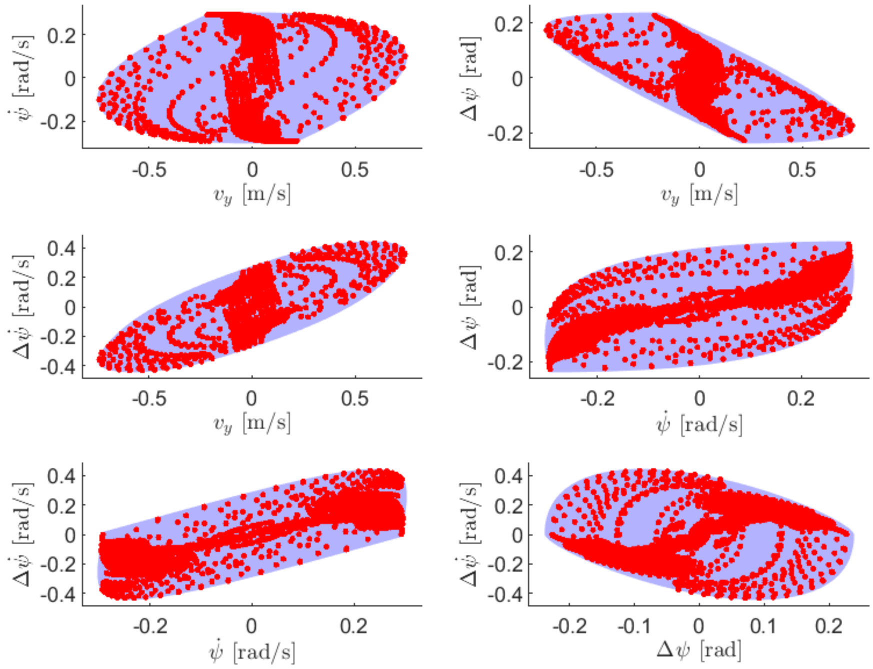

Figure B.4: Full reachable state space for 8 degrees steering angle in 5 seconds.

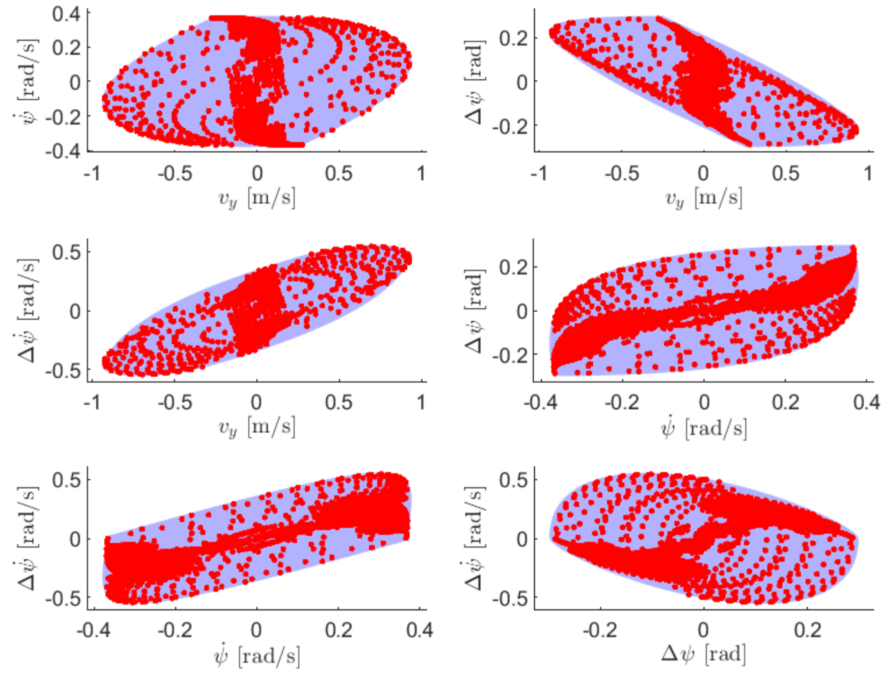

Figure B.5: Full reachable state space for 10 degrees steering angle in 5 seconds.

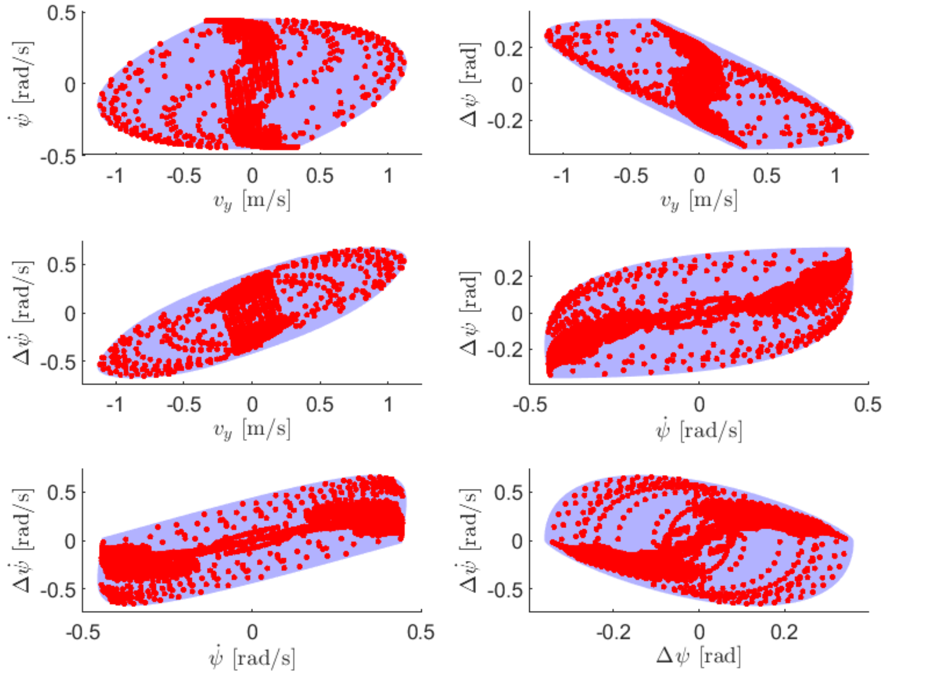

Figure B.6: Full reachable state space for 12 degrees steering angle in 5 seconds.

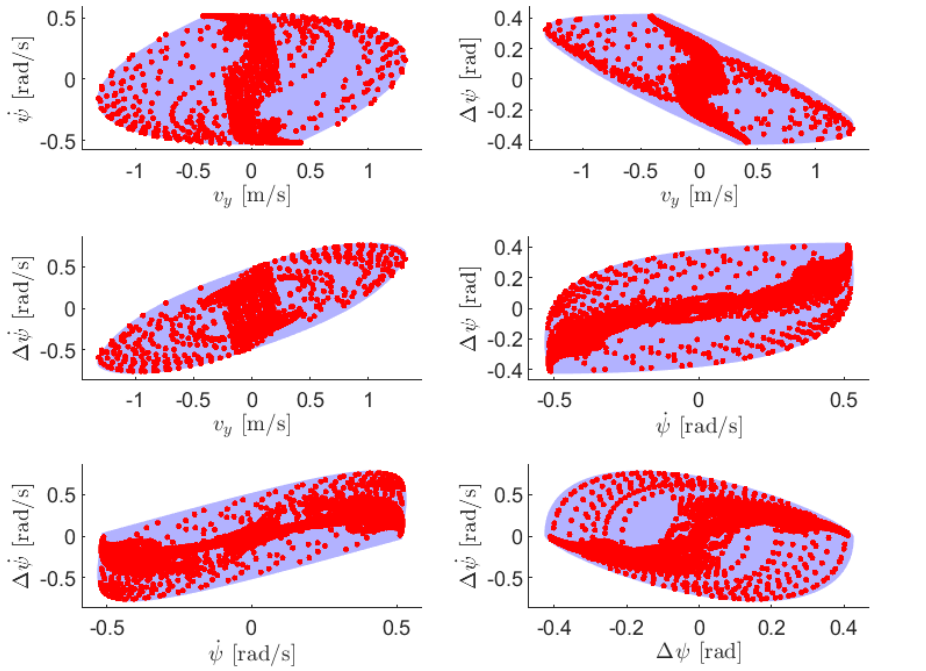

Figure B.7: Full reachable state space for 14 degrees steering angle in 5 seconds.

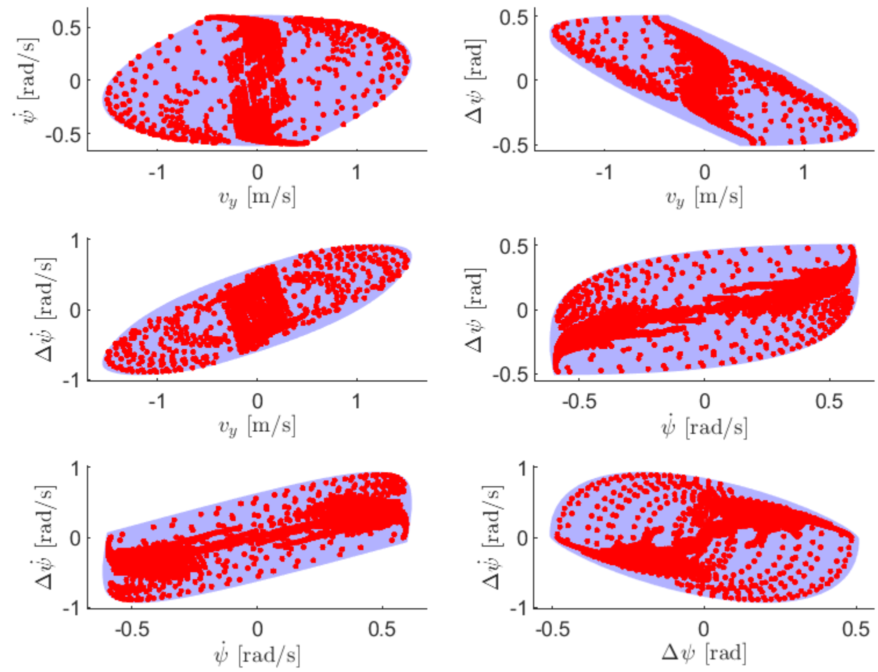

Figure B.8: Full reachable state space for 16 degrees steering angle in 5 seconds.

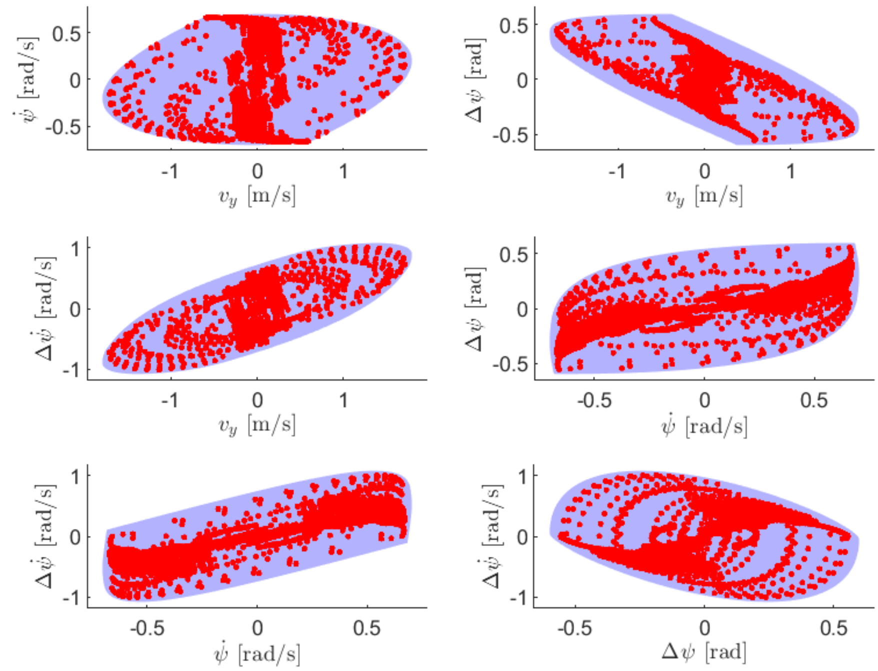

Figure B.9: Full reachable state space for 18 degrees steering angle in 5 seconds.

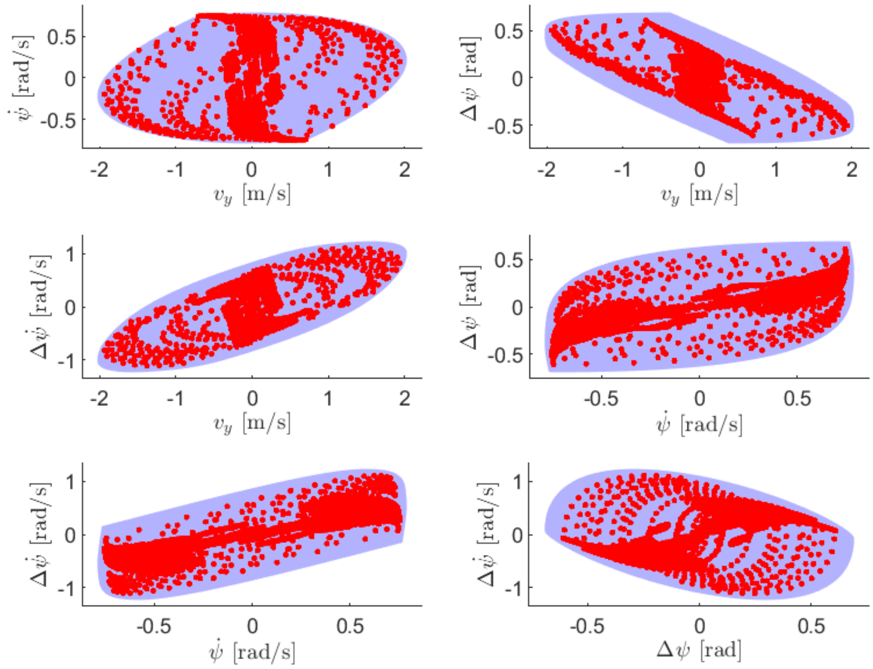

Figure B.10: Full reachable state space for 20 degrees steering angle in 5 seconds.

B.2 Lane Change Dynamics

This section shows the reachable sets with the RRT generated states for all the lane change maneuvers in the test suite discussed in Ch. 6.

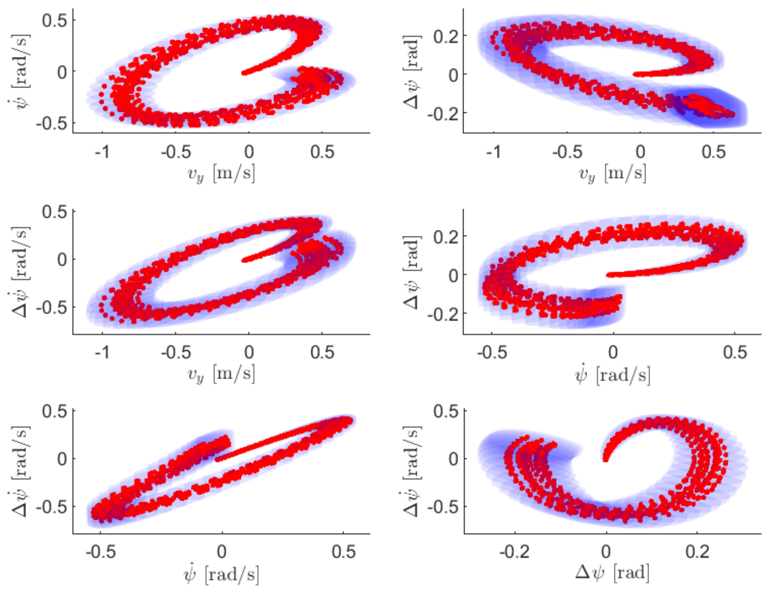

Figure B.11: Phase plane projections for sinusoidal maneuver of 2 seconds

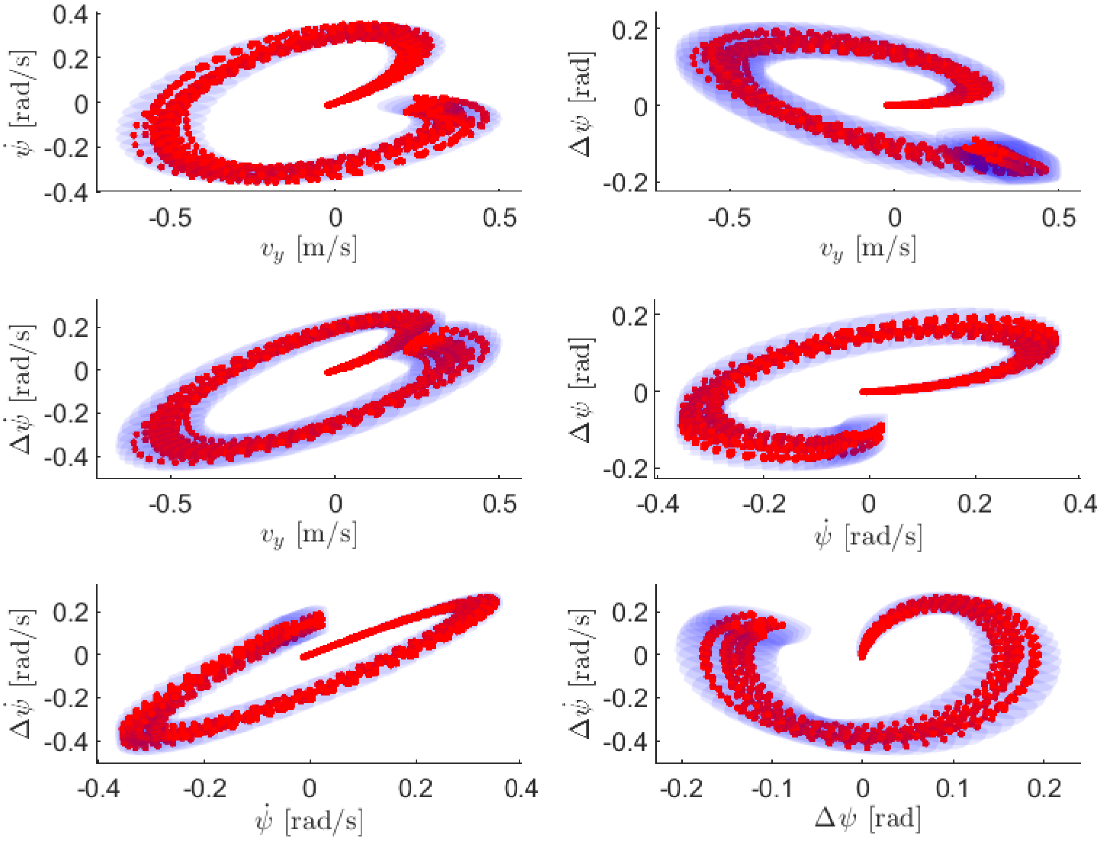

Figure B.12: Phase plane projections for sinusoidal maneuver of 2.5 seconds

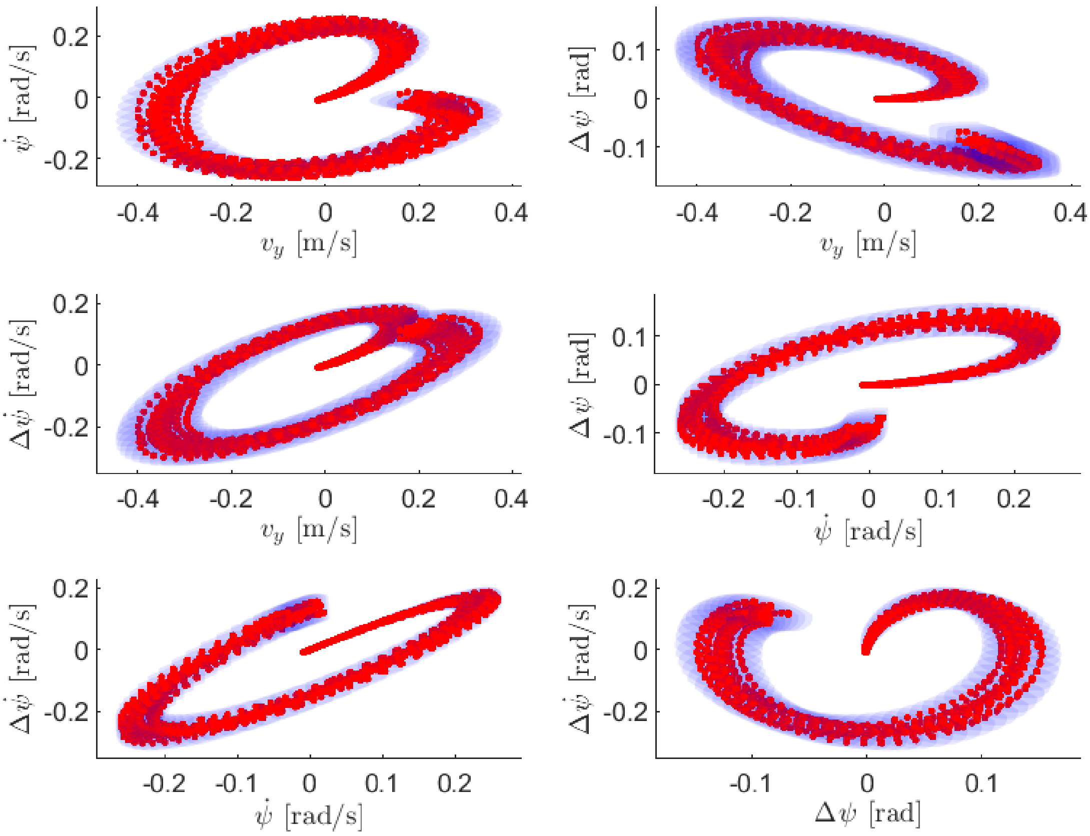

Figure B.13: Phase plane projections for sinusoidal maneuver of 3 seconds

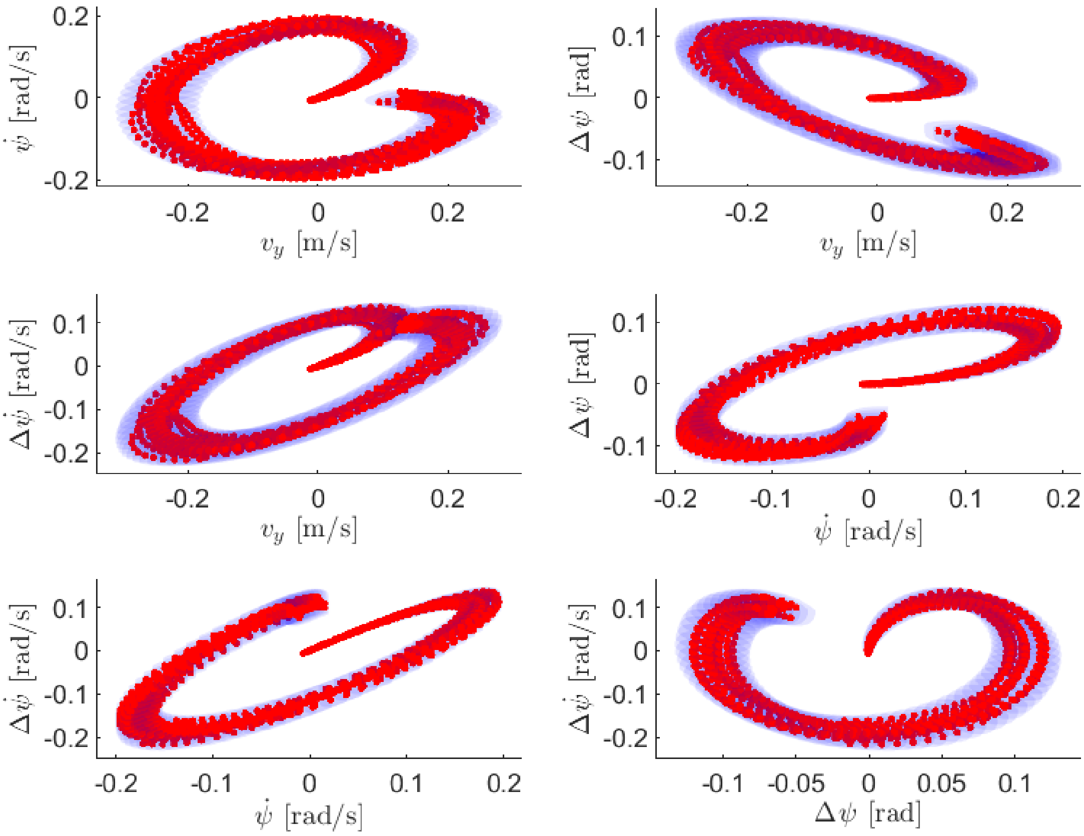

Figure B.14: Phase plane projections for sinusoidal maneuver of 3.5 seconds

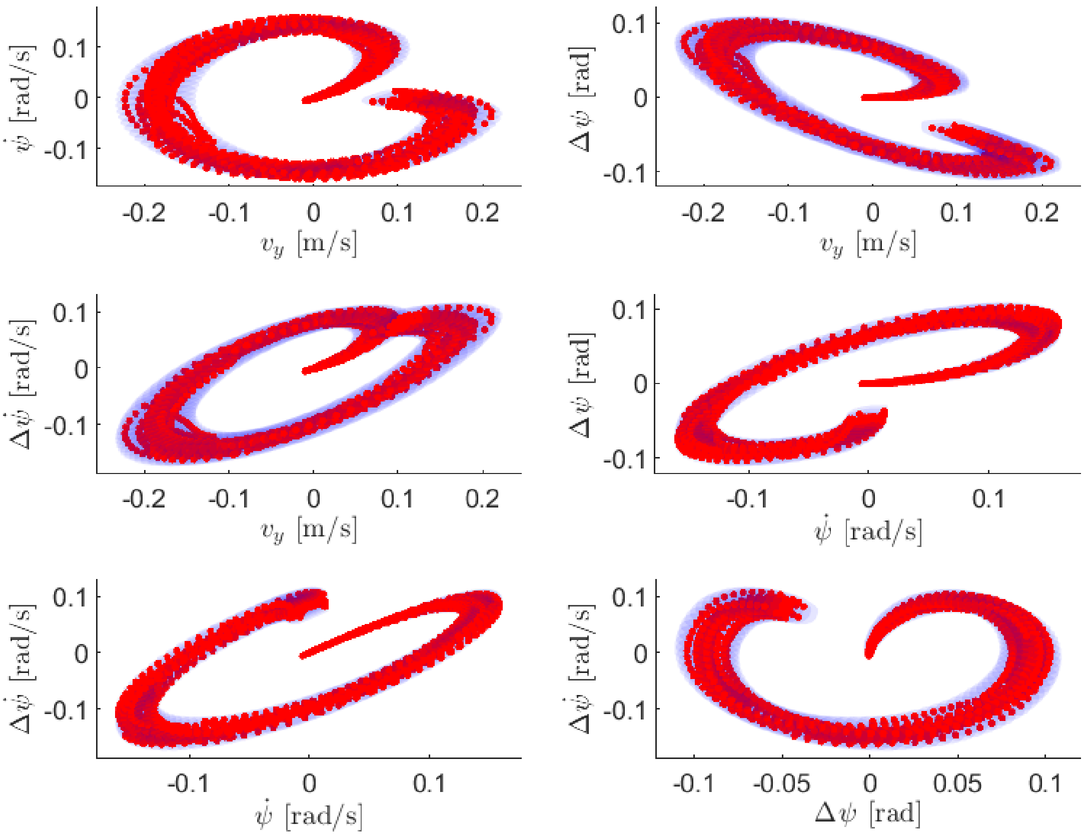

Figure B.15: Phase plane projections for sinusoidal maneuver of 4 seconds

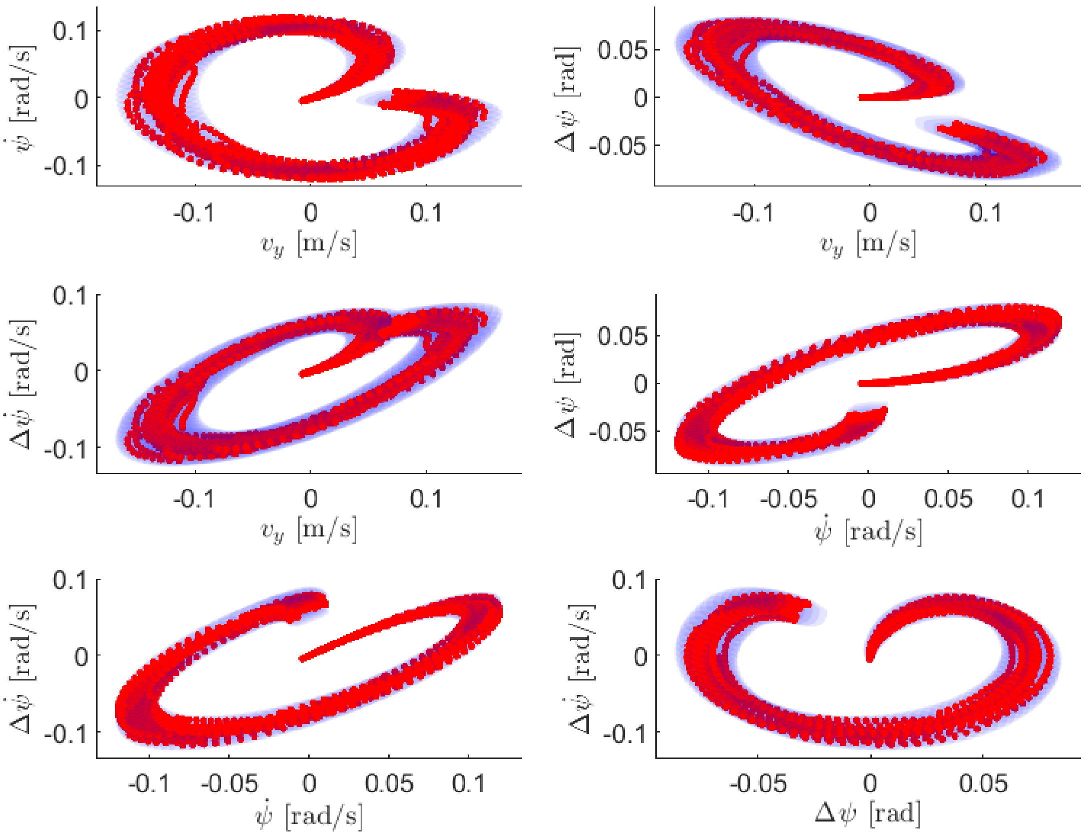

Figure B.16: Phase plane projections for sinusoidal maneuver of 4.5 seconds

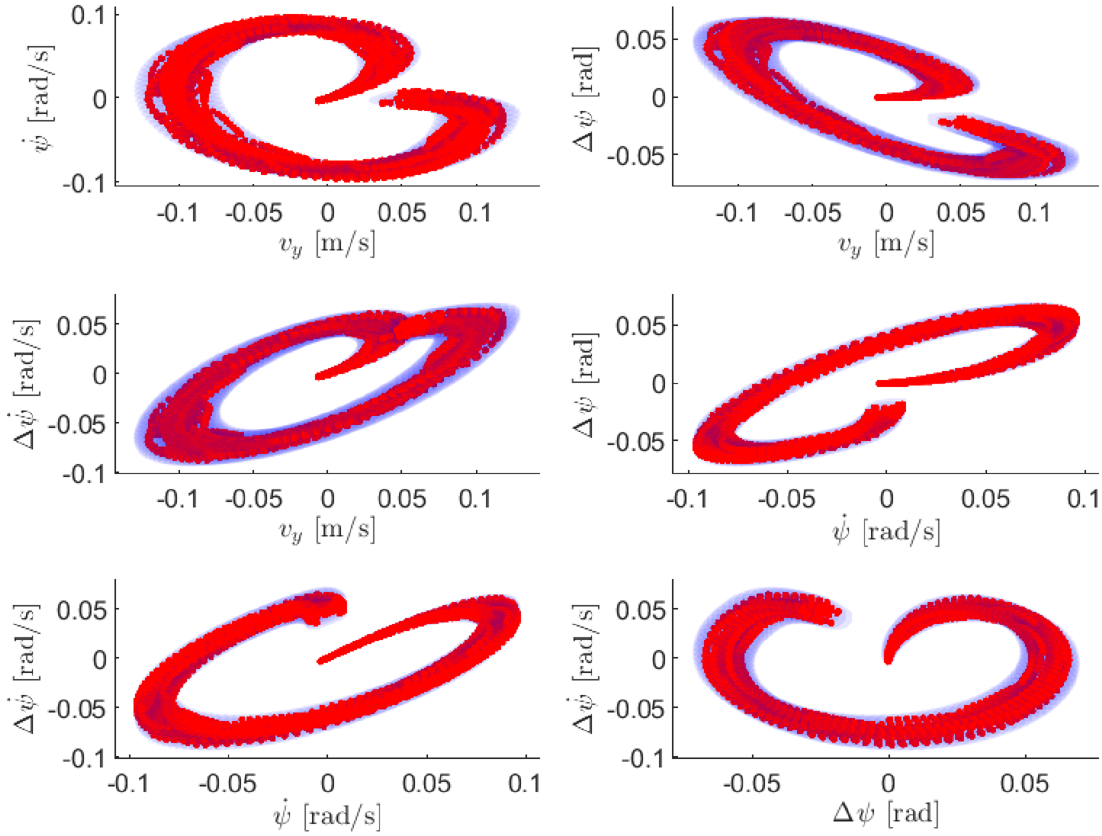

Figure B.17: Phase plane projections for sinusoidal maneuver of 5 seconds

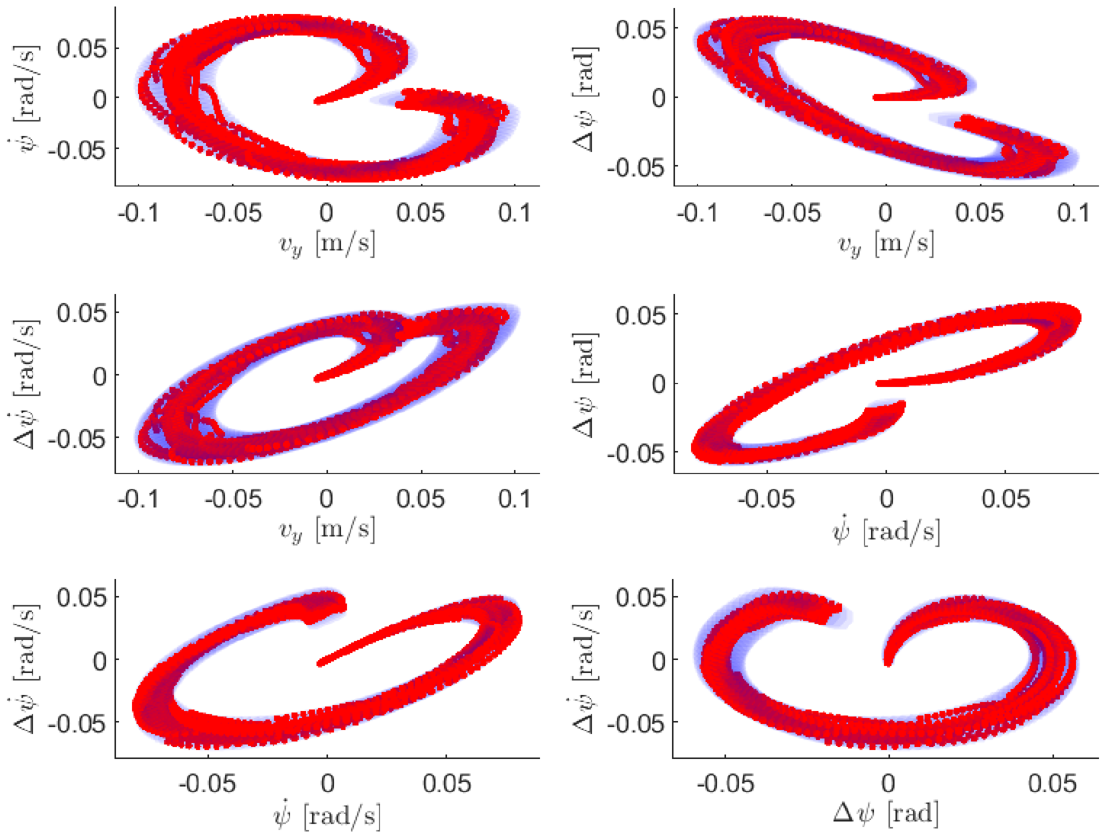

Figure B.18: Phase plane projections for sinusoidal maneuver of 5.5 seconds

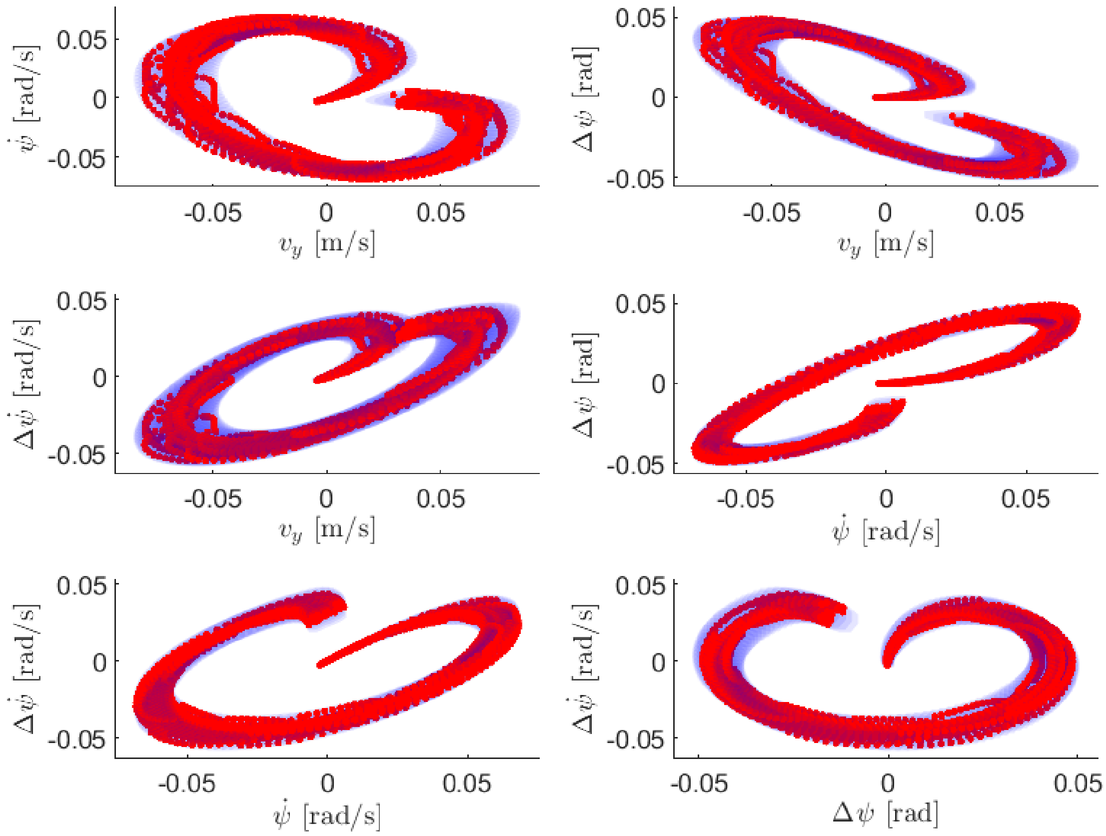

Figure B.19: Phase plane projections for sinusoidal maneuver of 6 seconds

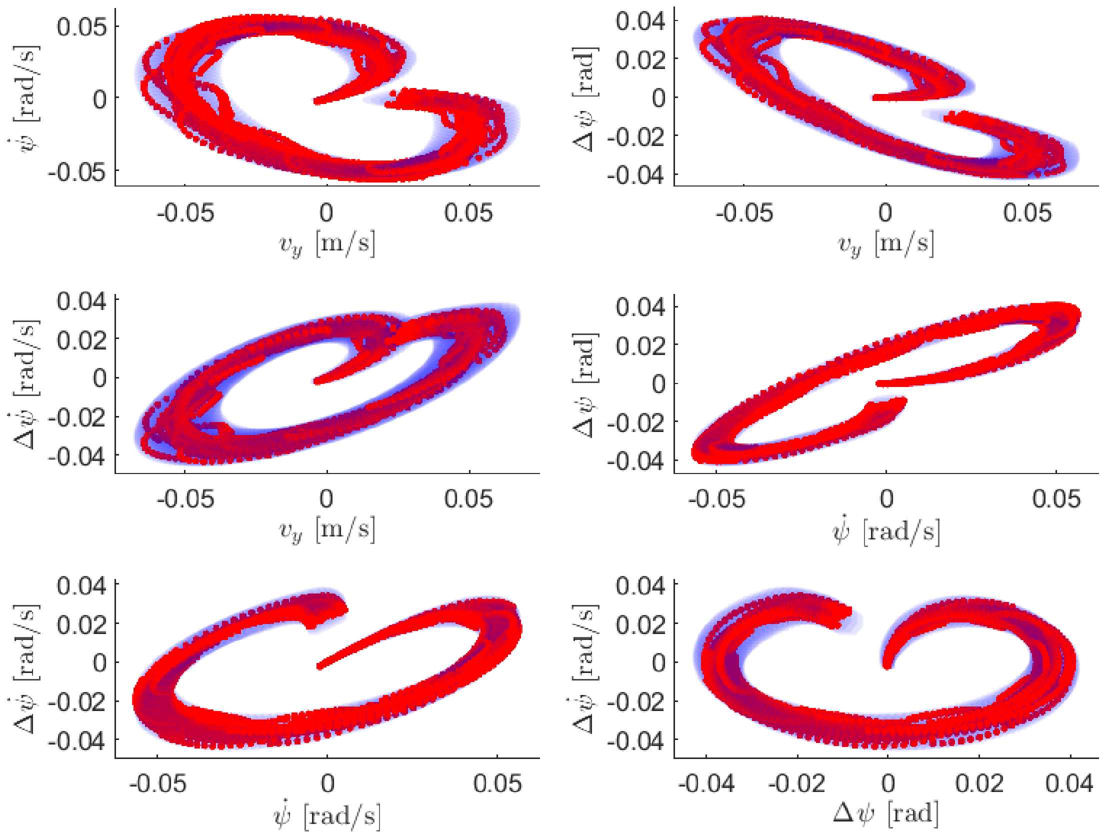

Figure B.20: Phase plane projections for sinusoidal maneuver of 6.5 seconds

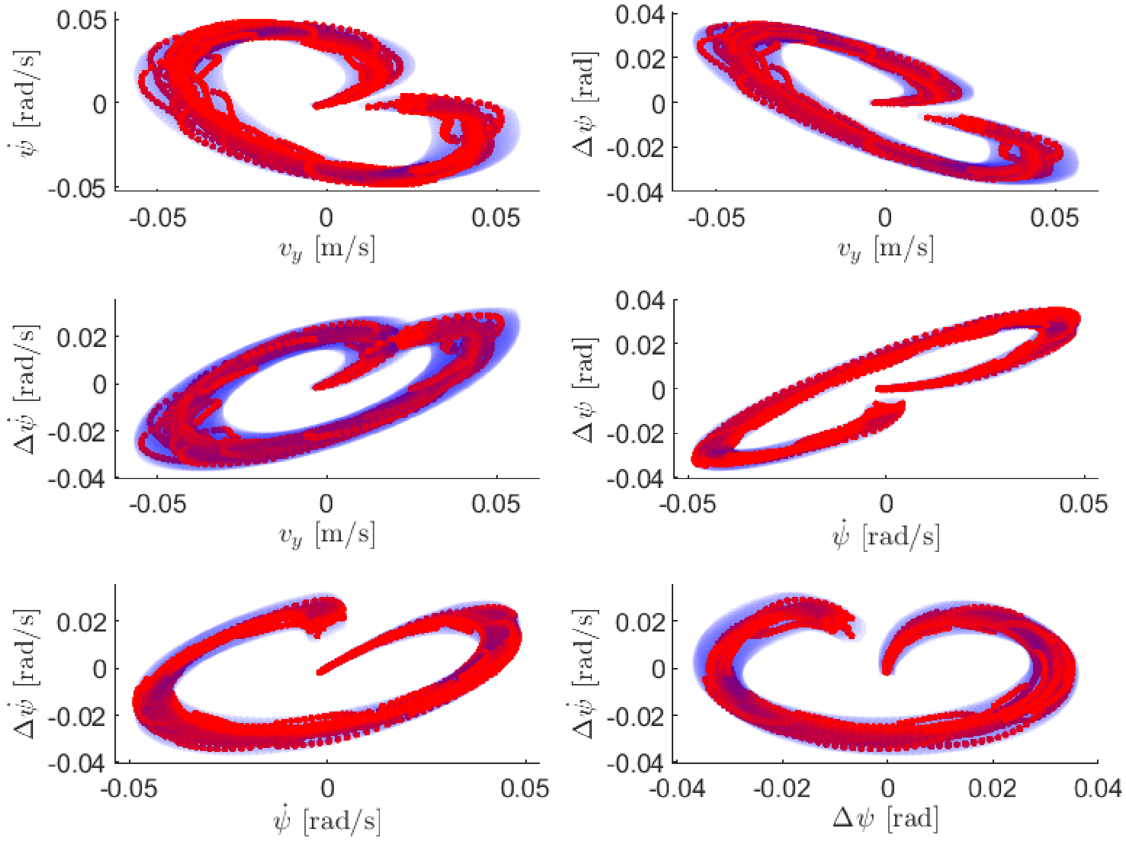

Figure B.21: Phase plane projections for sinusoidal maneuver of 7 seconds

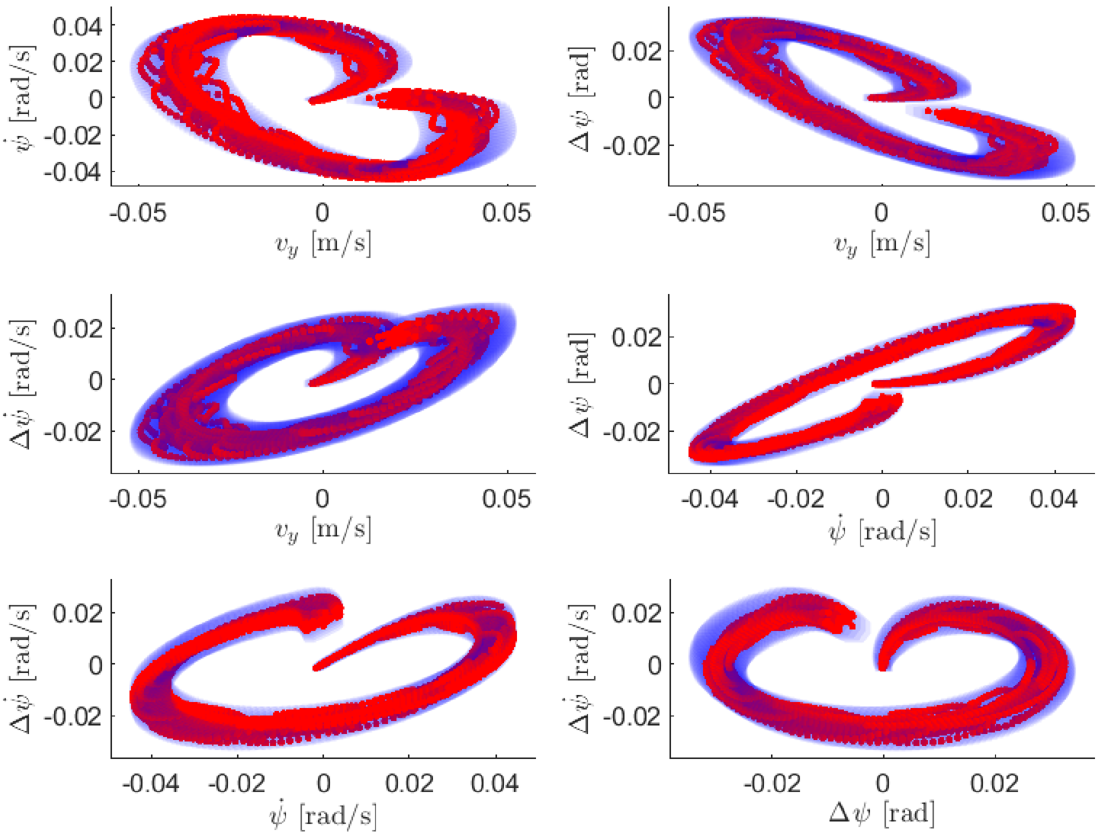

Figure B.22: Phase plane projections for sinusoidal maneuver of 7.5 seconds

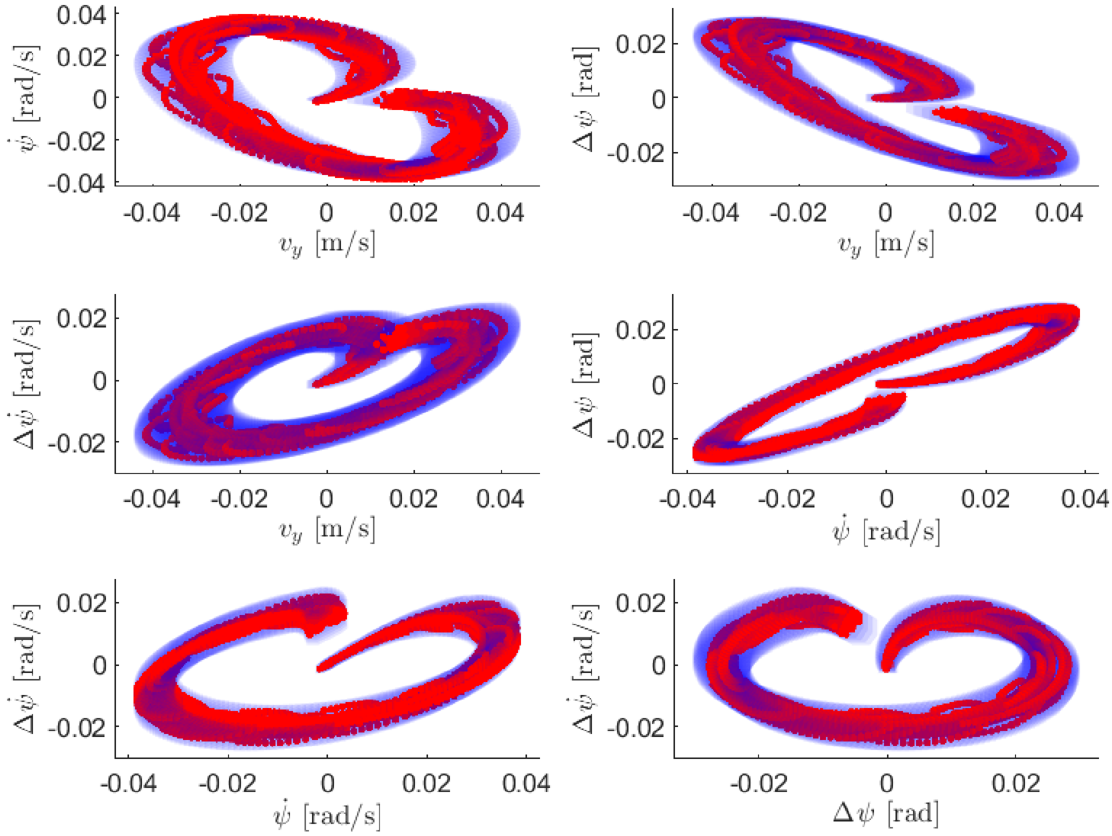

Figure B.23: Phase plane projections for sinusoidal maneuver of 8 seconds

B.3 VTM Simulations

In this section, the VTM simulations are shown on top of the reachable sets obtained in Chapter 6.

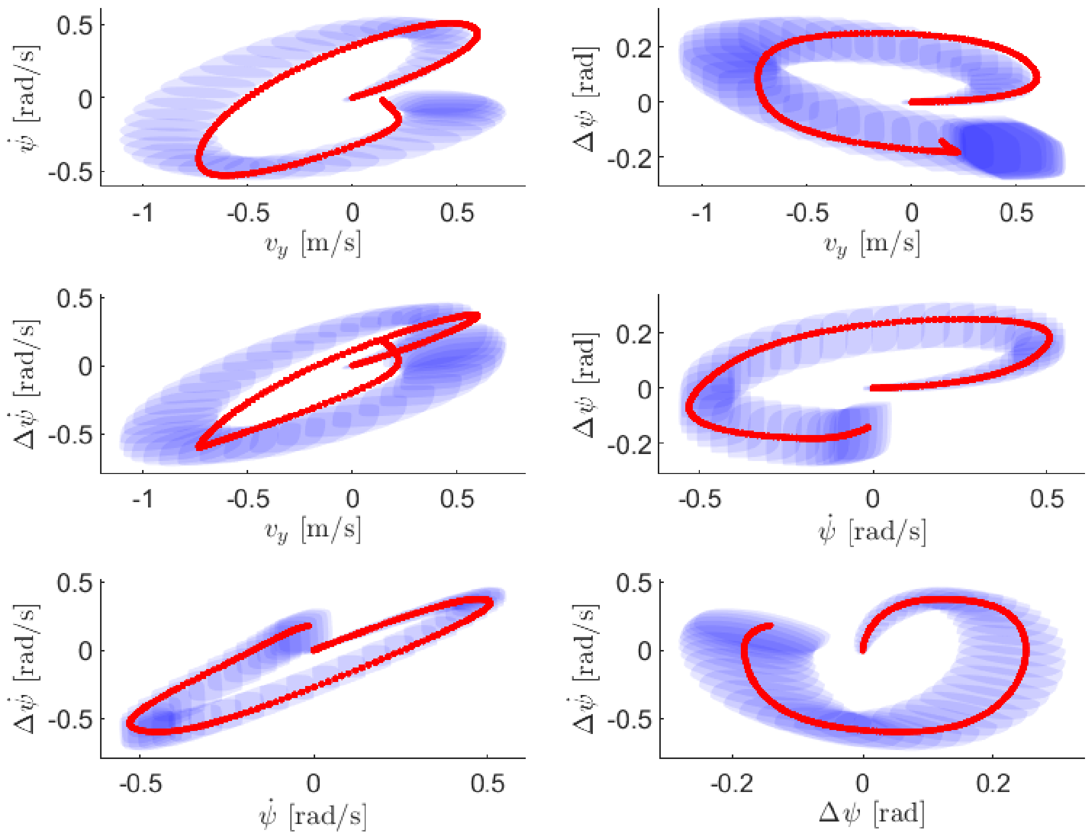

Figure B.24: Phase plane projections and VTM simulation for sinusoidal maneuver of 2 seconds

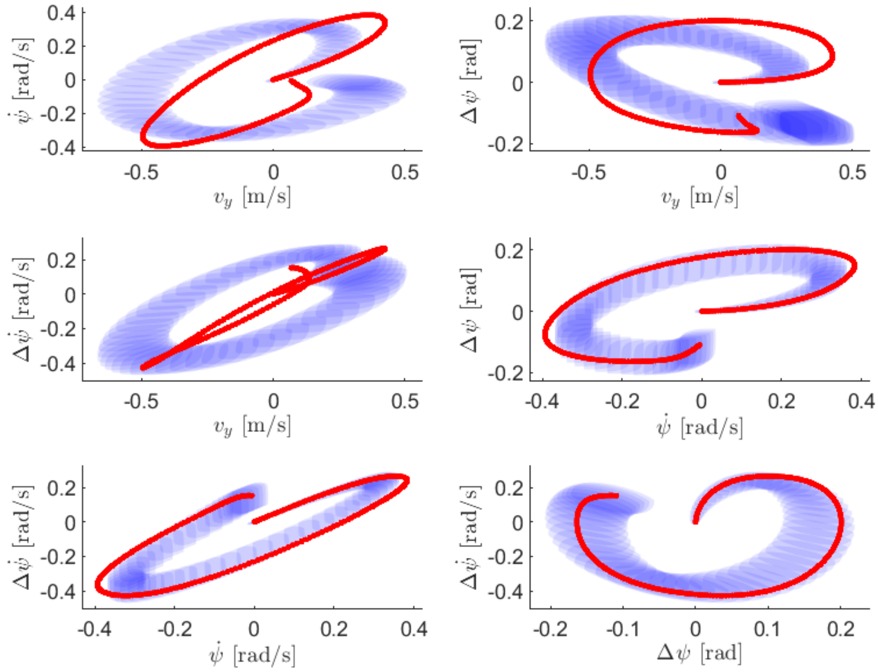

Figure B.25: Phase plane projections and VTM simulation for sinusoidal maneuver of 2.5 seconds

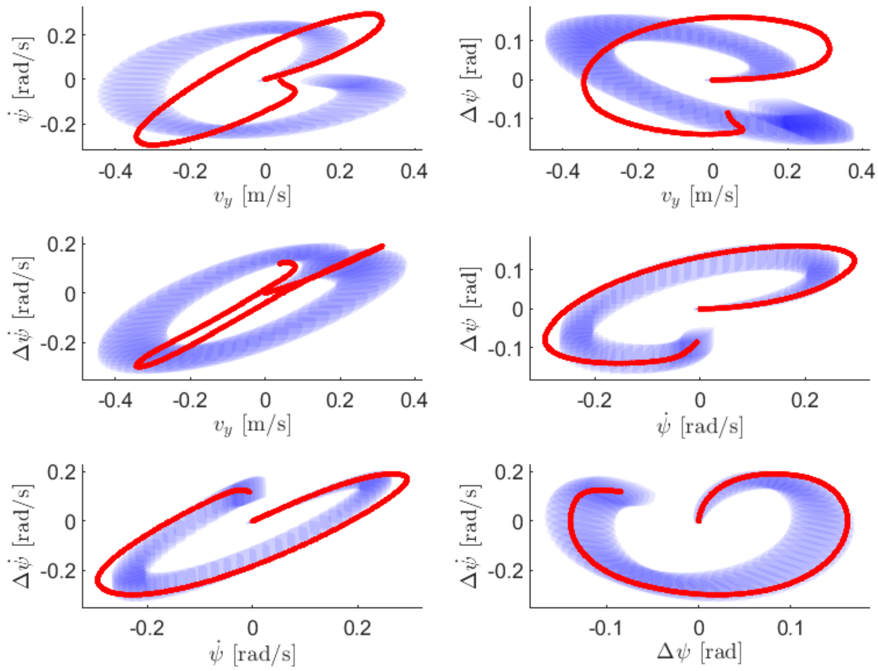

Figure B.26: Phase plane projections and VTM simulation for sinusoidal maneuver of 3 seconds

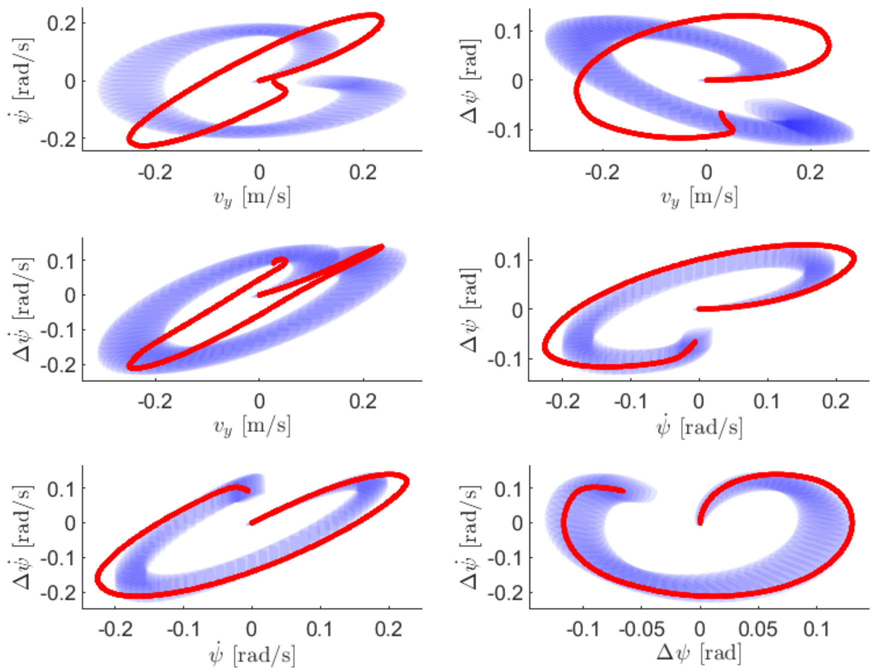

Figure B.27: Phase plane projections and VTM simulation for sinusoidal maneuver of 3.5 seconds

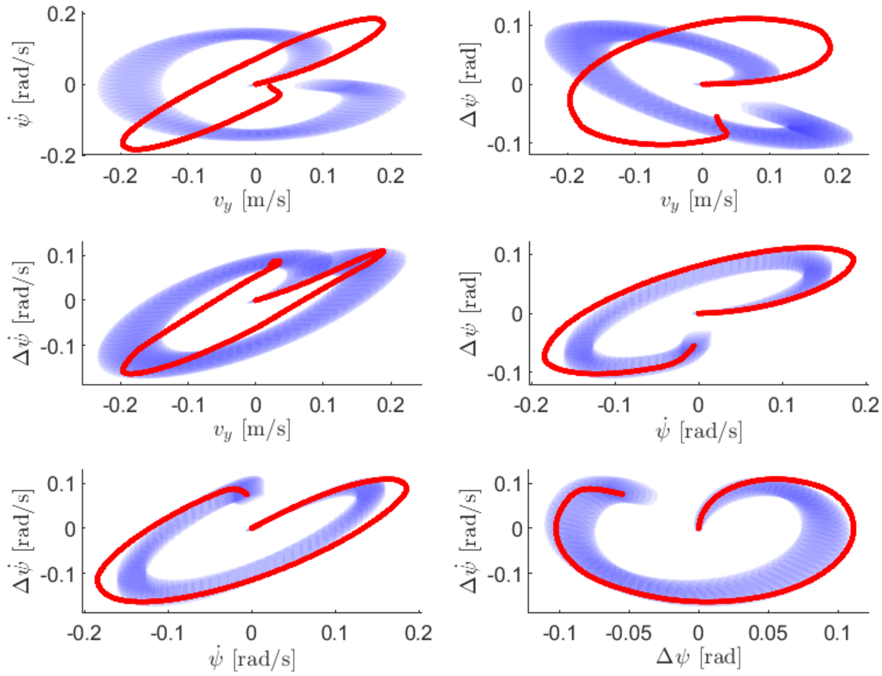

Figure B.28: Phase plane projections and VTM simulation for sinusoidal maneuver of 4 seconds

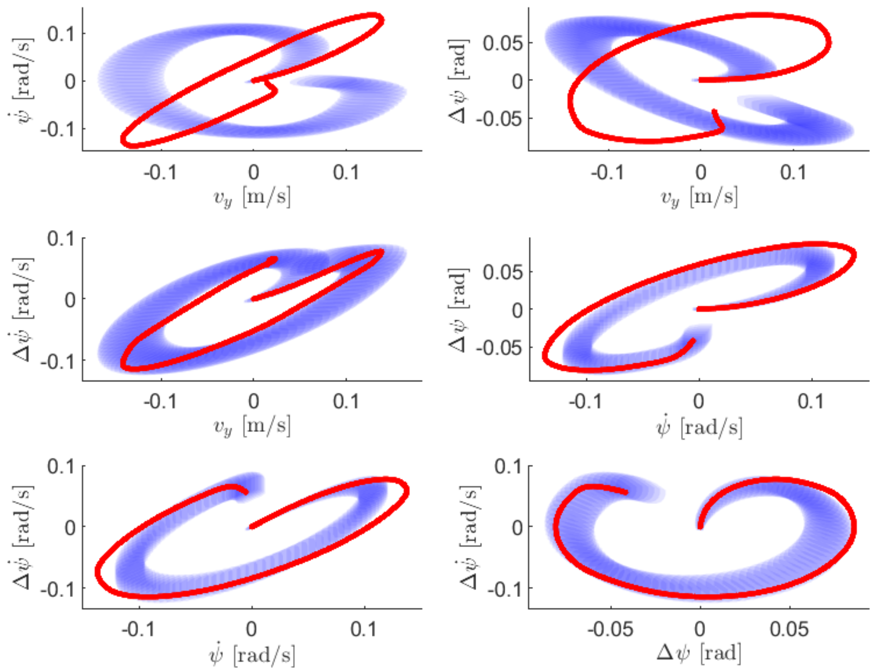

Figure B.29: Phase plane projections and VTM simulation for sinusoidal maneuver of 4.5 seconds

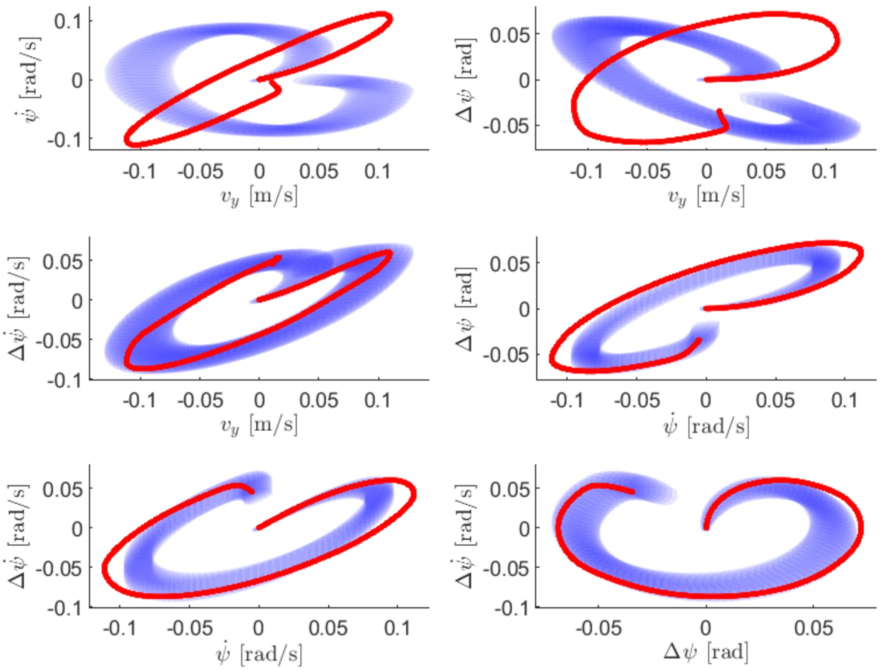

Figure B.30: Phase plane projections and VTM simulation for sinusoidal maneuver of 5 seconds

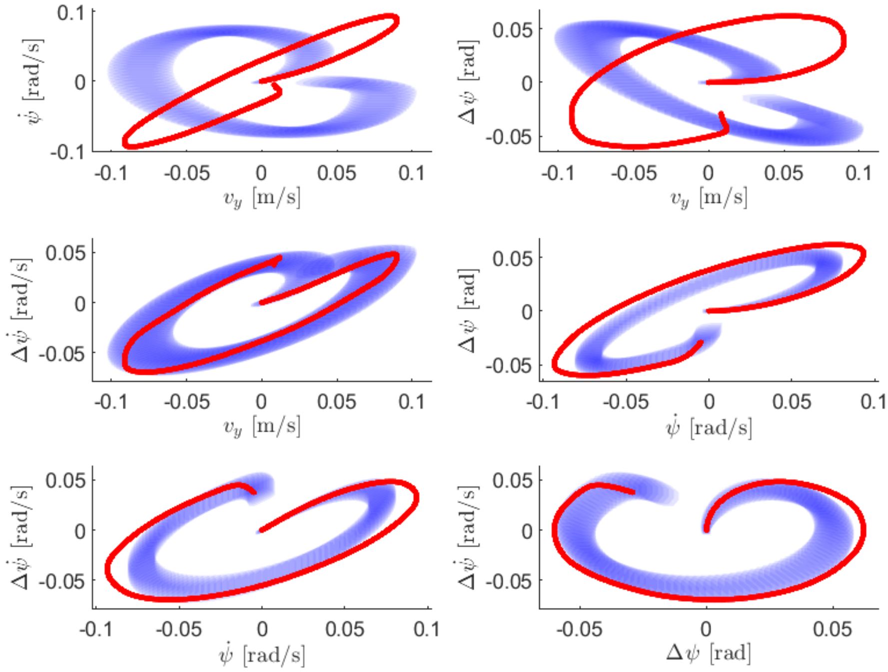

Figure B.31: Phase plane projections and VTM simulation for sinusoidal maneuver of 5.5 seconds

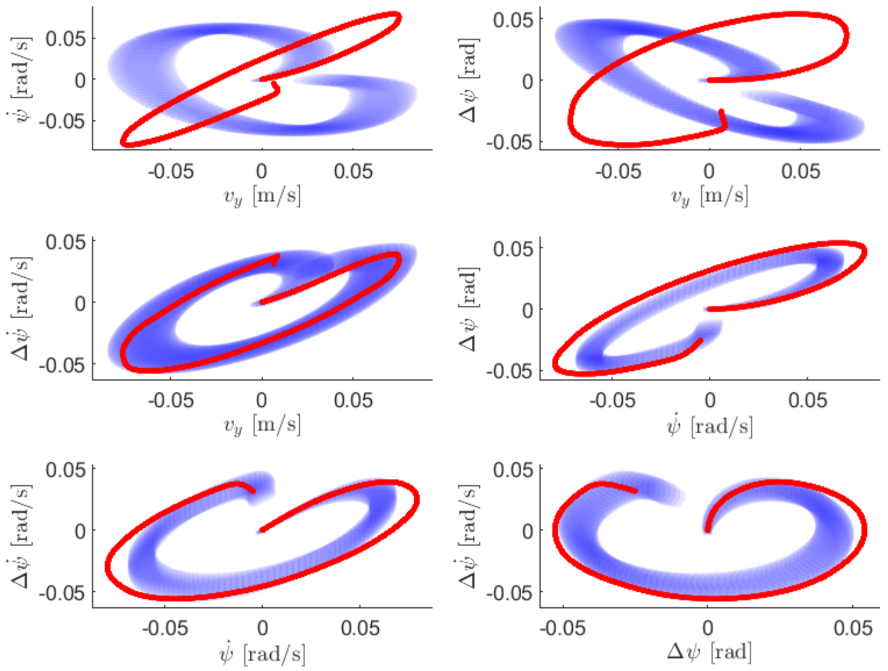

Figure B.32: Phase plane projections and VTM simulation for sinusoidal maneuver of 6 seconds

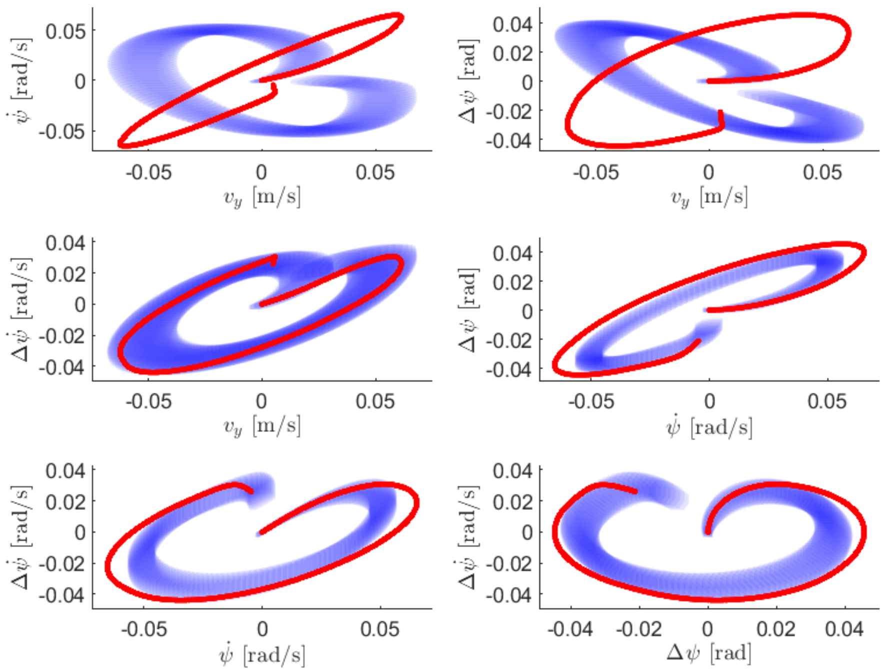

Figure B.33: Phase plane projections and VTM simulation for sinusoidal maneuver of 6.5 seconds

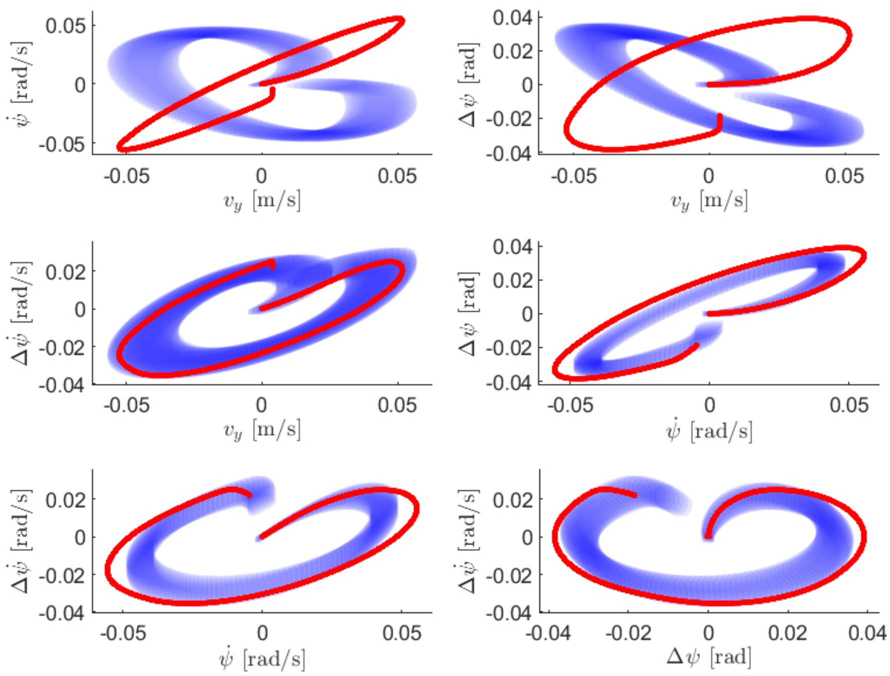

Figure B.34: Phase plane projections and VTM simulation for sinusoidal maneuver of 7 seconds

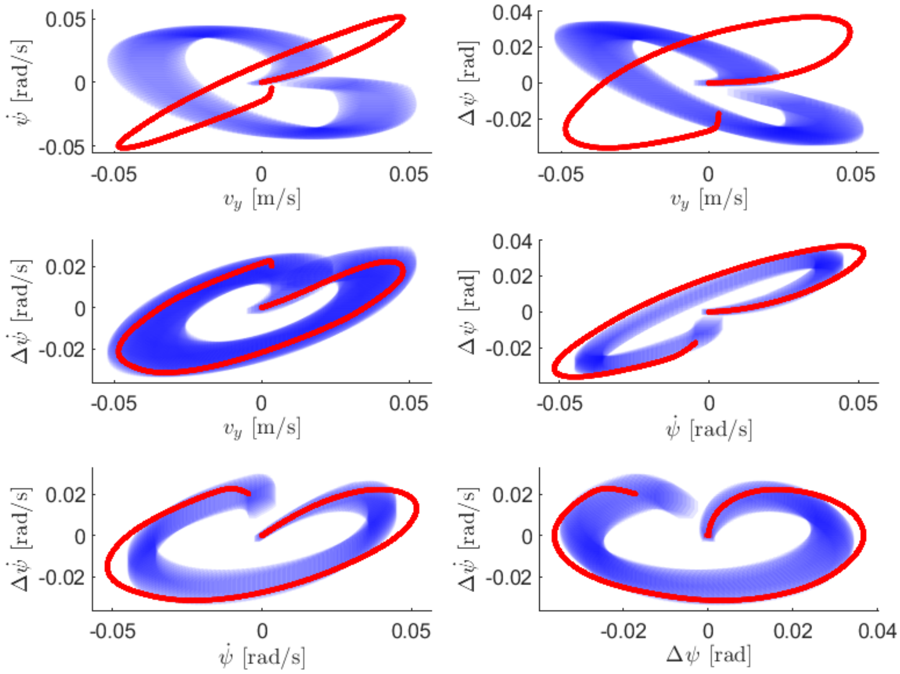

Figure B.35: Phase plane projections and VTM simulation for sinusoidal maneuver of 7.5 seconds

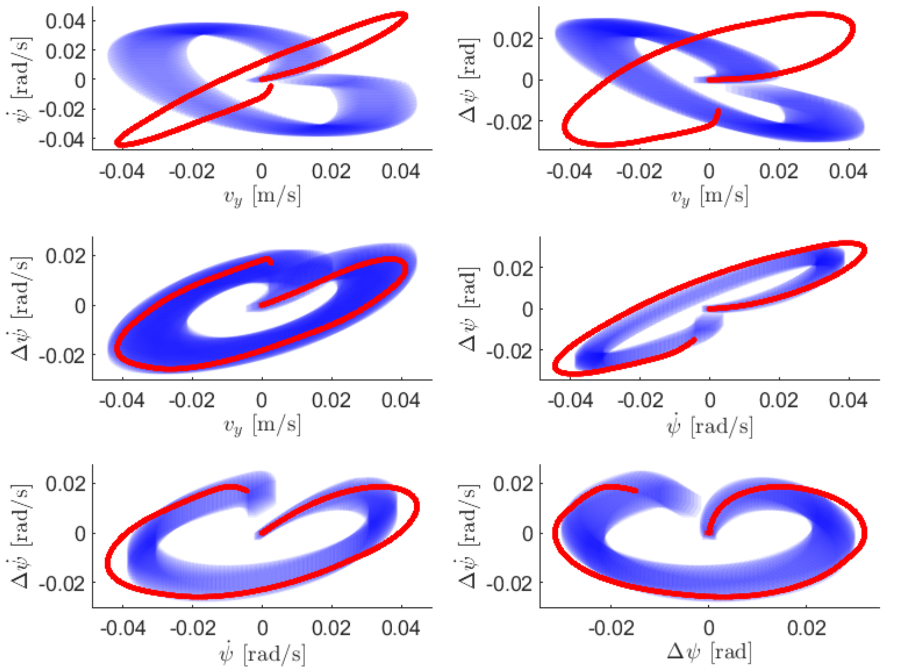

Figure B.36: Phase plane projections and VTM simulation for sinusoidal maneuver of 8 seconds